ÉCOLE DE TECHNOLOGIE SUPÉRIEURE
UNIVERSITÉ DU QUÉBEC

THESIS PRESENTED TO
ÉCOLE DE TECHNOLOGIE SUPÉRIEURE

IN PARTIAL FULFILLMENT OF THE REQUIREMENTS FOR A
MASTER'S DEGREE WITH THESIS IN ELECTRICAL ENGINEERING
M. A. Sc.

BY
Charles TRUDEAU

ELECTROSTATIC DEPOSITION OF GRAPHENE FOR USE IN PHOTO-CONDUCTIVE SWITCH

MONTREAL, OCTOBER 16, 2015

BOARD OF EXAMINERS (THESIS M.A.Sc.)

THIS THESIS HAS BEEN EVALUATED

BY THE FOLLOWING BOARD OF EXAMINERS

Prof. Sylvain G. Cloutier, Thesis Supervisor
Department of Electrical Engineering, École de technologie supérieure

Prof. Ricardo Zednik, Chair, Board of Examiners
Department of Mechanical Engineering, École de technologie supérieure

Mr. Martin Bolduc, External Evaluator
INO (Institut National d'Optique)

THIS THESIS WAS PRENSENTED AND DEFENDED

IN THE PRESENCE OF A BOARD OF EXAMINERS AND THE PUBLIC

OCTOBER 7, 2015

AT ÉCOLE DE TECHNOLOGIE SUPÉRIEURE

ACKNOWLEDGMENTS

This project would not have been possible if not for the help and guidance of many individuals. I will take the time to thank each of them personally. First of all I would like to thank my parents Alain Trudeau and Renee Gaulin for their continuous support and love in all matters of life but specifically for their support in my studies since I was a child, without them none of this would be possible. I would also like to thank my Thesis supervisor Sylvain G. Cloutier for his guidance in this project and his support when things did not go according to plan, I would also like to thank him for taking me in his research group, believing in me and my competence and providing an incredible work environment, it has been a pleasure to be under his supervision during my time at l'Ecole de Technologie Superieur. I would like to thank my good friend Cedric Sommers for his lifelong friendship and for introducing me to Sylvain Cloutier and his research. I will also take the time to thank each and every student in my research group since they all played a part even if not directly in this project. To Francois Xavier Fortier, I thank you for your technical advice, for your help with interfacing instruments and for our morning conversations over coffee. I would like to thank Xiaohang Guo for his light hearted attitude and our discussions on all matters. Debika Banerjee also played a part in the incredible working environment which I call our research group, I thank her for her sometimes jokester attitude which always lightens the mood in the office and also for her intelligent input in our technical discussions. I would like to thank Jaime Benavides for being a role model in terms of his hard working aptitude, for his expertise in chemical engineering and for our discussions on all matters of life. Felipe Gerlein became another role model of mine for his intelligence and relaxed attitude which is extremely welcome in times of stress, I thank him for this and for his help on anything relating to lasers and optics. Although Haythem Rehouma has not been with us for very long, I would like to thank him nonetheless for our morning conversations and for his input in technical discussions. Finally I would like to thank Nelson Landry, a research assistant to our research group, for all his help in any matter of instrumental set-up, design and fabrication. His help in matters of ordering parts and his connections to other laboratories and research personnel was also greatly appreciated, not to mention all his technical help on all matters.

ELECTROSTATIC DEPOSITION OF GRAPHENE FOR USE IN PHOTOCONDUCTIVE SWITCH

Charles TRUDEAU

ABSTRACT

Graphene, a material made up from a single atomic layer of honeycomb structured sp2 bonded carbon atoms, has been gaining interest in the last decade for its integration in optoelectronic devices in a wide range of fields. Many methods of graphene growth and deposition have been developed over the years. These methods range from high cost and high quality of deposited graphene to low cost and low quality of deposited graphene, depending on the applications wanted. An overview and comparison of these methods is presented in this work. More focus is placed on one such deposition method; the electrostatic deposition of graphene. This work aims to show the possibility to deposit micro graphene sheet arrays directly for the use in optoelectronic device active layers, such as bolometers and photoconductive switches. Improvements to the current technologies involving deposition of graphene using electrostatic forces have been investigated, more precisely, improvements to the control of the shape, size and position of the deposited graphene. These improvements are realised primarily via surface etching of the graphitic material used for deposition by pulsed UV Laser radiation. Etching of the graphitic material is performed to limit and therefore control the size of the deposited graphene. Patterning of the deposition substrate is also explored as a method of modifying local electric field strengths, moreover the possibility of direct deposition of graphene onto pattern SiO2 substrate to create suspended membranes is explored. However, deposition of graphene onto un-patterned SiO2 substrate are the main deposition results presented in this work. The optoelectronic properties of the deposited graphene were studied. More precisely, the deposited graphene is shown to have a direct electrical response to incident light of multiple wavelengths, thus making it suitable for photoconductive switch devices. The calorimetric properties of the deposited graphene were also studied, these results, however, were less conclusive, casting doubt on the effectiveness of graphene as a bolometer active layer. Improvements to the homogeneity of the cleaving process used in the electrostatic deposition of graphene were performed and are shown to lead to large scale graphene depositions, previously only thought to be achievable with more costly methods of graphene growth. A simple and accurate method of characterising the number of graphene layers present in the deposition is developed using the center of a single fitted gaussian curve on the 2D graphene Raman peak.

Keywords: Bolometer, Electrostatic Deposition, Graphene, Optoelectronics, Photoconductive switch, Raman Spectroscopy

DÉPÔT ÉLECTROSTATIQUE DE GRAPHÈNE POUR L'INTÉGRATION DANS DES INTERRUPTEURS PHOTOCONDUCTEURS

Charles TRUDEAU

RÉSUMÉ

Le graphène, un matériau constitué d'une seule couche atomique de carbone sp2 structurée en nid d'abeilles, attire beaucoup d'intérêt dans la dernière décennie pour son intégration dans des dispositifs optoélectroniques dans un large éventail de domaines. De nombreuses méthodes de croissance et dépôt de graphène ont été développés au fil des ans. Ces méthodes vont de coût élevé et de haute qualité du graphène déposé à des méthodes à faible coût et faible qualité du graphène déposé, selon les applications voulues. Une vue d'ensemble et une comparaison de ces méthodes est présentée dans ce travail. Un accent est mis sur un tel procédé de dépôt: le dépôt électrostatique de graphène. Ce travail vise à montrer la possibilité de déposer des matrices de feuille de graphène directement pour l'utilisation comme couches actives pour des dispositifs optoélectroniques tels que les interrupteurs photoconducteurs et les bolomètres. Des améliorations aux technologies actuelles impliquant le dépôt de graphène par force électrostatique sont présentées, plus précisément, sur le contrôle de la forme, la taille et la position de la déposition. Ces améliorations sur le contrôle du graphène déposé sont réalisées principalement par une gravure de la surface du matériau graphitique utilisé pour le dépôt par laser pulsé de rayonnement UV. La gravure du matériau graphitique est effectuée pour limiter et donc contrôler la taille du graphène déposé. Une gravure du substrat de déposition est également explorée comme un procédé de modification des intensités du champ électrique locale, outre la possibilité de dépôt direct du graphène sur un substrat de SiO2 engravé pour créer des membranes en suspension est exploré. Cependant, le dépôt de graphène sur un substrat de SiO2 non-modifié sont les principaux résultats de dépôt présentées dans ce travaille. Les propriétés optoélectroniques du graphène déposé ont été étudiés. Plus précisément, le graphène déposé a une réponse électrique directe à la lumière incidente de plusieurs longueurs d'onde, ce qui le rend convenable a l'utilisation pour des couches actives d'interrupteur photoconducteur. Les propriétés colorimétriques du graphène déposé ont également été étudiés, ces résultats, cependant, étaient moins concluants, jetant un doute sur l'efficacité du graphène comme couche active de bolomètres. Les améliorations apportées à l'homogénéité du processus de clivage utilisé dans le dépôt électrostatique du graphène peuvent conduire à des dépôts à grande échelle. Auparavant, les dépôts a grande échelle étaient uniquement réalisables avec des méthodes plus coûteuses de croissance de graphène. Un procédé simple et précis de la caractérisation du nombre de couches de graphène présents dans les dépôts a été mis au point. Cette méthode est réalisée à partir du centre d'une régression gaussienne sur la pic Raman 2D du graphène.

Mots-Clés: Bolomètre, Dépôt Électrostatique, Graphène, Interrupteur Photoconducteur, Optoélectronique, Spectroscopie Raman

TABLE OF CONTENTS

Page

LIST OF TABLES

Page

LIST OF FIGURES

Page

LIST OF ABREVIATIONS

AFM	Atomic Force Microscopy
CVD	Chemical Vapour Deposition
DI	Deionised
EM	Electromagnetic waves
FWHM	Full Width at Half Maximum
HOPG	Highly Ordered Pyrolytic Graphite
IPA	Isopropyl Alcohol
IR	Infra Red
I-V	Current - Voltage
Mins	Minutes
MWNT	Multi-Walled Nano-Tube
PMMA	Poly(methyl methacrylate)
PVC	Poly(vinyl chloride)
R_room	Resistance at room temperature
R_low	Resistance at low temperature
SEM	Scanning Electron Microscopy
SMU	Source Measure Unit
SWNT	Single-Walled Nano-Tube
TSL	Tunnable Semiconductor Laser
UV	Ultra Violet
VI	Visual Interface

LIST OF SYMBOLS AND UNITS OF MEASUREMENTS

Electrical Units

V	volt
kV	kilovolt
mA	miliamp
A	amp
Ω	ohm
kΩ	kilo-ohm
mW	miliwatt
W	watt

Geometric Units

nm	nanometer
μm	micrometer
mm	millimeter
cm	centimeter
m	meter
"	inches
cm^{-1}	wavenumber

Ratio Symbols

wt/wt	weight ratio
D/G	D over G ratio
%	percentage

Thermal Units

°C	degree Celsius
mK	mili-Kelvin
K	Kelvin

Temporal Units

s	seconds
mins	minutes
h	hours
GHz	gigahertz
MHz	megahertz
kHz	kilohertz
Hz	hertz

Weight Units

g	grams

INTRODUCTION

Graphene, a material made up from a single atomic layer of honeycomb structured sp2 bonded carbon atoms, has been gaining interest in the last decade since it was first separated from bulk graphite in 2004 (Hancock, 2011). The main interest from this material comes from its peculiar electronic properties as a zero bandgap semiconductor with a linear energy dispersion at the touching point of the conduction and valence bands. No other known materials exhibit such behaviours. Due to this unique dispersion relation, charge carriers within the graphene structure can be modelled as massless Dirac fermions (Hancock, 2011) (Bunch, 2008) (Sidorov et. al., 2007) compared with massive carriers found in materials which follow parabolic energy dispersions. This massless carrier model gives rise to unique transport properties found in no other material. This is why Andre Geim and Konstantin Noveselov received the 2010 Nobel Prize in Physics for the discovery and the "groundbreaking experiments regarding the two-dimensional material graphene"(Novoselov, K.S. et. al.,2004).

Graphene has been used and studied extensively in the last decade since it was first separated from bulk graphite by repeated cleaving of a graphite surface with household scotch tape (Geim, A.K., 2012). Since then, many research and development groups have been exploring the physical, optical and electric properties of single and few-layered graphene (Gilgueng et. al. 2009) (Gunasekaran & Kim, 2009) (Beidaghi et. al. 2012). Some important phenomena observed by these groups, to name a few: the anomalous quantum Hall and Berry's phase effect (Fal'Ko, Vladimir I., 2008) high field degeneracy splitting (Zhang, Y. et. al., 2006), quantum confinement (Allen, M.T. et. al., 2012) and massless carrier transport properties (Chernozatonskii et. al., 2014) (Kliros, 2010). Many groups have also specialised in the production of graphene-like materials such as single-layered graphene, few-layered graphene and single- and multi-walled carbon-nanotubes (Guldi et. al. 2005) (Palser, 1999) (Kykamis et. al., 2005). As a result, there is now a multitude of methods of creating these materials. Some of these methods include the direct construction of graphene from gases (Pollard,

2011) and some deal with separating graphene from bulk graphitic materials (Sidorov, 2009), however all these methods have as an end goal to "deposit" graphene onto a substrate, these methods are therefore described as "graphene deposition methods". Many groups have also started to integrate graphene materials into functional devices such as photovoltaic devices (Kykamis et. al. 2002) (Camacho et. al., 2007) (Sgobba & Guldi, 2007), opto-electronic devices (Jianjun et. al., 2006), high frequency resonators (Van der Zande et. al., 2010), field effect transistors (Dharmendar et. al., 2011), etc.

In this work , single and few-layered graphene is shown to be able to be separated from bulk graphitic material and deposited via electrostatic forces. The size and position of the deposited graphene sheets is shown to be controllable to a certain degree and that these deposited sheets can be introduced as the active layer in optoelectronic devices. These graphene-based devices are shown to be sensitive to light sources and induce a measurable change in resistance. In chapter 1, a review of graphene properties and the theory behind these properties is put forward and explained. Also, an introduction to current optoelectronic device technologies, a theoretical review of these technologies and how graphene properties relate to these devices is included in this chapter. Chapter 2 deals with the many existing graphene deposition and characterisation methods, the reasoning behind the deposition method choice of this work and how it relates to optoelectronic device fabrication. Chapter 3 includes a detailed look at the experimental methodology of the electrostatic deposition of graphene onto patterned and un-patterned SiO2 substrates that is used in this work. This chapter also includes the results of the deposition experiments. Chapter 4 takes the deposition results found in the previous chapter and gives analytic details on the characterisation process of the resulting deposited graphene. The characterisation of the number of gaphene layer deposited and of the optoelectronic properties of the deposited graphene is performed in this chapter.

CHAPTER 1

GRAPHENE FOR OPTOELECTRONIC DEVICES

1.1 Graphene, wonder material?

Recent advances in the field of graphene deposition have led way to more advances in our understanding of the properties of this novel material. This crystalline zero bandgap semiconductor with linear energy dispersion offers many peculiar electrical properties such as massless charge carriers that are unique to graphene. These unique properties have prompted researchers in fields such as material science to consider graphene as a wonder material with almost unlimited applications. In this work, one such application: the use of graphene as the active layer in photoconductive switches and bolometer devices will be explored. The optoelectronic properties of these devices will be put to the test to help answer if graphene is really a wonder material. A theoretical review of the phonon and energy dispersion properties, the electrical properties and the optical properties of graphene follows in this chapter.

1.1.1 Electrical Properties and energy dispersion relations

The peculiar electronic properties of graphene originate from its unique energy dispersion. In this part of the chapter, the energy dispersion of monolayered graphene and that of bi-layered graphene is studied and its effect on the electrical properties and phonon relations are explained. Figure 1.1 shows the 2 dimensional energy dispersion relations of graphene, a zero-bandgap semiconductor compared to a typical semiconductor (Hatsugai, 2010). In this figure, the linear energy dispersion relation of graphene near the Dirac point is easily identifiable compared to the parabolic nature of the energy dispersion in typical semiconductors. The touching of the valance and conduction bands of graphene,which gives rise to the "zero-bandgap" designation, is also clearly visible.

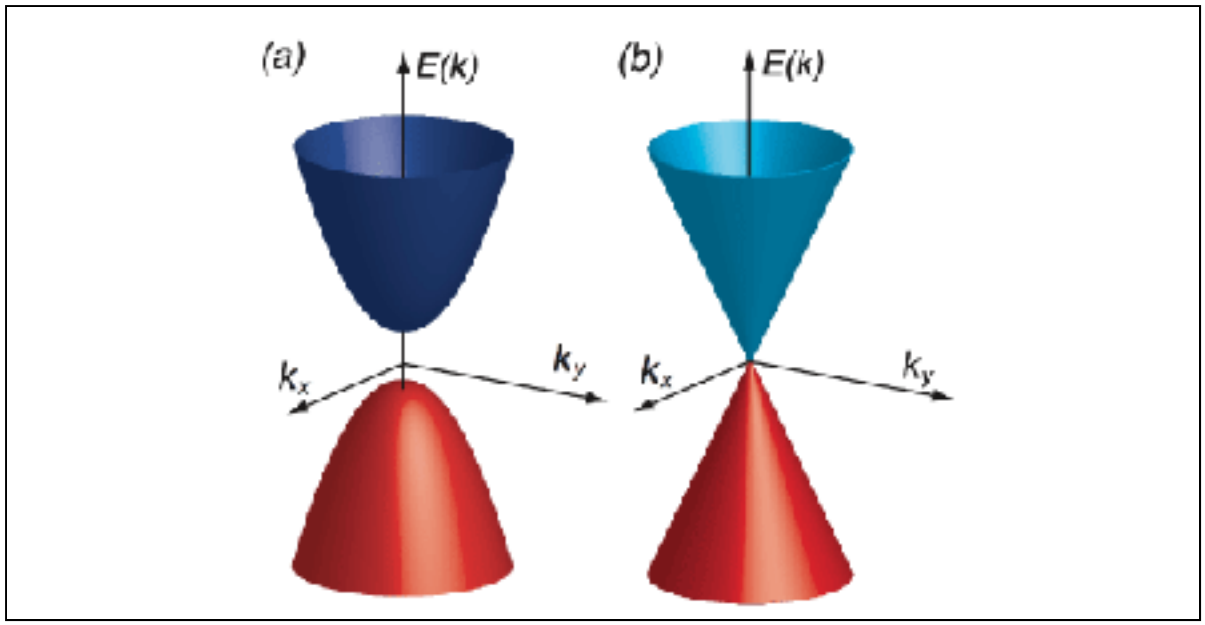

Figure 1.1 Energy dispersion of a) typical two-dimensional semiconductor and b) of zero-bandgap graphene semiconductor
Taken from Hatasugai (2010)

The intrinsic properties of the energy dispersion relations of monolayered graphene have been shown to produce some unusual electrical properties. One such property, that has gained major interest in the recent years, is the linear energy dispersion relation of graphene. Such an energy dispersion relation gives rise to theoretically massless charged carriers and thus theoretically infinite carrier mobilities. From Newton's second law (assuming that acceleration is the rate of change in group velocity) and crystal momentum relations, the mass of charged carriers can be calculated, this is shown in equations 1.1 to 1.5. Equation 1.1 is Newton's second law, where **F** is the force vector, m^* is the effective mass of the charged carrier and **a** is the acceleration of said carriers. In equation 1.2, the acceleration is assumed to be equal to the rate of change in group velocity $\boldsymbol{v_g}$ which is changed into reciprocal space, where ∇_k is the del operator in reciprocal space and $\omega(\boldsymbol{k})$ is the angular frequency. In equation 1.3, Newton's second law is applied to a crystal, where $\boldsymbol{p_{crystal}}$ is the crystal momentum. Equation 1.4 combines equations 1.2 and 1.3 to give an expression of the acceleration in terms of E(**k**): the energy dispersion relation, ħ: the reduced Plank constant

and **F**: the force vector. Equation 1.5 combines equations 1.1 and 1.4 to give an expression for the effective mass in terms of $\frac{\partial^2 \mathrm{E(k)}}{\partial \mathrm{k}^2}$; the curvature of the energy dispersion relation.

$$\boldsymbol{F} = m^* \boldsymbol{a} \tag{1.1}$$

$$\boldsymbol{a} = \frac{d\boldsymbol{v_g}}{dt} = \frac{d(\nabla_k \omega(\boldsymbol{k}))}{dt} = \nabla_k \left(\frac{d\boldsymbol{k}}{dt} \nabla_k \omega(\boldsymbol{k}) \right) \tag{1.2}$$

$$\boldsymbol{F} = \frac{d\boldsymbol{p_{crystal}}}{dt} = \hbar \frac{d\boldsymbol{k}}{dt} \tag{1.3}$$

$$\boldsymbol{a} = \nabla_k \left(\frac{F}{\hbar} \nabla_k \omega(\boldsymbol{k}) \right) = \left(\frac{1}{\hbar} \frac{\partial^2 \omega(\boldsymbol{k})}{\partial k^2} \right) \boldsymbol{F} = \left(\frac{1}{\hbar^2} \frac{\partial^2 E(\boldsymbol{k})}{\partial k^2} \right) \boldsymbol{F} \tag{1.4}$$

$$m^* = \hbar^2 \left[\frac{\partial^2 E(\boldsymbol{k})}{\partial k^2} \right]^{-1} \tag{1.5}$$

The curvature of a linear energy dispersion relation at the Dirac point is infinite and thus lead to an effective mass for the charged carriers of zero.

In practice, charge carrier mobilities in graphene have been measured to reach up to 15000cm^2/Vs (Geim & Novoselov, 2007), this deviation from the theoretical value has been explained to be due to defects introduced in the non-perfect graphene formation process (Geim & Novoselov, 2007) and depends on the channel width and length of the device used for measurement.

Another interesting property of the energy dispersion relation in graphene is the double resonance process in monolayered and bilayered graphene. (Mallard et. al., 2009) This double resonance process helps to explain the 2D graphene Raman peak and the splitting of this peak with increased number of layers. The 2D Raman peak (~2700cm^{-1}) found in graphene is due to two phonons with opposite momentum in the highest optical branch near the K point. The double resonance process links the phonon wave vectors to the electronic

band structure. This process for monolayered graphene is illustrated in figure 1.2. The Raman scattering process involving four virtual transitions: laser excitation of an electron-hole pair (vertical transition in figure 1.2), electron-phonon scattering with exchanged momentum q (horizontal transition in figure 1.2), electron-phonon scattering with negative exchanged momentum -q (horizontal transition in figure 1.2) and electron-hole recombination (vertical transition in figure 1.2). When the energy is conserved in these transitions, the double resonance conditions are met. The resulting 2D graphene Raman peak frequency is twice the frequency of the scattering phonon.

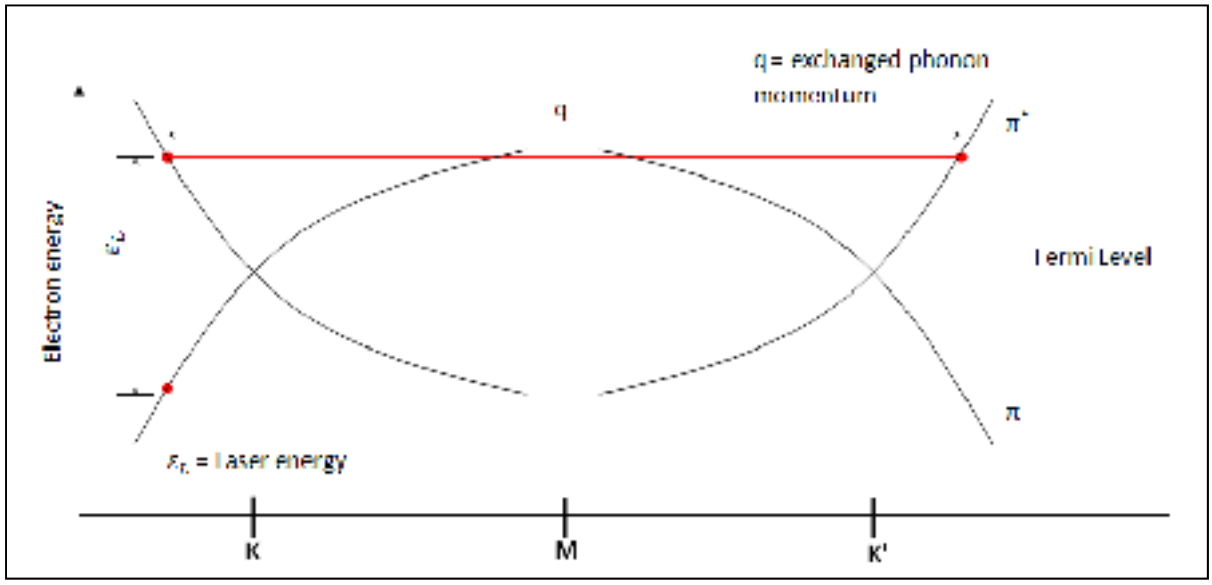

Figure 1.2 Monolayer graphene double resonance phonon relations

For bilayered graphene, the interactions of the graphene planes causes the π and π* bands to divide into four bands with a different splitting for electrons and holes (Zhenhua et. al., 2009) (Ferrari et. al., 2006), this is illustrated in figure 1.3. The 4 main resulting processes involve phonons with momenta q1B, q1A, q2A, and q2B, as shown in figure 1.3. There exists some other processes such as the four corresponding processes for the holes, and those associated to the 2 less intense optical transitions (not shown), these are associated to momenta almost identical to q1B, q1A, q2A, q2B and almost identical Raman shifts (Ferrari et. al., 2006). The main processes produce four different 2D sub-peaks in the Raman spectrum of bilayer

graphene. Similarly, further splitting of the 2D Raman peak occur with increased number of graphene layers (Ferrari et. al., 2006) (Mallard et. al., 2009). The Raman spectrum fingerprints for single-layer, bilayer, and few-layer graphene reveal changes in the electronic structure and electron-phonon interactions. This splitting in the 2D Raman peak of graphene allows for fast, unambiguous and nondestructive identification of graphene layers which will be explored in more detail further in this work.

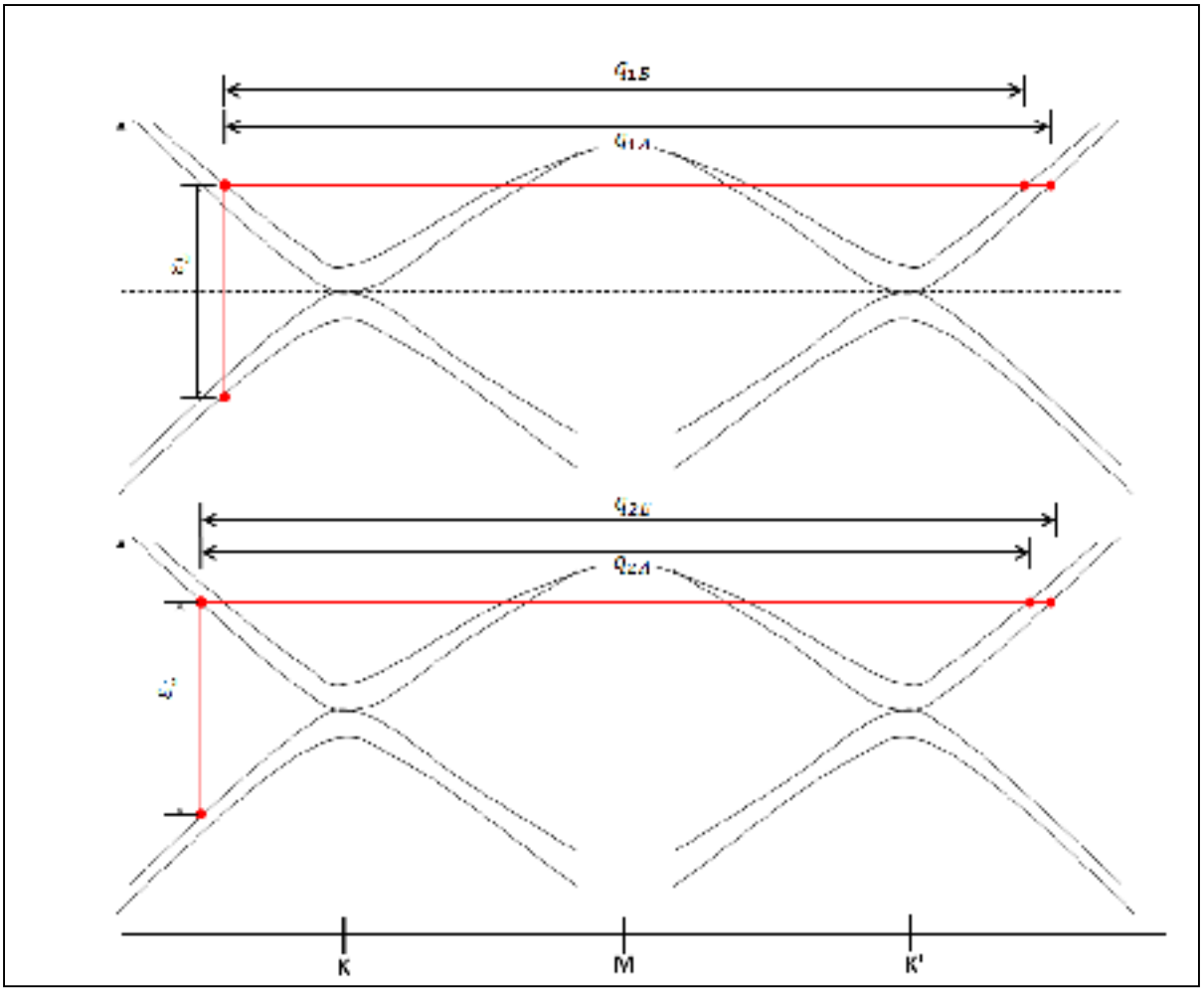

Figure 1.3 Bi-layered graphene double resonance phonon relations

Other non resonant phonon relation processes within the graphene lattice give rise to other Raman peaks (Mallard et. al., 2009), these are summarised in figure 1.4 and shown along

with the main graphene Raman spectrum features. The other main Raman features found for graphene are the D peak and the G peak found at ~1350 cm^{-1} and ~1590 cm^{-1} respectively. The G peak is associated with the doubly degenerate iTO and LO phonon mode and the D peak is associated with a second-order process involving an iTO phonon and a defect within the graphene lattice.

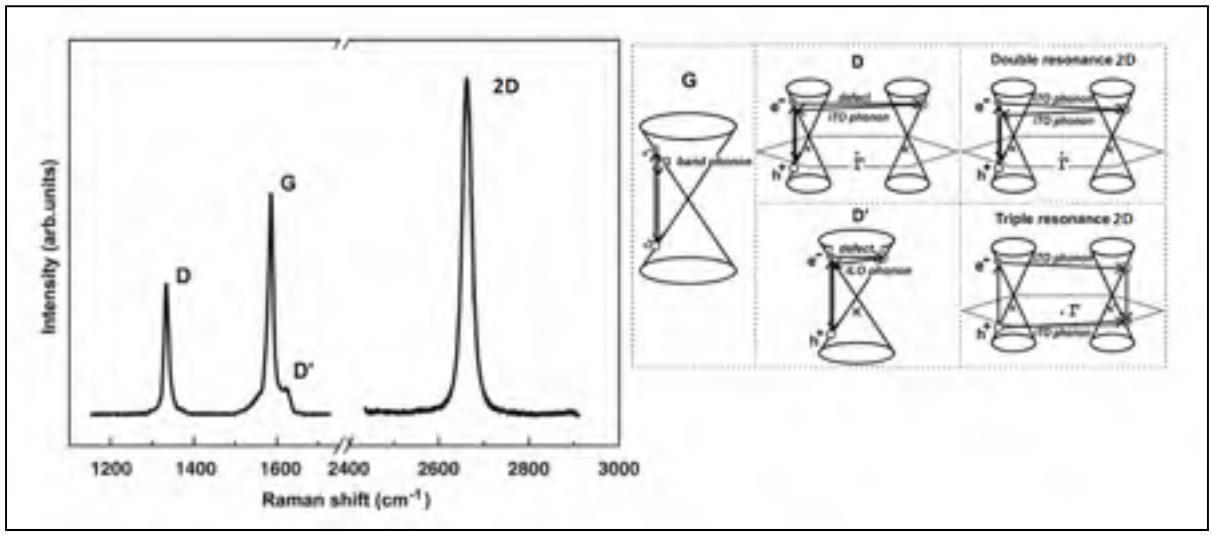

Figure 1.4 Main graphene Raman spectrum features and associated phonon relation processes Adapted from Mallard et. al. (2009)

1.1.2 Optical Properties

Optical properties of graphene-based materials offer the potential for multiple diverse applications in optoelectronics. For example, induced graphene bandgap photoluminescence has been explored as an alternative to fluorescent quantum dots (Bonaccorso et.al., 2010), or the optical limiting found in graphene-based materials has been used in passive manipulation of optical beams and as high intensity laser pulse protection (Liu et. al., 2009). Following is a review of the absorption, emission and non-linear optical properties of graphene.

Graphene sheets exhibit very low optical absorption over a broad spectral range from the ultraviolet to the near-infrared. The optical transparency of graphene is very high, over 90%

from 300nm to 2500nm wavelength (Bonaccorso et.al., 2010). Similarly to other carbon-based materials, the π-plasmon absorption is the main factor in photon harvesting by graphene (Eberlein, et. al., 2008). Figures 1.5 and 1.6 show the wavelength dependent transmittance of single-layered graphene and the total visible transmittance of different number of graphene layers respectively. As can be seen from these figures a ~2.3% to 4% of light absorbance per graphene layer is measured for a wide range of wavelengths. A small increase in absorbance to ~10% is seen at in the ultraviolet range of the spectrum at ~275nm.

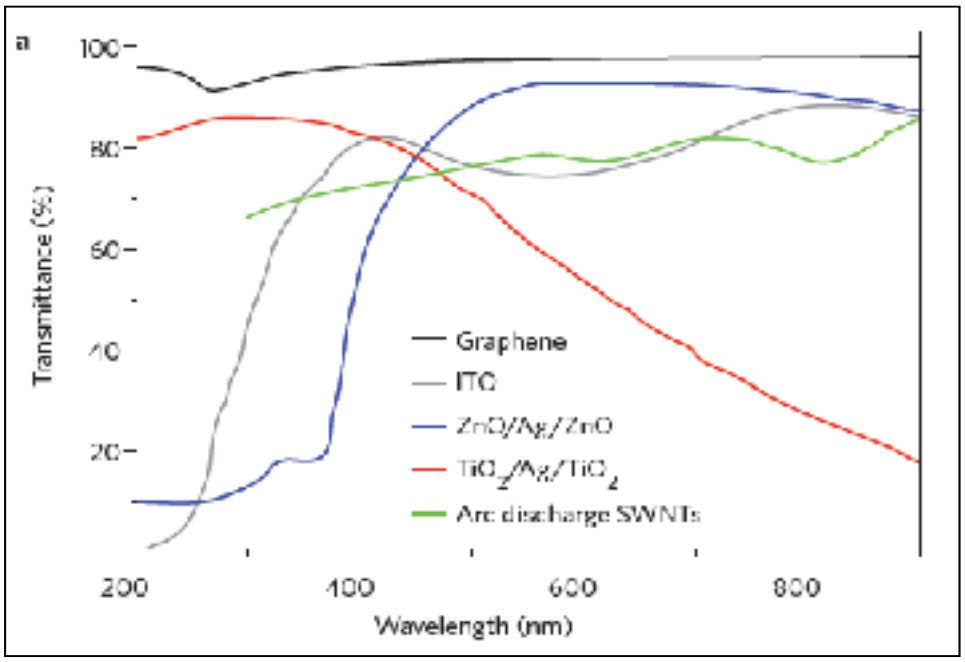

Figure 1.5 Transmittance for different transparent conductors: GTCFs39, single-walled carbon nanotubes (SWNTs), ITO, ZnO/Ag/ZnO and TiO2/Ag/TiO2
Taken from Bonaccorso et. al. (2010)

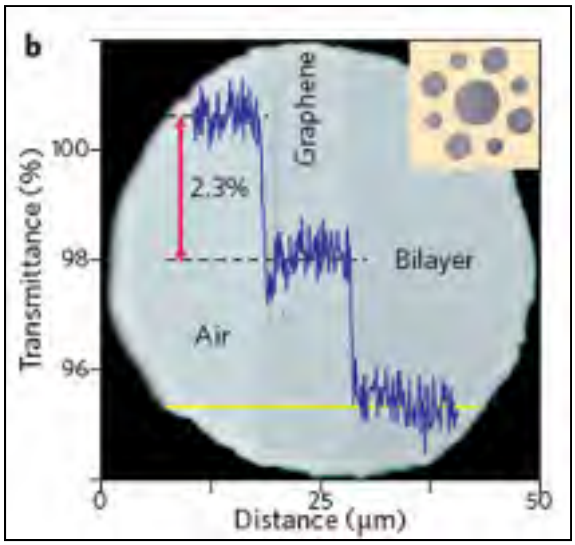

Figure 1.6 Transmittance for an increasing number of graphene layers
Taken from Bonaccorso et. al. (2010)

Zero bangap pristine graphene offers no emission or luminescence mechanism apart from thermal blackbody radiation, only by introducing a bandgap can this be done. Chemical and physical treatments to pristine graphene can be employed to artificially introduce a bandgap in graphene by reducing the connectivity of the π-electron network (Bonaccorso et. al., 2010). Since the photoluminescence of such an altered connectivity of the π-electron network depends greatly upon the treatment applied (Bonaccorso et. al., 2010) and that no such treatment is performed in this work, the emission properties of altered graphene are not studied further.

The non-linear optical properties of graphene and graphene-based materials are by far the most interesting. One of these effects is the optical-limiting effect previously reported in graphene (Liu et. al., 2009). Optical limiter exhibit linear transmittance at low light intensities and reduced transmittance at high intensities. Broadband (450-1064 nm) optical-limiting properties have been observed in graphene sheets prepared from substoichiometric graphene-oxides (Dai et. al., 2015). However, this optical limiting has been related to the environment surrounding the graphene sheets rather than being an intrinsic property of the

absorbing domains in the sheets (Dai et. al., 2015). Figure 1.7 shows the optical-limiting effects of graphene-based materials (Liu et. al., 2009).

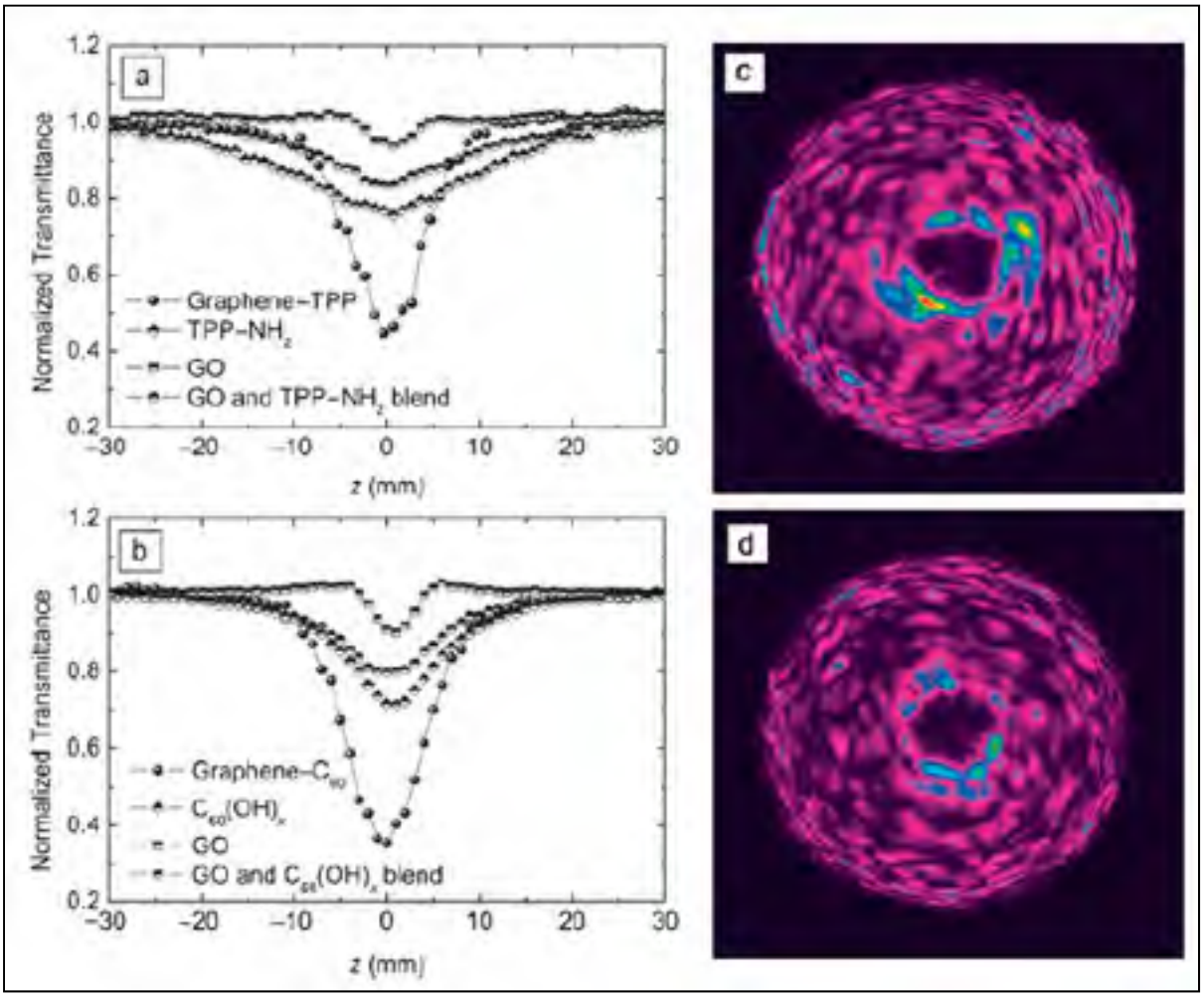

Figure 1.7 Non-linear optical properties of graphene and other carbon based materials Taken from Liu et. al. (2009)

1.2 Bolometers

Bolometers (sometimes called calorimeters) are devices which are able to measure the power of incident electromagnetic radiation via heating effects of a temperature-dependent conducting active layer. The word bolometer comes from the Greek words "bolometron" which translates roughly to "measurer of thrown things". Applications of bolometers are seen in a wide variety of fields spanning from dark matter detection in astronomy and particle physics (Gildemeister, 2000) to thermal imaging used in military grade night vision (Wood, 1993) and medical devices (Gorecki et. al., 2004). Bolometers can be used to measure incident radiation of most frequencies, however they are mostly used in infrared to terahertz radiation due to their high comparative sensitivity at these wavelengths (Richards, 1994). Outside of this range of frequencies there exists other devices which use different methods of detections that are more sensitive. In this part of the chapter, a review of the theory behind the method of light detection used in bolometers, the current bolometer technologies available and the proposed design of graphene based micro-bolometer devices is presented.

1.2.1 A Theoretical Review Of Bolometers

The following is a review of the principles of operation behind bolometer devices. Typically bolometer devices consist of an absorptive active layer connected to a thermal reservoir (Richards, 1994). Incident radiation comes into contact with the active layer of the bolometer which is then heated to temperatures above that of the thermal reservoir. This temperature change induces a change in resistivity in the temperature-dependent conducting active layer which can then be measured directly. Figure 1.8 shows a conceptual schematic of a bolometer device.

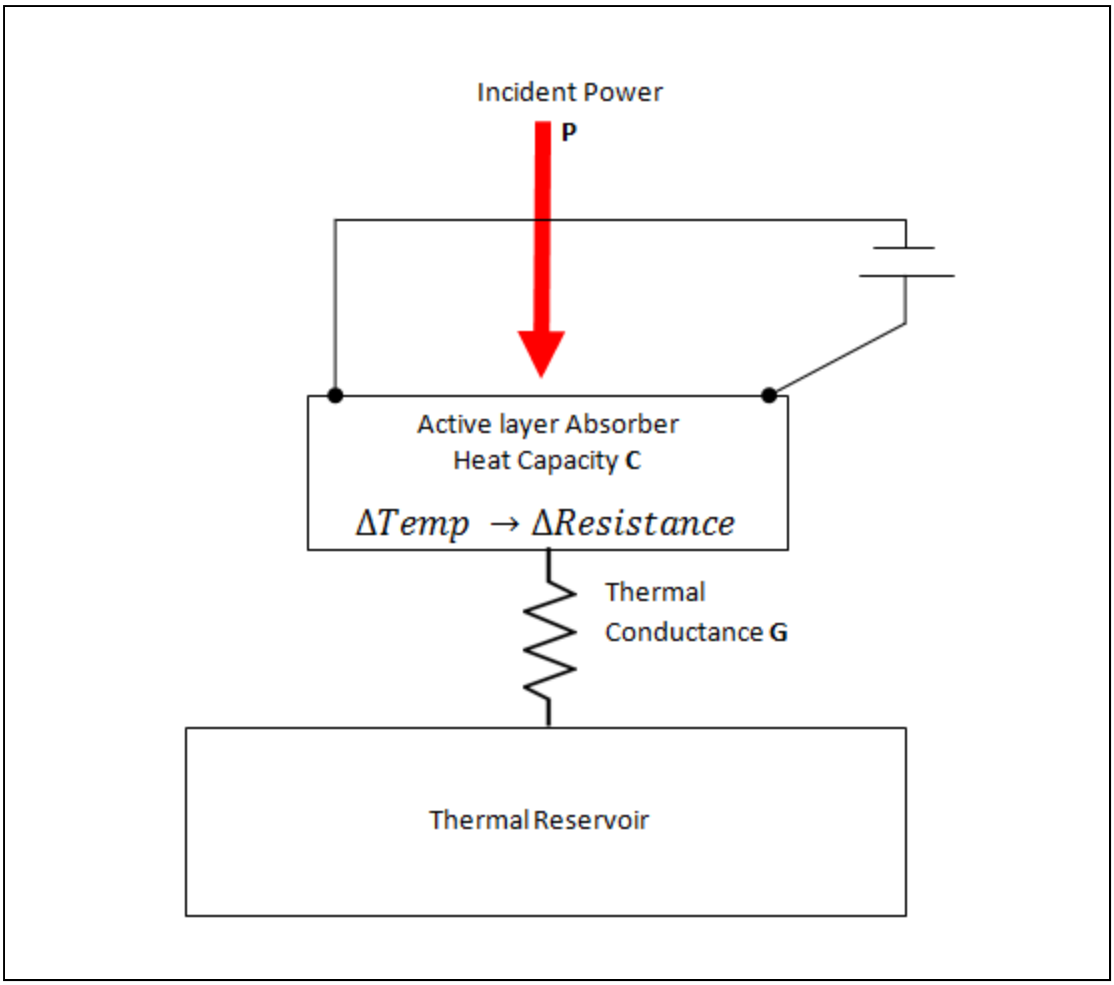

Figure 1.8 Conceptual schematic of a bolometer device. Active layer absorbs incident power P and heats up, ΔTemp = P/G. The active layer is connected to a thermal reservoir through a thermal conductance G

With the known temperature-dependent resistivity of the active bolometer layer, the thermal conductance and thermal impedance between the active layer and the thermal reservoir, the electrical responsivity of the device can be calculated with equation 1.6

$$S_r = I\frac{dR}{dT}\frac{dT}{dP} = \frac{\alpha(T)\,V}{G - \alpha(T)P_1}\left[\frac{V}{W}\right] \tag{1.6}$$

Where S_r = electrical responsivity, I = bias current, $\frac{dR}{dT}$ = change in resistance with temperature, $\frac{dT}{dP}$ = thermal impedance, $\alpha(T)$ = temperature coefficient of resistance, G = thermal conductance, P_1 = constant power of light source, V = bias voltage.

The response time or sampling frequency is an important property of any light sensitive devices, this is still true of bolometers. The response time of bolometer is based on the intrinsic thermal time constant which is equal to the ratio of the heat capacity of the active layer to the thermal conductance between it and the thermal reservoir. This is shown in equation 1.7.

$$\tau = \frac{C}{G}[s^{-1}] \tag{1.7}$$

Where τ = intrinsic thermal time constant, C = heat capacity of active layer and G is the thermal conductance between the active layer and the thermal reservoir.

1.2.2 Current Bolometer Technologies

The first bolometer designs consisted generally of a metallic active layer operated at room temperature. These designs have evolved over time, the metallic active layer is now mainly replaced with semiconductors or superconductor absorptive materials and many devices are operated at cryogenic temperatures to improve their sensitivity and response time (Coron, 1976). The active layers of most current bolometer technologies are more often than not suspended membranes, a thermal reservoir is thus created from the spaces surrounding the suspended membranes (Yoneoka et. al., 2011).

Most of the current bolometer technologies use germanium-based materials, such as doped crystalline germanium and diamond-germanium composites, as their active layer (Draine et. al., 1976). Germanium-based materials generally offer good absorbance in the infrared part

of the spectrum, relatively high heat capacities and low thermal conductivity between it and the thermal reservoir. (Low, 1961) (Draine et. al., 1976)

Recently, graphene is starting to gain interest as an active layer material in bolometers due to its particular electronic and transport properties (Hancock, 2011). Figure 1.9 shows the typical structure of a suspended microbolometer, this particular microbolometer's active layer is made up of two thin metal layers; an absorber and a thermistor.

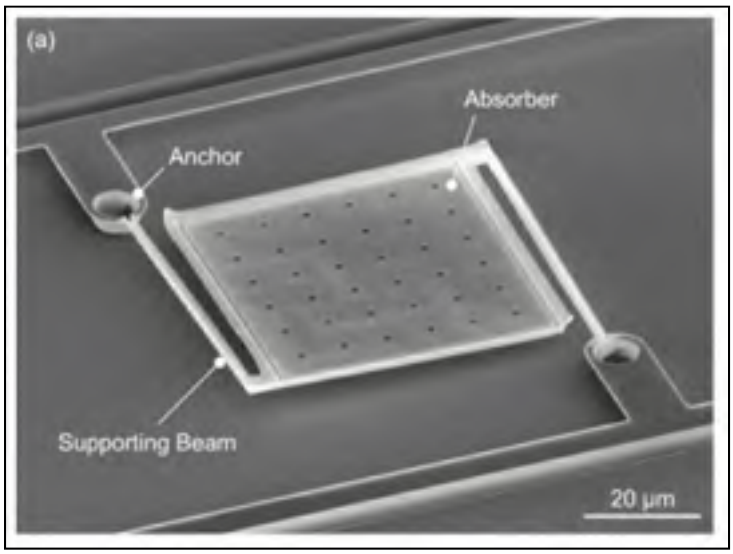

Figure 1.9 Microbolometer, suspended membrane made from two thin metal layers (absorber and thermistor) Taken from Yoneoka et. al. (2011)

1.3 Photoconductive Switches

Photoconductive switches are electrical switches which are based on the photoconductivity of an active material. This active material's electrical conductance increases as a function of incident light, much like a bolometer but without relying on heating effects. Generally photoconductive switches use semiconductors for the active layer, where light of energy greater than the semiconductor's bandgap is absorbed and generates free charge carriers. Since graphene is a zero bandgap semiconductor, it follows that there is no lower limit on the

photon energy capable of creating free charged carriers. Thus photoconductive switches that use graphene as an active layer should be sensitive to the whole electromagnetic spectrum.

1.3.1 A Theoretical Review Of Photoconductive Switches

As stated before, photoconductive switches rely on the photoconductivity properties of a semiconductor material. Photoconductivity is an opto-electronic phenomenon in which a material becomes more electrically conductive as a result of electromagnetic radiation absorption. When electromagnetic radiation of energy greater than the bandgap of said semiconductor is absorbed, the energy is enough to excite valence electrons to the conduction band thus increasing the number of free charge carriers and the overall electrical conductance of said semiconductor. If a voltage bias and a load resistor are added in series with a photoconductive material, a drop in voltage across the load resistor can be measured as an increase in current through the circuit is generated from the increase in electrical conductivity of the photoconductive material. A sketch of this basic photoconductive switch is presented in figure 1.10.

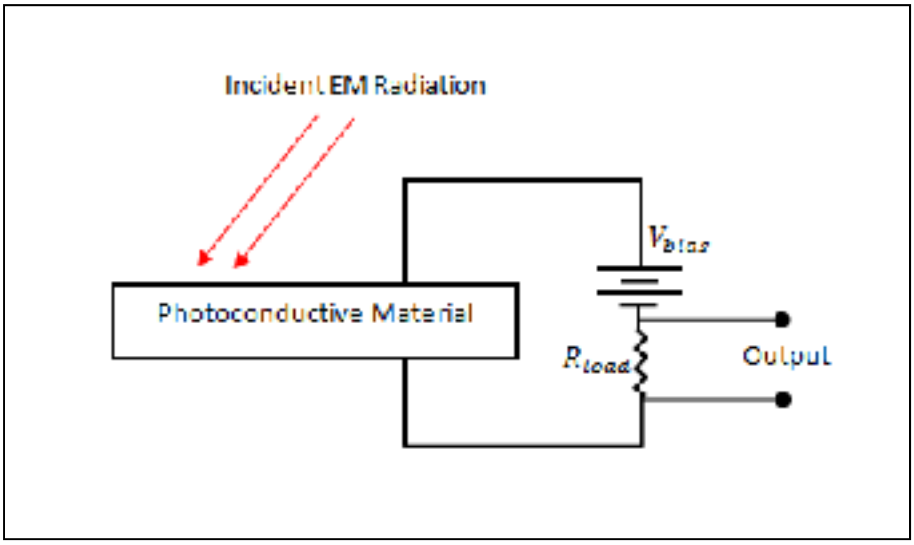

Figure 1.10 Sketch of photoconductive switch circuit design

When photoconductive materials are subject to cycles of light illumination, the current passing through them can be measured directly, the "switching" behaviour becomes apparent. A sketch of a typical response to cycles of light illumination is shown in figure 1.11. From the incident light cycling response, the sampling frequency can be calculated from the measured response and relaxation time. This relation is shown in equation 1.8, where τ is the sampling frequency in hertz, Δt_1 is the response time in seconds and Δt_2 is the relaxation time also in seconds.

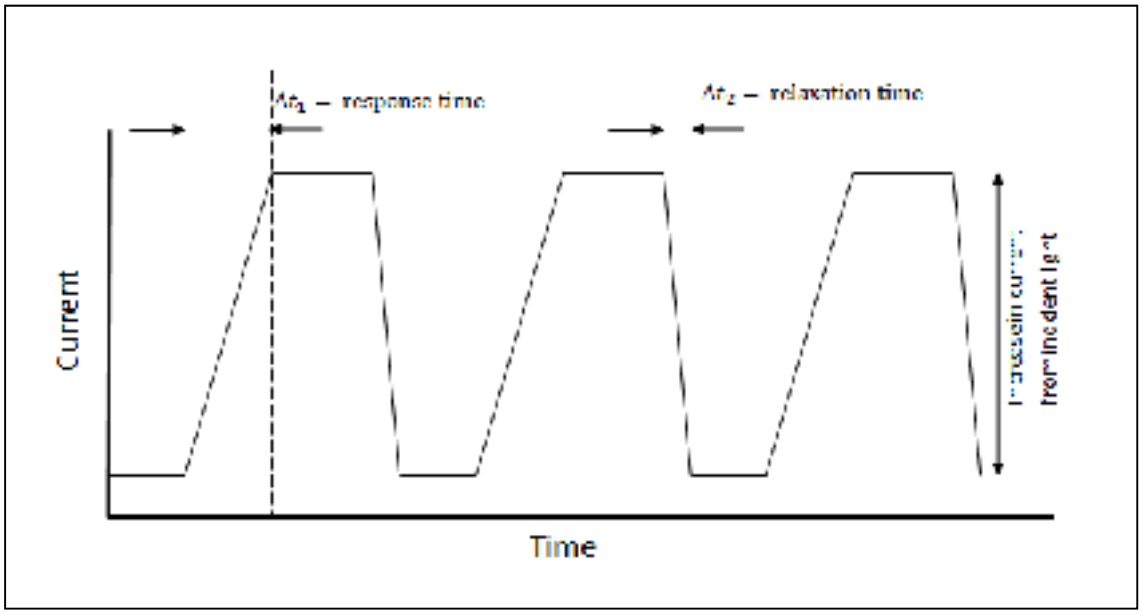

Figure 1.11 Sketch of typical photoconductive response to incident light cycling

$$\tau = \frac{1}{\Delta t_1 + \Delta t_2}[hz] \tag{1.8}$$

1.3.2 Current Photoconductive Switch Technologies

There exists different designs of photoconductive switches for different applications, all of these designs are generally of the metal-semiconductor-metal type. High voltage photoconductive switches are generally large devices, up to centimetres in length, with

electrical contacts on the end faces. For low power and high sampling frequencies, the devices are created with a small gap, a few microns in size, in a microstrip. For the highest sampling frequencies, sliding contact devices are created, where a point between the two parallel strips of a coplanar stripline is illuminated. These devices span a large range of applications, from generation of electrical terahertz pulses (Krokel et. al., 1989) (Smith et. al., 1989) to high-speed photodetectors in optical fiber communications (Kotaki et. al., 1987) and ultra-fast analog-to-digital converters (Miller, 2001). Figure 1.12 shows a schematic diagram and the operation concept of photoconductive terahertz emitters conceived by C.W. Berry and his team in 2013.

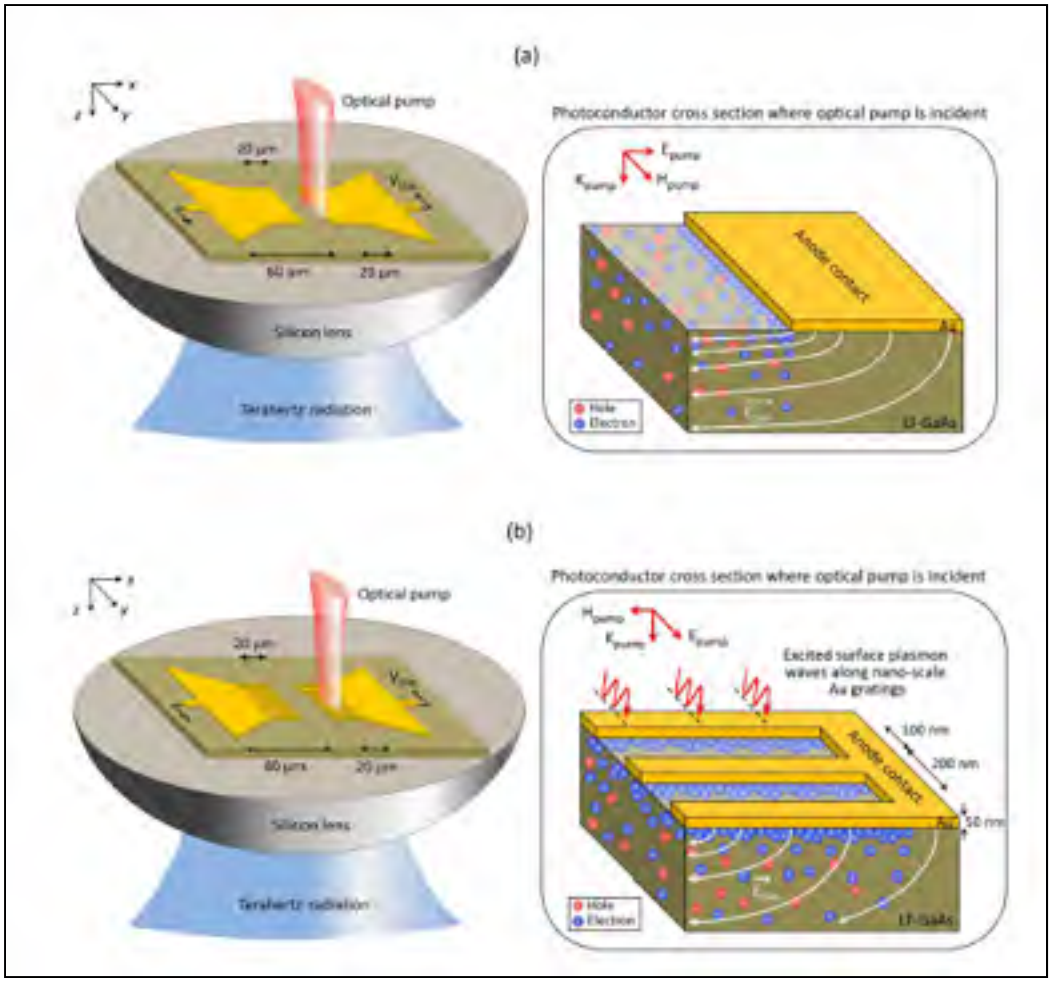

Figure 1.12 Schematic diagram and operation concept of photoconductive terahertz emitters
Taken from Berry et. al. (2013)

1.4 Graphene Optoelectronic Device Design

The aim of this work is to demonstrate an optoelectronic device such as a bolometer or a photoconductive switch using directly deposited graphene sheets as the active layer. The design behind such a device is similar to current technologies, which includes a suspended membrane as the active layer a thermal reservoir and contacts. By patterning "hole" features into the deposition substrate, it is possible to create thermal reservoirs which can then be covered by a deposited graphene sheet thus creating a suspended active layer membrane. Contacts can then be added and connected in a circuit with the other micro-devices in an array. Figure 1.13 illustrates the simple single photoconductive switch design, the choice of a base Si/SiO2 substrate comes from the availability and cost of such material but could be replaced by another material. This design is somewhat rudimentary, however it offers a basic stepping stone to further works on graphene-based bolometers and/or photoconductive switch. Figure 1.14 shows the design of the micro-devices acting as pixels as part of the whole array.

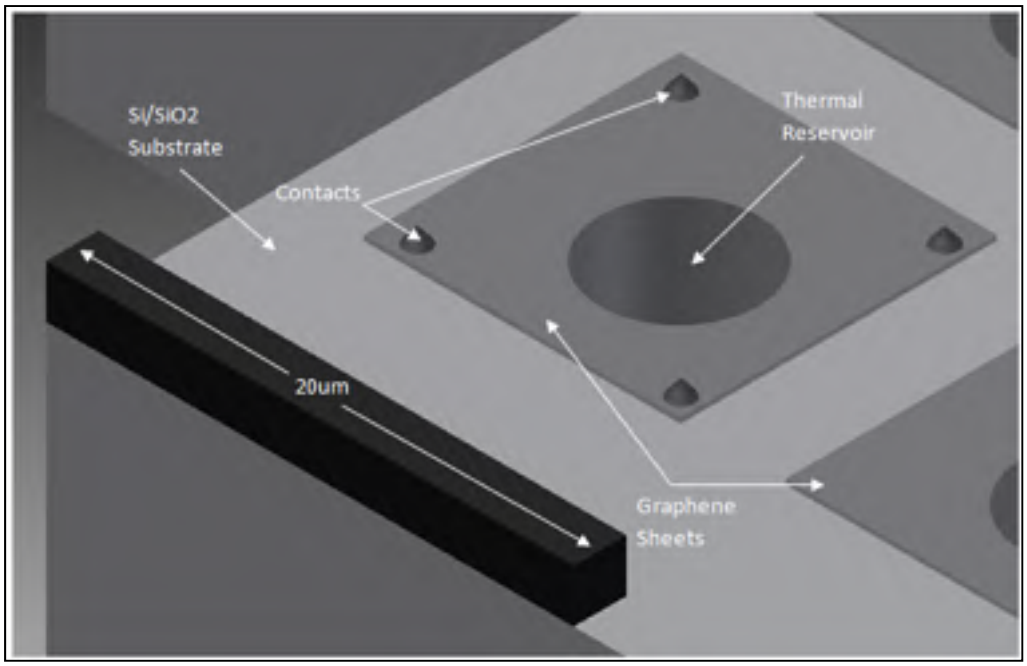

Figure 1.13 Graphene bolometer/photoconductive switch design, showing active layer graphene sheet, thermal reservoir and contacts

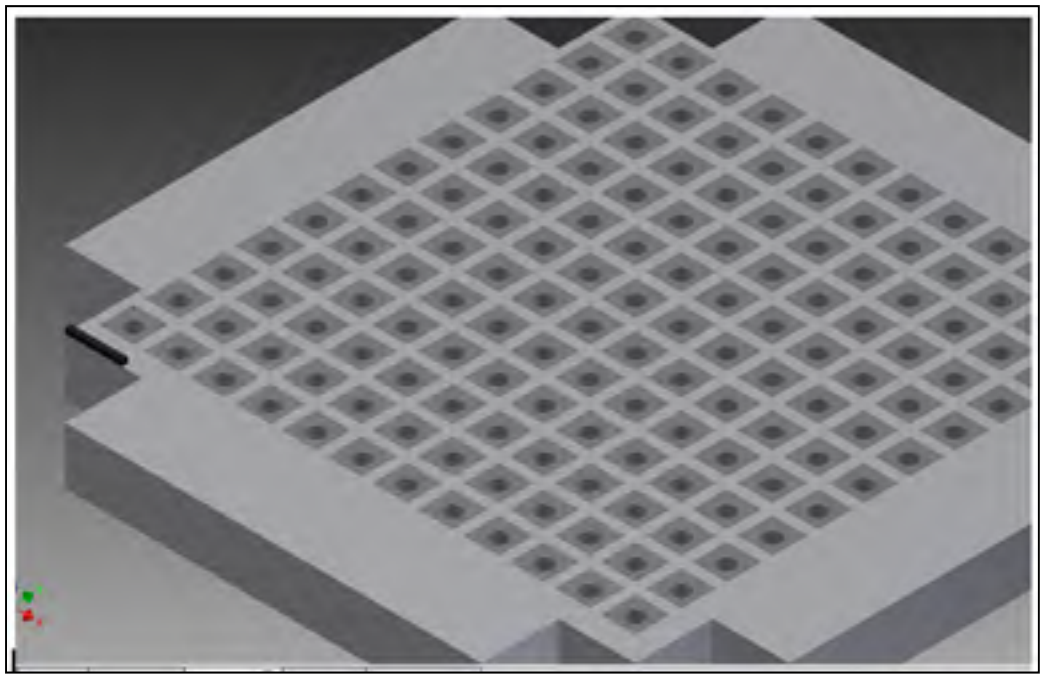

Figure 1.14 Graphene microbolometer/micro-photoconductive switch array design

CHAPTER 2

LITERATURE REVIEW OF GRAPHENE DEPOSITION AND CHARACTERISATION METHODS

2.1 Literature Review: Graphene Deposition

Different methods of graphene deposition have been developed over time by researchers. These different methods of deposition each offer their advantages and drawbacks, some methods allow for deposition on any substrate while others only permit deposition on electrical insulators or metallic surfaces. Another parameter that depends on the method of deposition chosen is the amount of time needed for the deposition of graphene, this vary hugely from minutes to days. The cost of materials and apparatus needed for the deposition is another factor in choosing which method of deposition is ideal for certain projects. These methods also differ with regards to the size of the deposition area of graphene and the precision at which it can be deposited. It is important to note that the precision at which graphene can be deposited refers to both the spatial precision of deposition and also the precision of the number of graphene layer deposited. In the first parts of this chapter, the three most popular methods of graphene deposition will be analysed in detail, their advantages and drawbacks will be evaluated, and possible improvements of the methods will be discussed.

2.1.1 Chemical Vapour Deposition

Chemical vapour deposition or CVD has become one of if not the most popular deposition method for graphene (Hancock, 2011) (Pollard, 2011). Although it is called a deposition method, in CVD the graphene is more grown then deposited. This method of deposition is perhaps the most precise method of deposition, although the most strenuous method as it takes the longest time and is possibly the most expensive method to deposit graphene on a chosen substrate.

In this subsection, the CVD method of graphene deposition will be analysed in detail, a complete methodology of this deposition method will be explained, and conclusions will be drawn in relation to the project presented in this work.

2.1.1.1 General Theory of CVD

In the CVD process, carbon atoms are made to adhere to the surface of a metal substrate in a controlled environment (Pollard, 2011) (Obraztsov, 2009). Other carbon atoms then follow but are pushed to the sides of first atoms thus creating a one atom thick layer of carbon, this carbon layer is then crystallised into graphene by reducing the temperature of the controlled environment (Pollard, 2011)(Obraztsov, 2009). As the graphene grows from nucleation points in the lattice, eventually they will come into contact with the graphene grown from neighbouring nucleation points and thus will create boundaries between each region as their lattice orientation will inevitably differ (Pollard, 2011)(Yu, et. al., 2011). The growth of the graphene lattices will come to a stop when each region grown from nucleation points will be surrounded by the boundaries at which point they are called domains (Pollard, 2011)(Yu, et. al., 2011). The domain boundaries can be represented as defects in the complete graphene layer as the bond between the carbon atoms at such a boundary does not follow the Bravais lattice structure present in the bulk of the domains (Pollard, 2011)(Yu, et. al., 2011).

These defects are of great importance on the quality of the final graphene layer since they act as barriers for charge transport (Yu, et. al., 2011) and thus negatively affect the electrical properties of the graphene which have been discussed sub-chapter 1.1.1 of this work. Therefore, it is important to try and minimize the number of boundaries and to maximize the size of the domains.

2.1.1.2 Methodology

For CVD, a metal substrate such as copper is chosen as the deposition medium. Annealing the metal substrate is an important first step to increase the domain size of the deposited graphene. This is done by heating the metal in a furnace to around 1000°C under low vacuum (Pollard, 2011) (Obraztsov, 2009). For the deposition of the carbon atoms on the metal substrate, methane and hydrogen gases are flowed through the furnace while it is kept at the annealing temperature (Pollard, 2011) (Obraztsov, 2009). The hydrogen molecules catalyses a chemical reaction between the surface of the metal substrate and the methane molecules, resulting in the deposition of the carbon atom from the methane onto the surface of the substrate (Pollard, 2011). Due to this reaction with the surface of the substrate, the carbon atoms are deposited as a one atom thick layer on the surface (Pollard, 2011) (Yu, et. al., 2011). The diagram in figure 2.1 illustrates the deposition of carbon atoms onto a copper substrate. The furnace is then cooled rapidly to crystallise the carbon atoms into a contiguous graphene layer (Pollard, 2011) (Obraztsov, 2009). This rapid cooling also decreases the density of nucleation points and thus minimizes the defects due to domain boundaries (Pollard, 2011) (Yu, et. al., 2011). If the furnace is cooled too slowly, the layer of carbon can also aggregate into graphite (Pollard, 2011).

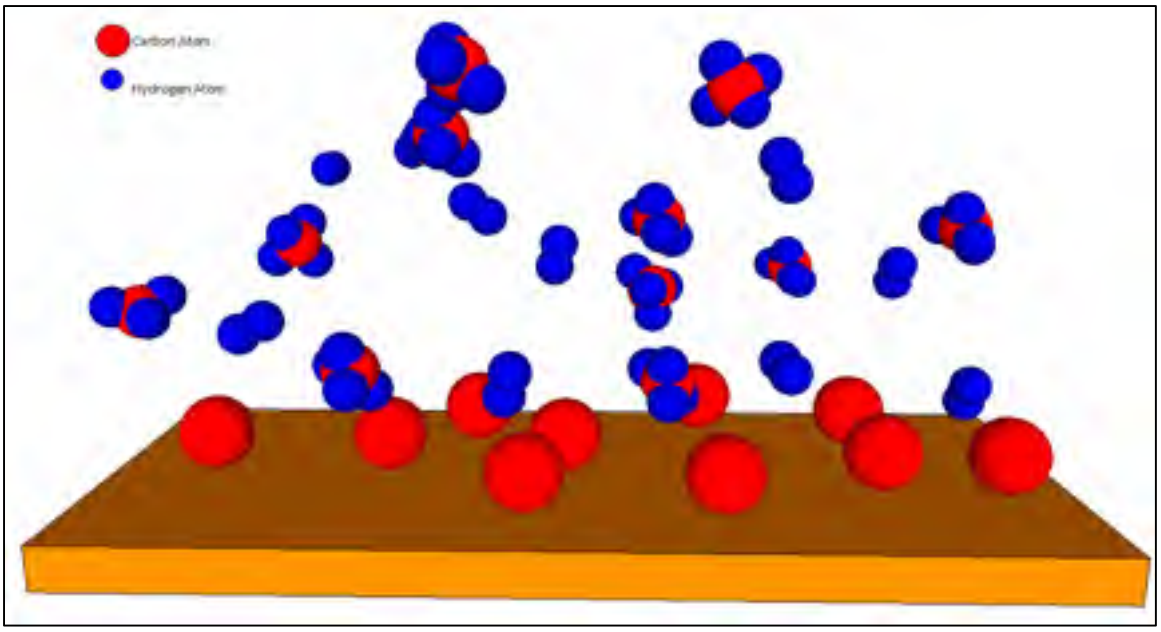

Figure 2.1 Diagram showing CVD growth of graphene on copper substrate

During the CVD process impurities can be introduced at many levels and can find their way into the final graphene layer. This introduction of impurities, be it from the substrate or the gases used in this method must be minimised or eliminated completely (Pollard, 2011) (Yu, et. al., 2011). Fortunately with experience, these impurities can be sufficiently minimised to create a graphene layer with a similar amount of impurities as exfoliated graphene flakes (Pollard, 2011). The difference between the thermal expansion between the graphene and the metal substrate can cause the graphene to wrinkle as it cools and crystallises (Kazi, et al., 2014). This effect can be minimised if proper annealing of the metal substrate is done (Kazi, et. al., 2014). Technically, this process of deposition can be used to create graphene sheets covering any sized substrate, however there are some limiting factors. One such factor is the size of furnaces available since the whole process needs to take place inside a furnace with a controlled environment (Pollard, 2011). Another limiting factor is the purity of the metal substrate used for the deposition since the metal needs to be perfectly smooth and devoid of defects to be able to create a single graphene sheet covering its entirety, these metal substrates can reach extremely high costs as their size increase.
(http://www.sigmaaldrich.com//materials-science/material-science-products.html?TablePage=108832768, visited August 2015)

2.1.1.3 Set-up and Materials

A simplified set-up of the apparatus needed to perform CVD is shown in figure 2.2. It includes a furnace and a quartz tube to provide the annealing for the metal substrate and the high temperatures needed for the process, a methane and a hydrogen gas line intake to the quartz tube to provide the gases needed for the deposition, an exhaust line to create the gas flow, a line to a vacuum pump to create the low vacuums needed for the metal substrate annealing and a crucible to hold the metal substrate inside the quartz tube and the furnace.

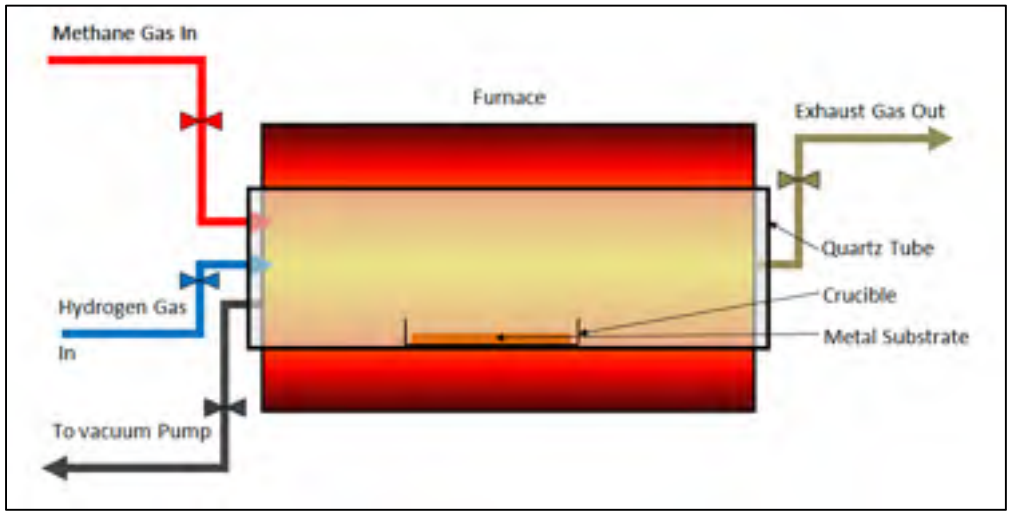

Figure 2.2 Diagram of furnace set-up for CVD

The flow rate of methane and hydrogen gas used in this method have an effect on the dynamics of the carbon deposition. An increase in methane provides more carbon atoms to be deposited and increases the number of nucleation points while an increase in hydrogen promotes the reaction between the methane and the surface of the metal substrate (Pollard, 2011).

Copper is only one of many metals that can be used as a deposition substrate, most transition metals can be used for such depositions. Other popular metals used in graphene CVD are cobalt and nickel (Pollard, 2011) (Kazi, et. al., 2014). Impurities and roughness of the substrate surface causes increases in the number of nucleation points and thus increases the defects due to graphene domain boundaries (Yu, et. al., 2011).

2.1.1.4 Transfer Process

Once the graphene is deposited on the metal substrate it can then be transferred to any other desired substrate, this transfer process can be used to create suspended devices. Starting with the metal substrate covered on both sides with deposited graphene, one side is spin coated with an Anisole-PMMA solution to create a protective layer. The graphene is then etched off the other side of the metal substrate generally using oxygen plasma. The metal substrate and deposited graphene are then placed, PMMA face up, on the surface of an etchant solution (depending on the metal substrate choice) such as Ferric-Chloride for copper. Once the metal substrate is etched completely, the membrane is then removed from the etchant solution and scooped into DI water multiple times to clean it. With the desired final substrate, the membrane is scooped out of the DI water, the device is then left to dry. The Anisol-PMMA thin film is then removed by soaking the dried device into Dichloromethane until the thin film is completely removed. The device is then rinsed with acetone and IPA to clean it once more. If suspended devices are desired, care must be taken during the drying processes, critical point drying must be performed to get the device out of any liquid. Critical point drying must be performed to avoid any damage and movement that would occur to the suspended graphene from removing it from a liquid solution (Pollard, 2011) (van der Zande et. al., 2010). This typical transfer process from a copper foil substrate to a final desired substrate is summarized in Table 1 with illustrated steps in Figure 2.3.

Table 2.1 Transfer process of deposited graphene from a copper foil substrate to final desired final substrate

Steps	Information
1	Copper with graphene deposited on both sides
2	Anisole-PMMA spin coated on one side to form protective layer
3	Etch graphene off PMMA-free side
4	Place copper-graphene-PMMA sample onto copper etchant solution
5	Let copper etch away completely
6	Scoop membrane and rinse in DI water
7	Scoop membrane out of DI water with desired final substrate
8	Let desired substrate and membrane dry
9	Remove PMMA with Dichloromethane solution
10	Rinse and clean with Acetone and IPA
Extra	Critical point drying for suspended devices

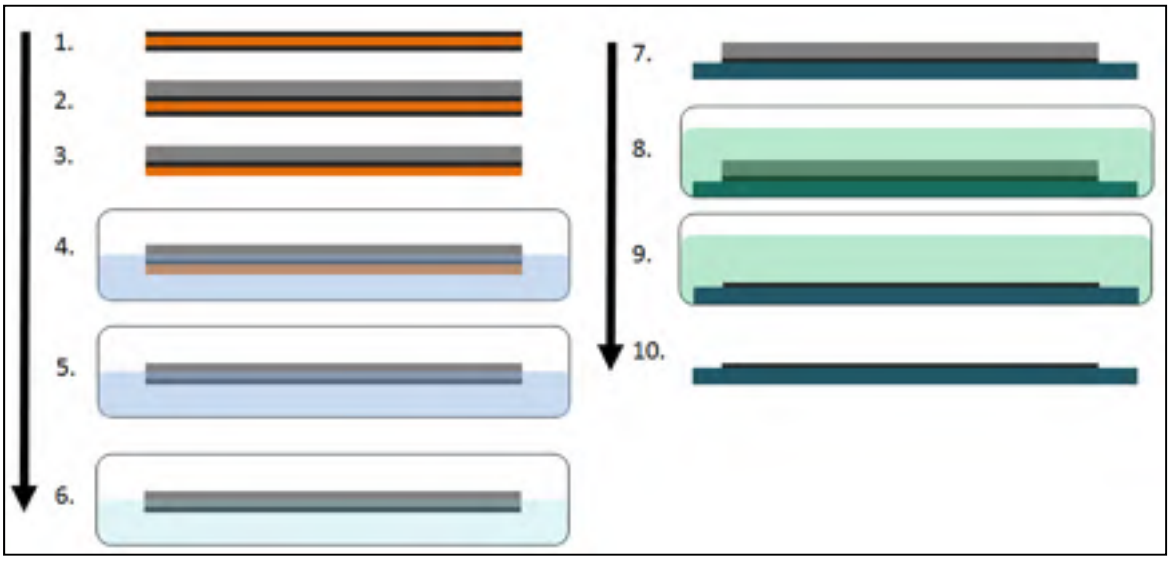

Figure 2.3 Schematic showing the steps in the transfer process of CVD graphene from a copper substrate to the desired substrate

2.1.1.5 Typical Results from CVD

As described above, the CVD of graphene along with the transfer process makes the creation of suspended graphene devices possible. In the following part of the chapter typical devices that can be created with this method will be examined along with their quality.

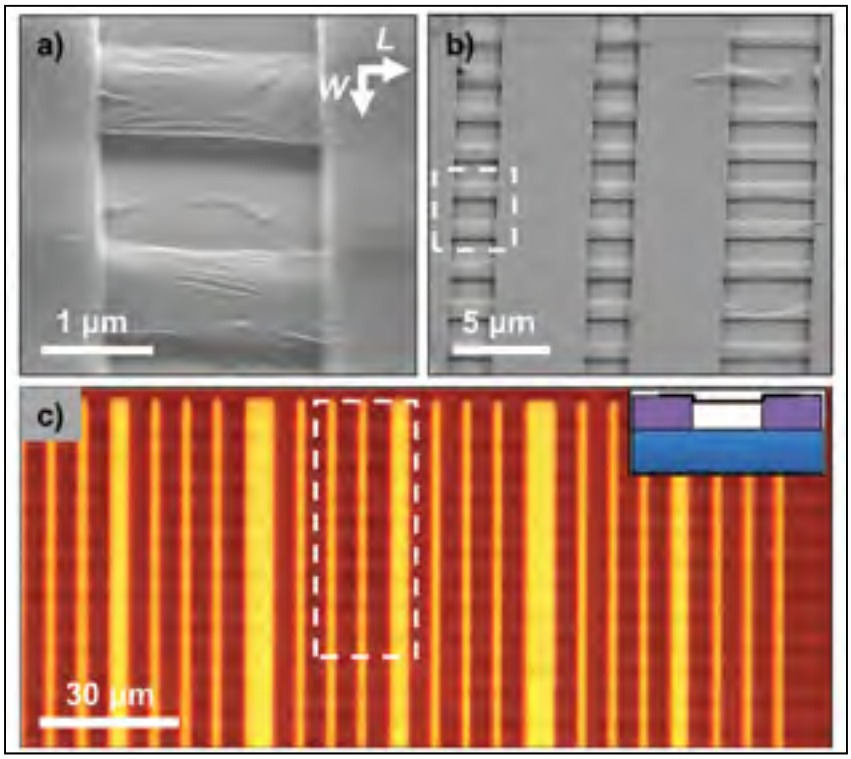

Figure 2.4 Suspended graphene resonators
Taken from van der Zande, et. al. (2010)

Figure 2.4 shows typical SEM images of suspended graphene ribbons over etched trenches, these were made by CVD of graphene onto copper and then transferred using critical point drying onto a pre-patterned silicon oxide substrate (van der Zande, et. al., 2010) . From Figure 2.4a) it can be seen that the graphene ribbons suspended over the 2um trenches show some deformation such as ripples (~10nm in amplitude) and some buckling of the ribbon (~100nm in amplitude) due to tension, shear and/or compression. The amount of deformations in this device varies between neighbouring suspended ribbons which signify that the tension, shear and compression in the graphene is somewhat variable. This variation is likely due to transfer process and/or the variable conditions of the CVD graphene prior to

the transfer. Moreover, for the longer suspended graphene ribbons, shown in Figure 2.4b), some large tears can be seen to occur in a few of the ribbons at mechanically weak grain boundaries inside the crystal matrix. Similar ripples and buckling to the short suspended graphene ribbons was also reported for the larger ribbons.

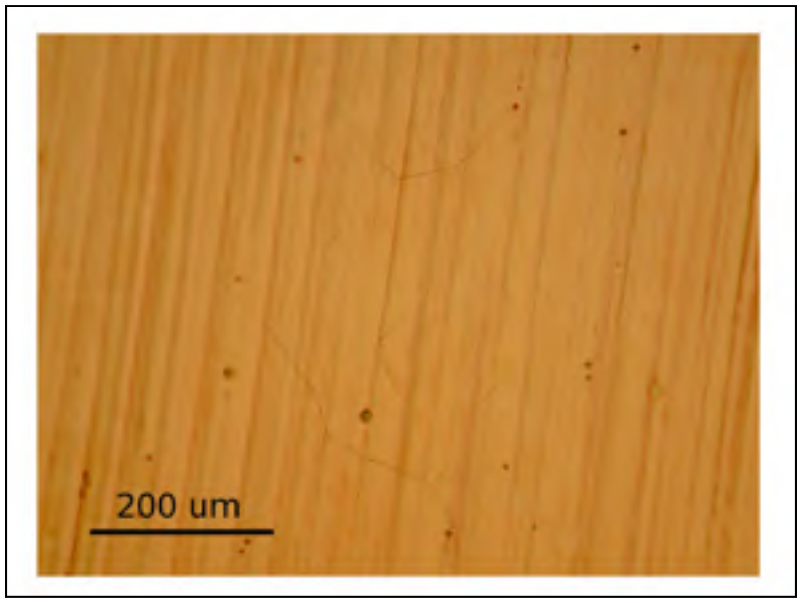

Figure 2.5 Optical microscope image of graphene on copper foil
Taken from Pollard (2011)

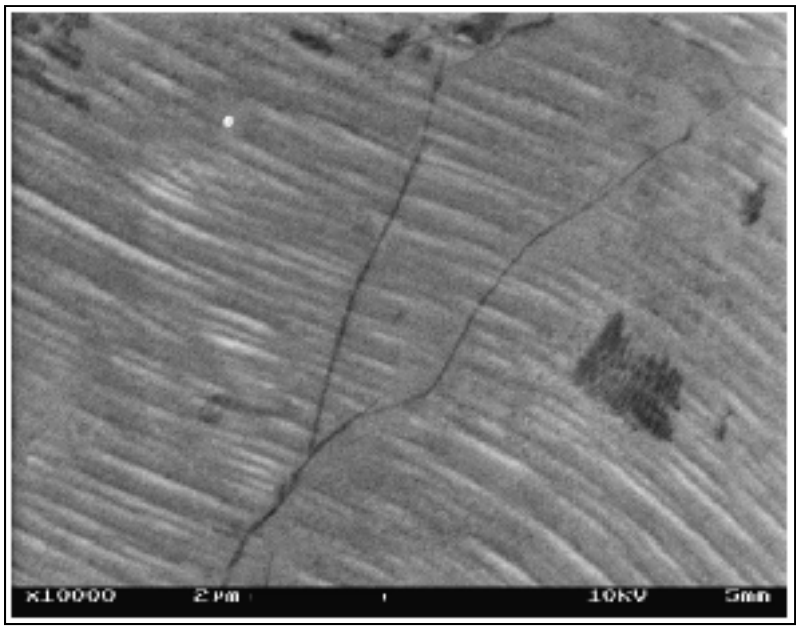

Figure 2.6 SEM image of graphene domains on copper
Taken from Pollard (2011)

Figure 2.5 shows an optical image of CVD graphene on a copper substrate (Pollard, 2011). It can be observed that the graphene is almost invisible, this is due to the graphene only absorbing ~2-4% of light per layer (Bonaccorso, et. al., 2010) and hence can barely be seen with the naked eye. Figure 2.6 shows an SEM image of the same CVD graphene on copper with a x10000 magnification to show the graphene domain boundaries (Pollar, 2011). The expected size of the graphene domains in CVD can vary extremely depending on many factors summarized in the sections above, these can range from less than a micron to a few hundred microns (Yu, et. al., 2011).

Figure 2.7 Microscope image of SiO2 wafer after graphene transfer
Taken from Pollard (2011)

Figure 2.7 shows a large CVD graphene membrane transferred onto a silicon oxide wafer (Pollard, 2011). Some complications occur when transferring such a large graphene membrane, as can be seen from the figure, the graphene membrane crumpled on itself in some places. This most likely occurred while removing the PMMA from the graphene membrane in dichloromethane.

2.1.2 Micro-Mechanical Deposition

Another method for creating graphene sheets and depositing them is the micro-mechanical deposition method (Jayasena, et. al., 2013) (Chun-hu, et. al., 2012). This method makes use of mechanical forces to separate graphene from a block of bulk HOPG, the sheets can then be manipulated using an AFM tip. Micro-mechanical deposition of graphene is not a popular method of deposition but still offers some advantages over other methods. The reproducibility of the quality, shape and size of the deposited graphene is one of the main

advantages (Chun-hu, et. al., 2012). However the manipulation of graphene once it has been deposited can be rather difficult and time consuming (Jayasena, et. al., 2013).

2.1.2.1 Micro-Mechanical Deposition Theory

The theory behind micro-mechanical deposition is straightforward, using mechanical forces to brake off single layers of graphene from an HOPG block (Jayasena, et. al., 2013) (Chun-hu et. al., 2012) (Xuekun et. al., 1999). One of these methods involves shaving off graphene sheets from the top of an HOPG block (Jayasena, et. al., 2013), as shown in figure 2.8. Another method involves using vibration forces between the HOPG block and the deposition substrate to remove the top layers of graphene from the HOPG block (Xuekun et. al., 1999), as shown in figure 2.9. The deposited graphene sheets can later be moved with care using an AFM tip (Xuekun et. al., 1999).

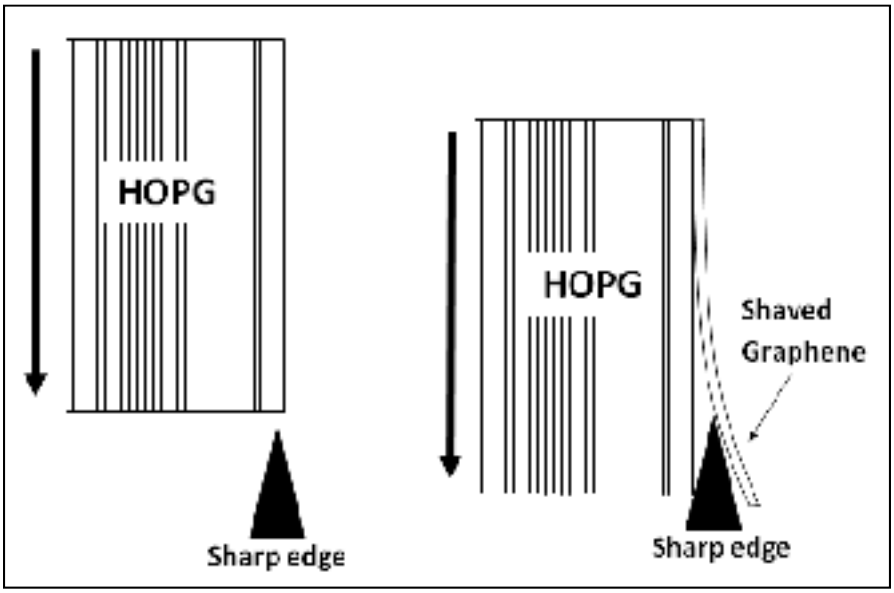

Figure 2.8 Graphene shaving from HOPG block.

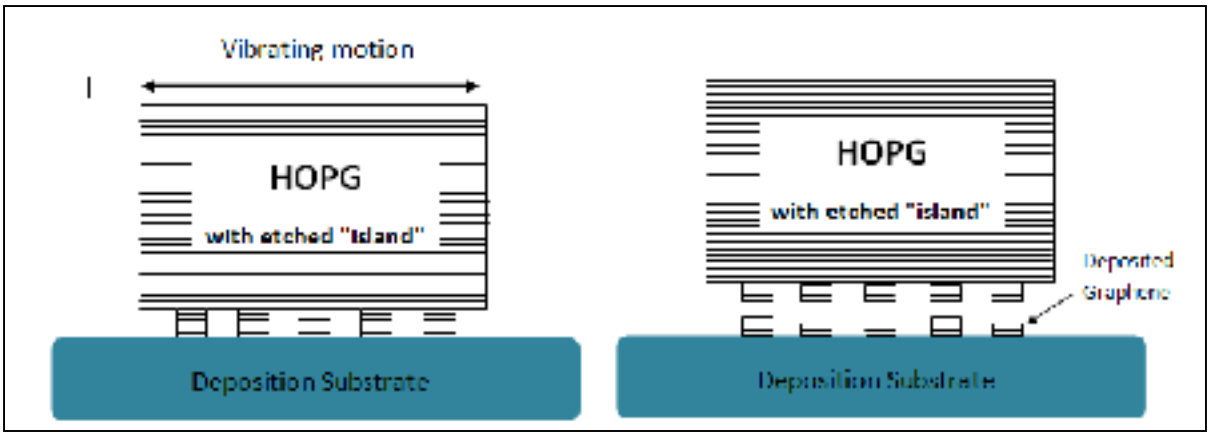

Figure 2.9 Depositing graphene using vibrations.

2.1.2.2 Methodology

This chapter will focus on micro-mechanical deposition of graphene from a patterned HOPG substrate. The first step is to pattern the HOPG substrate, this can be done using oxygen plasma (Pollar, 2011) (Xuekun, et. al., 1999). The HOPG is first cleaved using a razor blade to create ~1.5mm thick pieces of HOPG, a thin film of SiO2 is then deposited using plasma enhanced chemical deposition (Xuekun, et. al., 1999). The SiO2 layer is then patterned to create a negative mask for the patterning of the HOPG (Xuekun, et. al., 1999). Oxygen plasma is then used to etch the HOPG to create island on the surface of the cleaved pieces (Xuekun, et. al., 1999). The thin film of SiO2 is then removed with dilute HF (Xuekun, et. al., 1999). From here the islands can be manipulated directly with an AFM tip or deposited using mechanical vibrations onto the preferred substrate (Xuekun, et. al., 1999) (Chun-un, et. al., 2012), as shown in figure 2.9. Again, using an AFM tip the deposited graphene can then be manipulated to fabricate devices or structures (Xuekun, et. al., 1999).

2.1.2.3 Typical Results of Mirco-Mechanical Deposition

For the aforementioned method, the size and shape of the deposited graphene is very constant, whereas the number of graphene layers deposited varies depending on the amount of vibration force that was applied during the deposition (Xuekun, et. al., 1999) . As shown in figure 2.10, the size and size of each etched HOPG island is constant and forms a uniform array.

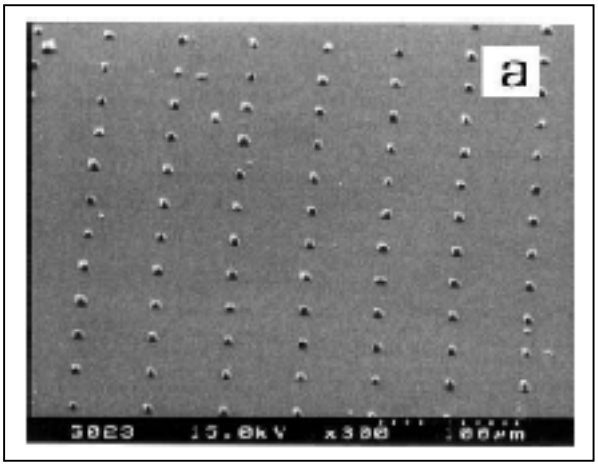

Figure 2.10 SEM image of the etched array of HOPG island
Taken from Xuekun, et. al. (1999)

The height of such islands can be controlled by controlling the parameters of the oxygen plasma etching (Xuekun, et. al., 1999). Figure 2.11 shows two different heights of HOPG island (b = 200nm & c = 9μm). The 200nm islands were found to be a good height for manipulation with an AFM tip (Xuekun, et. al., 1999). As can be seen from this image, the thicker islands have a larger base then tip size, this is due to the oxygen plasma etching (Xuekun, et. al., 1999).

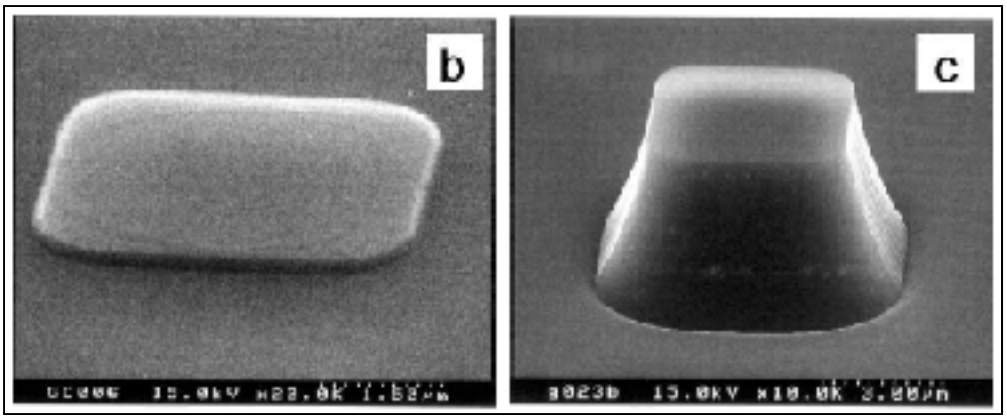

Figure 2.11 SEM image of HOPG islands of b) 200nm &
c) 9μm in height
Taken from Xuekun, et. al. (1999)

Figure 2.12 shows the results of the deposition process for 6 μm thick island (Xuekun, et. al., 1999). The size of each graphene sheet is rather constant, however some of the deposited graphene stayed in stacks (Figure 2.12a) while others were found to be fanned out into thinner sheets (Figure 2.12b) (Xuekun, et. al., 1999). Very thin layers of graphene up to single layers, where observed to be deposited in the fanned out depositions compared to the stacked depositions (Xuekun, et. al., 1999). The thinnest sheets of graphene deposited using this method were found in the more fanned out deposition which were observed to occur with increased "rubbing" between the HOPG and the SiO2 (Xuekun, et. al., 1999).

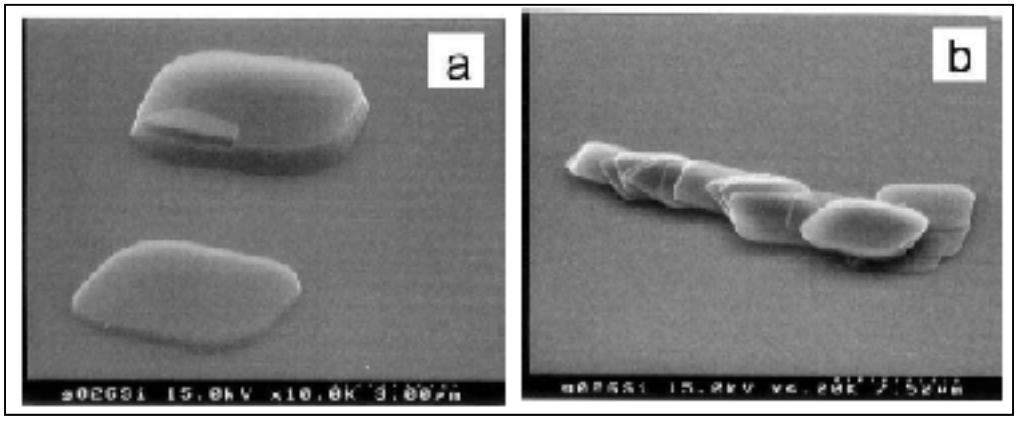

Figure 2.12 SEM image of deposited graphene sheets
Taken from Xuekun, et. al. (1999)

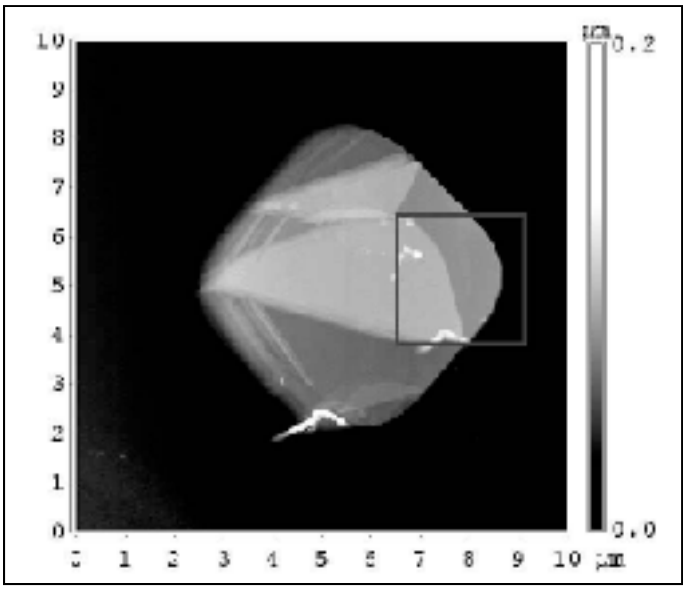

Figure 2.13 AFM tapping mode image of deposited graphene sheet
Taken from Xuekun, et. al. (1999)

Figure 2.13 shows the height profile of one such deposited graphene sheet using AFM tapping mode. The graphene sheet deposited in this image is rather thick (up to ~100nm) thus is in the order of 100 atomic layers, with some of the layers folding back on themselves (Xuekun, et. al., 1999).

2.1.3 Electrostatic Deposition

The electrostatic deposition of graphene, much like the micro-mechanical deposition method, is another method of removing graphene from a bulk graphitic material to a desired substrate (Sidorov, et. al., 2007) (Sidorov, 2009). This method of deposition makes use of electrical charges and fields to separate the gaphene and deposit it directly on the wanted substrate (Sidorov, 2009). This technique is not as popular as other techniques of graphene deposition since the size and quality of the deposited graphene is not as easily controllable as the other methods, especially the CVD method with better spatial selectivity (Sidorov, 2009) (Pollard 2011). Although this method has some drawbacks it is not without advantages, the electrostatic deposition of graphene offers what is probably the cheapest and fastest way to

deposit graphene (Sidorov, 2009) (Geim, 2012). As an emerging technique, it also offers room for improving the technique to minimize any of the drawbacks associated with this method of deposition.

2.1.3.1 Electrostatic Deposition Theory

Electrostatic deposition of graphene uses electrical charges and fields to separate already loosened graphene from a bulk graphitic material such as HOPG (Sidorov, 2009). By applying a large electrical potential between two electrodes supporting a bulk graphitic material and an insulating deposition substrate, a large electrical field can be generated. The loose graphene sheets on the surface of the bulk graphitic material opposing the electrode becomes charged due to the applied electrical potential (Sidorov, et. al., 2007) (Sidorov, 2009). By bringing the bulk graphitic material with the charged loose graphene sheets into contact with the insulating deposition substrate, the charged loose graphene sheets separate from the bulk graphitic material due to the increased electrical field applying a force greater than the force of adhesion between the bulk graphitic material and the loose graphene sheets (Sidorov, 2009). A sketch of the interaction between the loosened graphene sheets and the deposition substrate is illustrated in figure 2.14. The separated charged graphene sheets are attracted to the grounded electrode and then adhere to the insulating deposition substrate, and thus are deposited. This process is shown in figure 2.15.

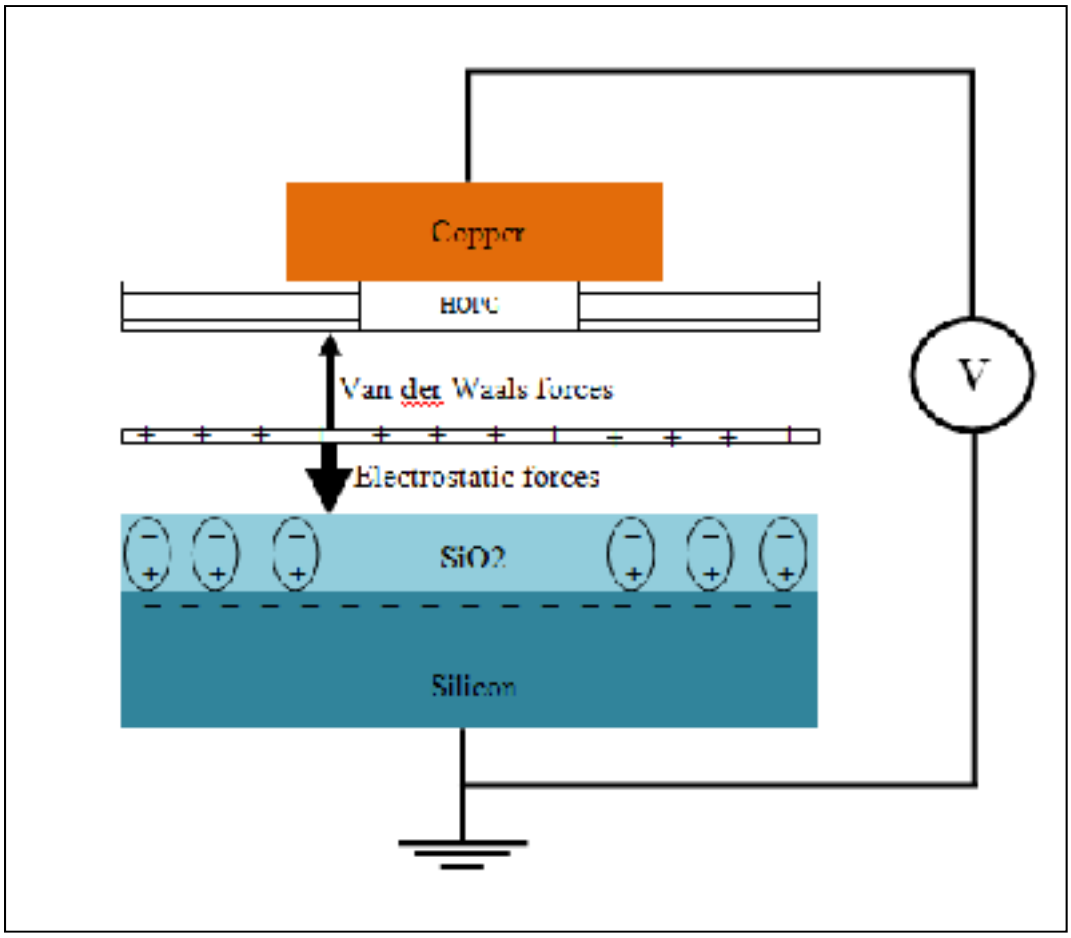

Figure 2.14 Sketch of the interactions between the loosened graphene sheets and the deposition substrate

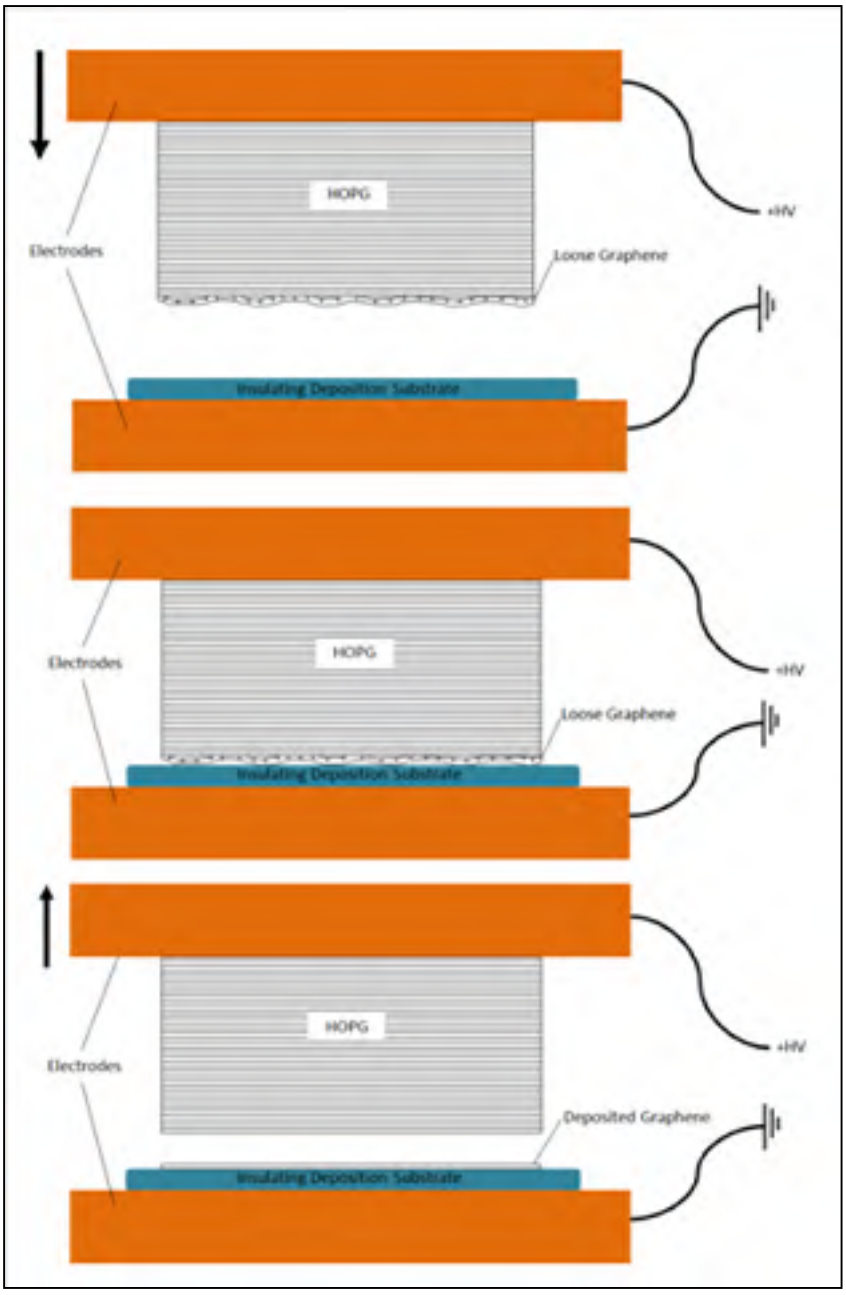

Figure 2.15 Electrostatic deposition of graphene from a bulk graphitic material to an insulating deposition substrate

Some of the limiting factors of this method can be seen straight away, one such limiting factor is the fact that the deposition substrate needs to be insulated from the grounded electrode otherwise the electrical field will vanish when the bulk graphitic material is brought into contact with the deposition substrate (Sidorov, 2009). If the wanted deposition substrate

is not an insulator, then an insulating material layer must be placed between the deposition substrate and the grounded electrode. This problem can also be counteracted by performing a first deposition onto an insulating material and then transferring the graphene onto the wanted final substrate much like for the CVD of graphene (Sidorov, 2009) (Pollard, 2011).

Another problem that occurs is with the amount of loose graphene present on the surface of the bulk graphitic material. The manipulation of such a material will inevitably create some loose graphene sheets on the surface. However upon the first deposition, these loose sheets will be deposited and only bulk graphitic material will be left. Therefore a method of loosening graphene sheets from the bulk material is needed. Thankfully such methods exists, any cleaving of the bulk graphitic material will create loose graphene sheets on the cleaved surfaces. For example, cleaving of a bulk graphitic material can be done with a razor blade or even with scotch tape (Sidorov, 2009) (Jayasena, et. al., 2013).

Another problem that can occur during the electrostatic deposition of graphene is electrical shorting between the bulk graphitic material and the grounded electrode. The electrical field due to the large electrical potential can be strong enough to ionise the surrounding air and thus create a path for the charge to follow. By performing the deposition inside of a nitrogen atmosphere, any shorting or arcing of the electrical current can be avoided (Sidorov, 2009).

Since the loosening process of the top graphene layer is somewhat unsystematic, the remaining adhesion forces between the loose graphene sheets and the bulk graphitic material can vary extremely (Sidorov, 2009) (Xuekun, et. al., 1999) (Jayasena, et. al., 2013). Therefore, a theoretical calculation of the electrical potential needed to deposit such sheets would be futile and an experimental approach is needed.

2.1.3.2 Methodology and materials

The electrostatic deposition of graphene can done from any bulk graphitic material, there are many such materials that can be used. Kish graphite and single crystal natural graphite are

materials that can be used for this deposition method (Sidorov, et. al., 2007) (Sidorov, 2009) (Geim, 2012). However, one bulk graphitic material stands out above the rest, highly oriented pyrolytic graphite or HOPG (Sidorov, 2009). HOPG is formed of compacted graphene layers with a common stacking axis but with a varying in-plane orientations (http://www.2spi.com/catalog/new/hopgsub.php, visited 5th June 2013). The common stacking axis of HOPG makes it the perfect material for electrostatic deposition, since it stabilises the loosening process of the top graphene layers and makes the deposition of a wanted number of layers more feasible and less of a random process (Sidorov, 2009).

One side of the HOPG is cleaved to loosen the top graphene layers from the bulk, the "scotch-tape" method is preferred for its simplicity and repeatability (Sidorov, 2009). This method consists of applying a piece of household adhesive tape to one side of the HOPG. Any air pockets between the tape and the HOPG are removed by flattening the tape with plastic tweezers, creating a more uniform adhesion between the two. The tape is then peeled from one side effectively cleaving the HOPG by removing top graphene layers (Sidorov, 2009). Even with the precautions taken, the cleaved graphene layers are removed inhomogeneously causing some of the remaining graphene on the HOPG to dislocate both vertically and laterally, thus creating the loose graphene sheets which are needed for the electrostatic deposition to work (Sidorov, 2009). Such cleaving needs to be done systematically before the deposition process.

The other side of the HOPG is then attached to a small copper electrode, silver epoxy or another conducting adhesive is used. This electrode is connected to the positive terminal of a high voltage source. The second electrode which is connected to the ground terminal of the high voltage source and will host the deposition substrate. Therefore, it needs to be large enough to stage such a substrate, a copper plate of dimensions larger than the deposition substrate is needed. An insulating layer is also needed to create a charge barrier between the grounded electrode and the deposition substrate (Sidorov, 2009). Mica sheets can be used as this insulating layer which also reduces the possibility of voltage breakdown between the two electrodes. The deposition substrate is then placed on top of the mica sheet.

The bulk graphitic material is then brought into contact with the deposition substrate for a couple of seconds while the electrical potential is applied. The loose graphene sheets on the surface are separated from the bulk graphitic material and deposited onto the deposition substrate (Sidorov, 2009). The electrical potential needed to deposit a wanted number of graphene layers vary depending on the deposition substrate, the size of the electrodes and the thickness of the insulating mica sheets (Sidorov, 2009). A potential of 1-10 kV is generally needed to deposit up to ~10 layers of graphene, with lower potentials depositing less layers (Sidorov, 2009). Potentials as low as 50V have been reported for single layered graphene on very thin substrates (~250nm) (Sidorov, 2009).

2.1.3.3 Typical Results from Electrostatic Deposition

Since electrostatic deposition of graphene relies heavily on the inhomogeneous loosening of top graphene layers from bulk graphitic material, it is expected that the resulting deposited graphene will also be inhomogeneous in size, number of layers deposited and in quality. Figures 2.16 and 2.17 show typical electrostatically deposited graphene with a deposition voltage of 5kV on SiO2 substrate (Sidorov, et. al., 2007).

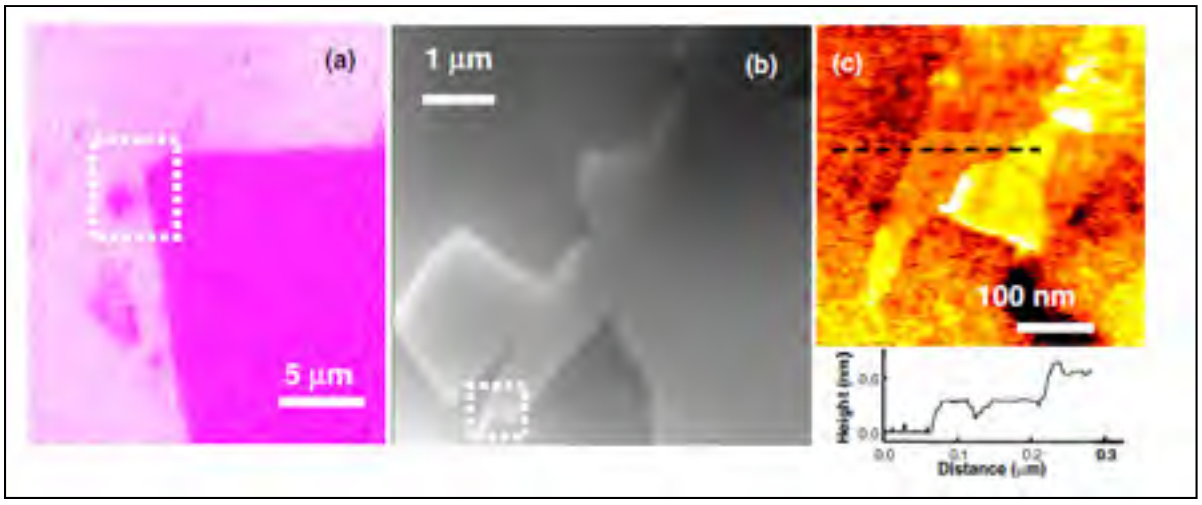

Figure 2.16 Optical (a), SEM (b) and AFM (c) images of a graphene sheet produced by electrostatic transfer. A SEM image of the region depicted by the dashed box in (a) is shown in (b). The dashed box in (b) corresponds to the AFM image and the line scan shown in (c) Adapted from Sidorov et. al. (2007)

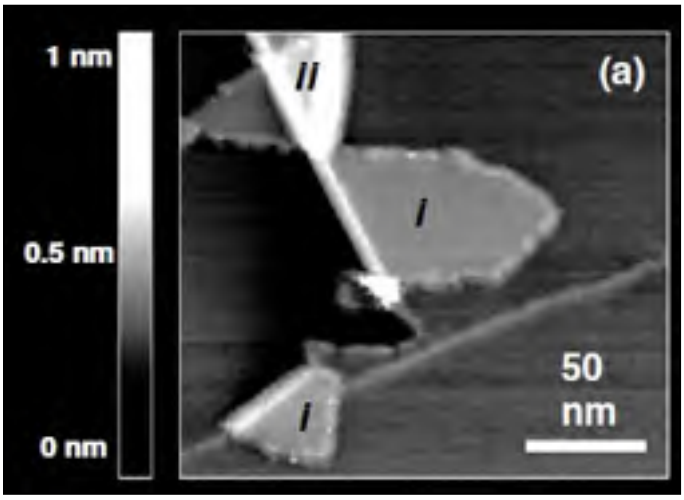

Figure 2.17 Scanning tunnelling microscope images of (a) single (i) and double (ii) folded graphene Adapted from Sidorov, et. al. (2007)

Figure 2.17 shows an optical, SEM and AFM images of the deposited graphene. It can be observed from these images that the deposited graphene varies in the number of layers, where some regions are single layered, others double and even triple layered graphene (Sidorov, et. al., 2007). Figure 2.18 shows a scanning tunnelling microscope image. This image also shows the variation in the number of graphene layers deposited (Sidorov, et. al.,

2007). It can also be observed in these two figures that the shape of the deposited graphene is rather irregular. The height profile in Figure 2.17c) shows some irregularities in the thickness of the graphene sheets, this can be linked to small tears or breaks within the graphene lattice due to the inhomogeneous cleaving process (Sidorov, et. al., 2007).

2.1.4 Comparison of the different methods of deposition

In this chapter, three different methods of graphene deposition have been summarised, each with its own advantages and shortcomings. These points will be put into context and made evident in this section.

Chemical vapour deposition is by far the best method of deposition if the quality of the final deposited graphene is the only criteria looked at. This method offers precise control of the number of layers of graphene deposited with a good control of the size of the graphene domains and thus the quality of the graphene. In CVD, the size of the final graphene sheets is controllable via oxygen plasma etching and the fabrication of devices and suspended devices is possible via a transfer process. This means that for now, CVD offers the best possible graphene for the fabrication of devices. The drawbacks of CVD are not in terms of the final graphene product but in terms of the time and equipment needed to perform these deposition. CVD is the most time consuming of the three methods of deposition, even more so if the transfer process is needed to fabricate devices. This means that CVD is a great method for laboratory experiments but is not suitable for large scale industrial device fabrication.

Micro-mechanical deposition on the other hand, offers a mid quality but somewhat homogeneous final deposited graphene. The size of the deposited graphene can also be controlled with etching of the HOPG before deposition. The major drawback with this method is the lack of control of the number of layers of graphene deposited. The fabrication of devices also requires the manipulation of the graphene after being deposited, this is another time consuming step that needs high precision and training. Therefore this method is also unsuitable for large scale industrial device fabrication. The vibration forces involved in

this deposition method make it unsuitable for direct deposition for most device fabrication as it would possibly cause damage to the final devices.

The short deposition time and the simplicity of the equipment needed for electrostatic deposition are the primary advantages of this method. However, the shape, size and number of layers deposited is not easily controlled currently with this method when compared to other methods. This means that device fabrication with deposited graphene via electrostatic forces is not yet up to par with other methods of deposition. Electrostatic deposition is one of the least studied methods of deposition for graphene presently and therefore could offer room for improvement to make it suitable for large scale industrial device fabrication.

2.2 Literature Review: Graphene Characterisation

The characterisation of graphene optoelectronic properties and graphene layer morphology are important to evaluate the quality of deposited graphene sheets for their use in any device architecture. Graphene layer characterisation methods have been developed since the first single layered graphene sheets were produced. In this chapter, four methods of graphene layer characterisation will be analyzed, these methods include; AFM thickness measurements, SEM characterisation, optical layer counting and Raman spectroscopy. Generally two or more of these methods are used simultaneously to give a more accurate characterisation of the number of layers. (Sidorov, 2009) (Hidefumi et. al., 2010) In this work, it is proposed to improve on one of these methods to develop a quick and accurate characterisation method for the number of graphene layers present in the deposited sheets. The optoelectronic, mainly the calorimetric properties of the deposited graphene will also be evaluated. These properties are important to evaluate the response of optoelectronic devices based on the deposited graphene.

2.2.1 Methods of Layer Characterisation

There are four main methods of graphene layer characterisation currently used in the world of graphene deposition. The first is the AFM (atomic force microscopy) measurements, to directly probe the thickness of the deposited graphene with atomic-level resolution. This method is time consuming and requires expensive instrumentation (Sidorov et. al., 2007). Another method is the SEM (scanning electron microscopy) image brightness measurements which differentiate the number of layers via charge accumulation on the surface of different number of graphene layers. This method is a very indirect and can be difficult to performed with an insulating deposition substrate such as SiO2 (Hidefumi et. al., 2010). Then there is optical characterisation, this is a very basic qualitative method of characterisation, it relies on counting the graphene layers with an optical microscope. This method uses the light absorption of graphene and relies on brightness differences similarly to the SEM characterisation method (Bonaccorso et. al., 2010). Finally there are Raman spectroscopy methods of layer characterisation. These methods rely on the direct probing of phonon energies within the graphene layers. One of these methods uses the graphene D/G peak intensity ratios which gives a relative estimate of the ratio between sp2 and sp3 carbon atoms which varies for different number of graphene layers. Another method uses the evolution of the 2D graphene peak, this method probes the double resonance phonon processes found for different number of graphene layers. Raman spectroscopy methods of layer identification can be very accurate but require pristine graphene and lose accuracy with defects within the graphene lattice (Sidorov, 2009)

2.2.1.1 AFM Thickness Measurements

AFM thickness measurements is a straight forward method of layer characterisation. The thickness of the deposited graphene is directly measured with an AFM. The measured step height between the graphene and deposition substrate can differ from the actual step height due to differences in Van der Walls force interaction of the AFM tip with the graphene and the deposition substrate. It should also be noted that the thickness of graphene layers can

change over time due to a relaxation of the sp3 bonds within the graphene and/or the introduction of moisture between the deposition substrate and the graphene (Sidorov et. al., 2007). This effect can be seen in figure 2.18, this figure shows the height differences of deposited graphene measured 45 days apart. It can be seen from this figure that the height of the graphene for the dashed lines 1 and 3 do not vary much after 45 days, however, the height of the graphene for the dashed lines 2 and 4 almost doubles.

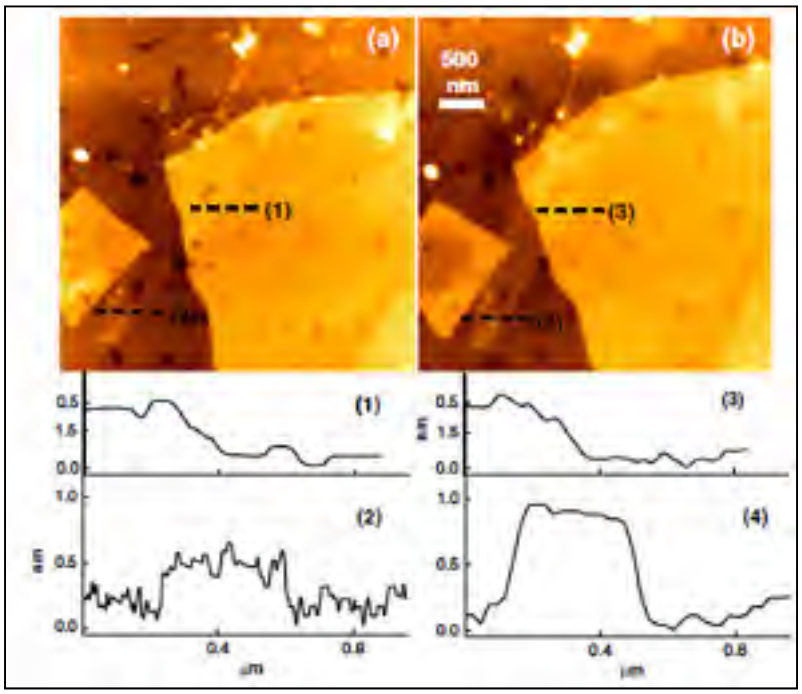

Figure 2.18 Height differences of the graphene (a) 1 day after deposition and (b) 45 days later after leaving it in a laboratory environment. The AFM height profiles (1)–(4) correspond to dashed lines (1)–(4), respectively, in (a) and (b). In either (a) or (b) the nearly square sheet on the left is 5 monolayers thick, while the large sheet on the right is 7 layers thick
Adapted from Sidorov et. al. (2007)

The thickness of one graphene layer is evaluate at ~0.35nm which can relax to ~0.8nm with time (Sidorov et. al., 2007). This relaxation in the thickness of the graphene layers makes this method not reliable as a stand-alone graphene layer characterisation method.

2.2.1.2 SEM and Optical Characterisation

SEM characterisation of graphene layers is a very popular method of characterisation as it offers another straightforward characterisation method with better accuracy than that of the AFM thickness method (Sidorov et. al., 2007) (Hidefumi et. al., 2010), although it is a rather qualitative method of characterisation. SEM measurements result in contrast images in which the number of graphene layers can easily be identified. The contrast variations in the image are due to the conductivity differences and charge accumulation between the graphene and the deposition substrate (McMullan, 1995).

Optical characterisation using visible light (390 to 700nm) can be done in either transmission or reflection modes depending on the deposition substrate used (transparent substrate needed for transmission mode). The visible light absorbance for each layer of graphene is known to be ~2-4% (Bonaccorso et. al., 2010), this will result in contrasts images in which the number of graphene layers can be identified by the difference in light absorption. Figure 2.19 shows a comparison of the optical and SEM images showing the contrast differences for different number of graphene layers on different deposition substrate.

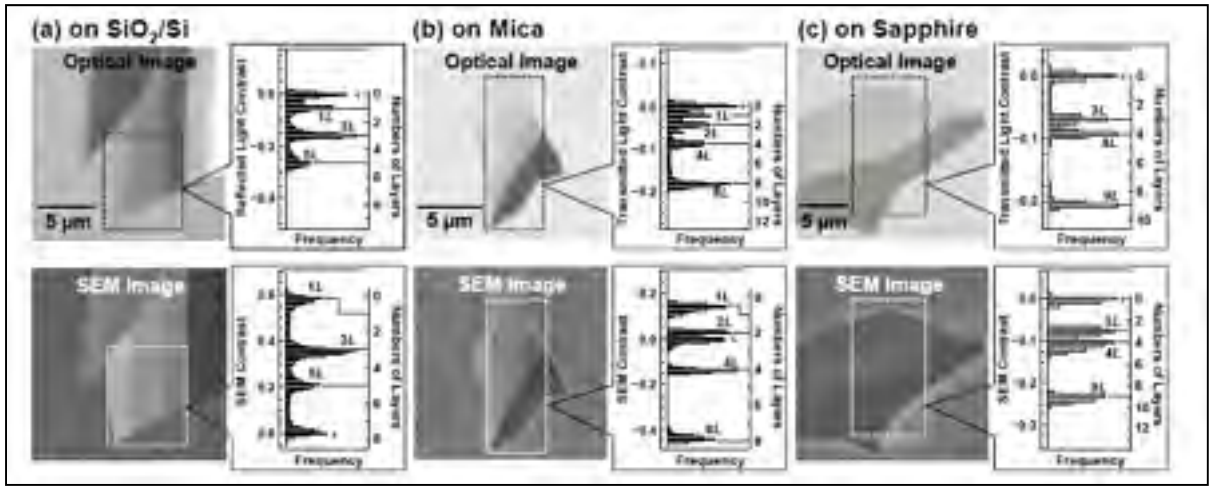

Figure 2.19 Comparison of optical and SEM methods for determining the number of graphene layers on various substrates, (a) SiO2/Si, (b) mica, and (c) sapphire
Taken from Hidefumi et. al. (2010)

As can be seen from this figure, identification of single layered graphene via optical characterisation is difficult since the contrast between a single layer of graphene and the deposition substrate is small. This difference in contrast is more visible with the SEM images, clearly showing the difference between the deposition substrate and any deposited graphene (Hidefumi et. al., 2010). This optical characterisation method is only accurate until ~7 layers of graphene where it becomes more opaque. Whereas the SEM characterisation method is accurate for a much greater range of graphene layers.

2.2.1.3 Raman Spectroscopy

There exists a couple of graphene layer characterisation methods that use Raman spectroscopy. Raman spectroscopy uses a coherent light source to probe vibrational modes within the substrate. These methods include 2D graphene Raman peak evolution and D/G graphene Raman peak ratio mapping (Ferrari et. al., 2006). These two methods offer different accuracies of graphene layer characterisation. The D/G Raman peak ratio mapping method is quite accurate for pristine graphene, however defects within the graphene lattice are known to affect the intensity of the D peak and hence the D/G peak intensity ratio (Ferrari et. al., 2006) (Graf et. al., 2007). Figure 2.20d) illustrates how the D/G ratio can be used to characterise the number of graphene layers, the integrated intensities of the D and G peaks are plotted with a dashed and solid line respectively. It can also be observed that this ratio changes abruptly at the edges of the layers of graphene.

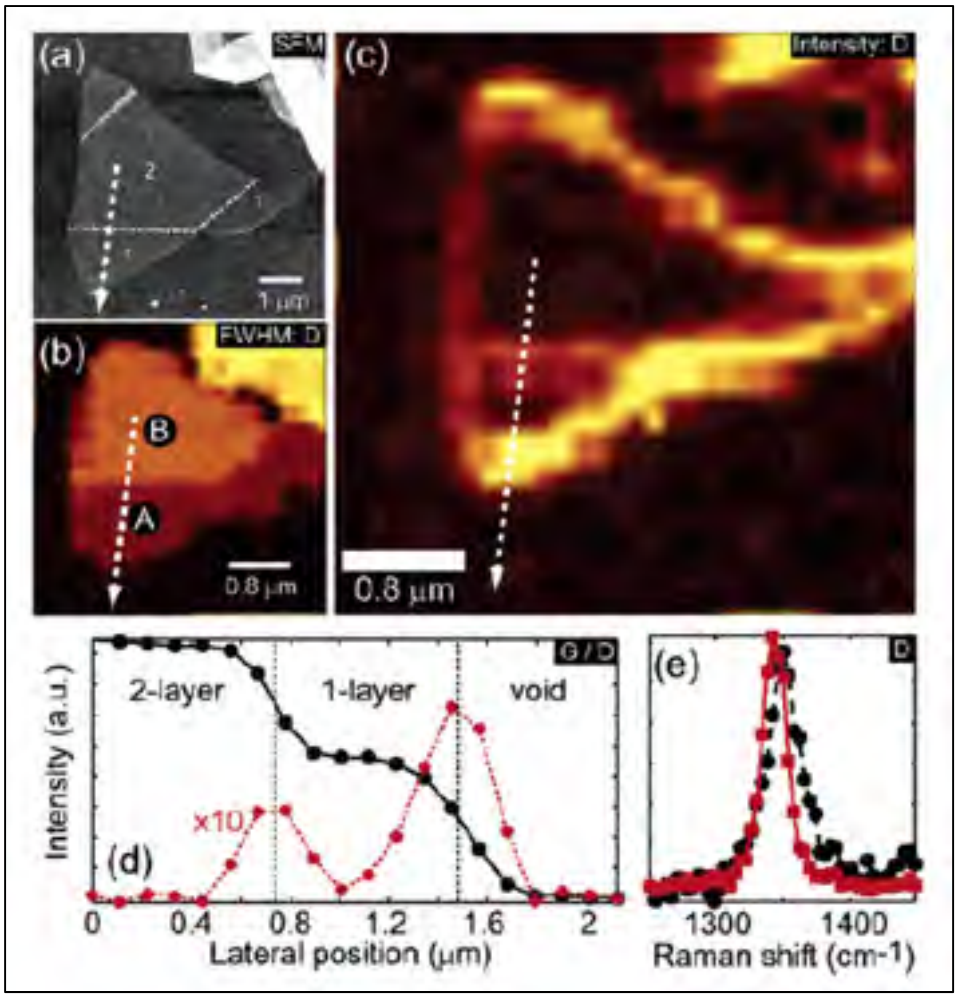

Figure 2.20 a)SFM micrograph, b)FWHM of the D' line, c)Raman mapping of the integrated intensity of the D line, d)integrated intensity of the G peak (solid line) and integrated intensity of the D line (dashed line), e) D peak for the edges (dashed for 2 to 1 layer, and solid for 1 to 0 layers) Adapted from Graf et. al. (2007)

The peak evolution method seem to be more accurate for a broader range of variations in graphene lattice quality. The 2D graphene Raman peak is known to split into multiple peaks for increasing number of graphene layers (Malard et. al., 2009). Figure 2.21 shows this splitting of the 2D peak with the resulting Raman spectra from one layer to 4 layers of graphene and for HOPG. It can be observed that the relative center of this peak shifts towards higher wavenumbers with increasing number of layers. It can also be noted that the width of the resulting peak increases with the number of layers. The 2D peak is also know to split in

single layered graphene when treated at high temperatures (> 2200°C) (Mallard et. al.,2009), since such heat treatments are not performed in this work, this effect will not be further taken into account.

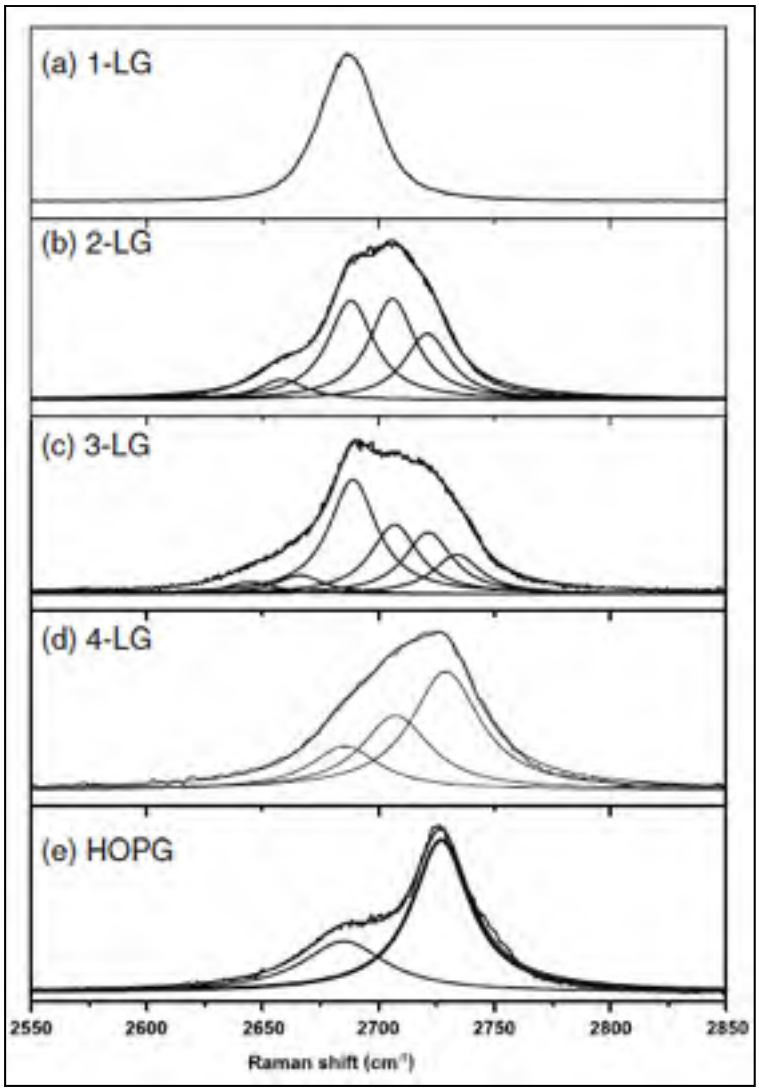

Figure 2.21 2D graphene Raman peak evolution
Taken from Malard et. al. (2009)

This characterisation method is effectively two methods, since both the center and the width of the resulting 2D graphene Raman peak can be used to characterise the number of graphene layers. This method will be used as the primary method of layer identification for this work

since it offers a good accuracy that does not depend on graphene lattice integrity (Mallard et. al., 2009).

2.2.2 Optoelectronic Properties Characterisation

The optoelectronic properties of deposited graphene is of interest if it is to be used as the active layer in optoelectronic devices. As seen in the first chapter, the calorimetric properties of the active layer of a bolometer are proportional to the bolometer response. Another property that is investigated is the direct electrical response of the deposited graphene with an incident light source, which is of importance for both bolometers and photoconductive switches.

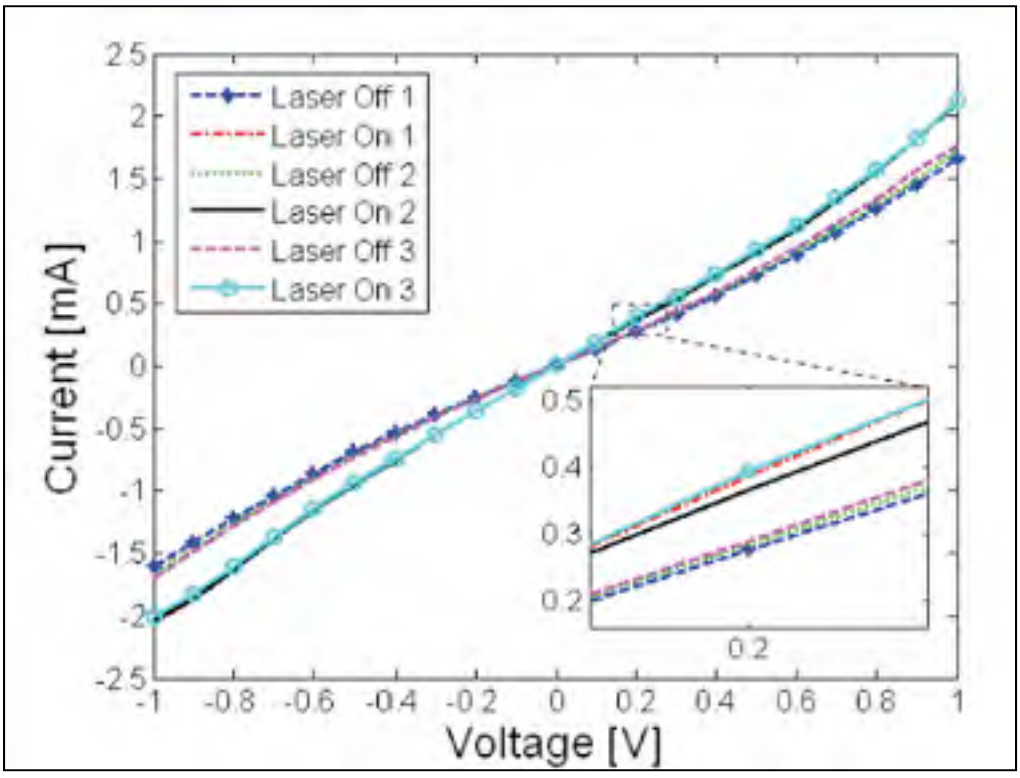

Figure 2.22 I-V curves of Graphene sample recorded by the iterative laser switching on and off
Taken from Gilgueng et. al. (2009)

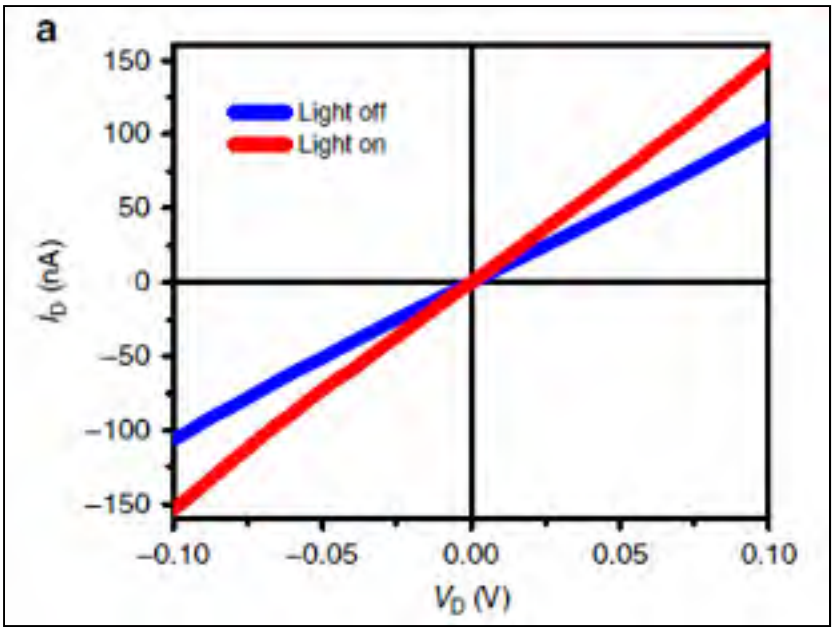

Figure 2.23 I–V curves of Graphene Sample with and without 532nm illuminations
Adapted from Zhang et. al. (2013)

Figures 2.22 & 2.23 show typical direct electrical response of graphene with an incident light source of 120mW (IR) (Gilgueng et. al., 2009) and 5.57nW (visible light) (Zhang et. al., 2013) respectively. The resistivity of the graphene decreases as the incident light source is switched on, demonstrating that graphene can be used as a photoconductive material for optoelectronic devices.

Figure 2.24 shows the two point resistance measurements taken at room temperature and at 100mK for multiple graphite samples, it can be observed that there is a wide range of resistance change between room and low temperature measurements and that the general trend is an increase in resistance at lower temperatures. It can also be noted that the samples with high room temperature resistances (> 10kΩ) increased in resistance to a much greater degree (Bunch, 2000).

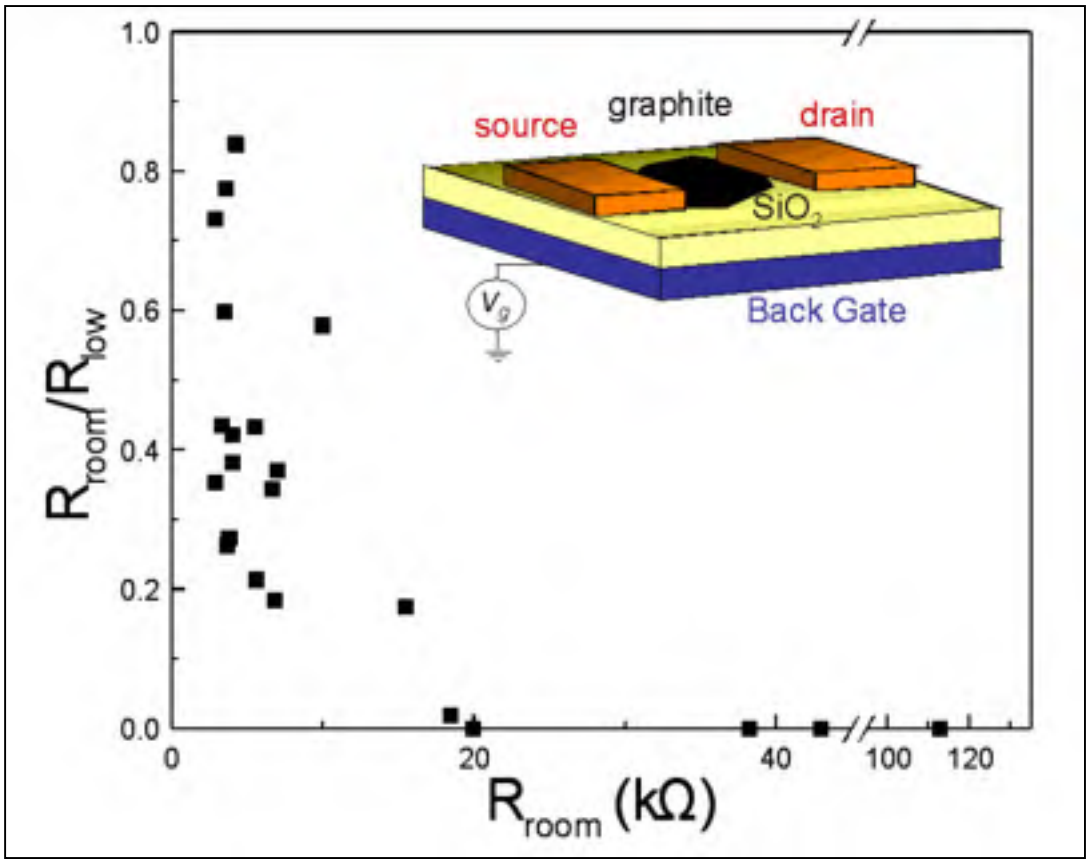

Figure 2.24 A scatter plot of the ratio of the low (T ~ 100 mK) to room temperature 2-point resistance versus the room temperature 2-point resistance for all the devices for which there is low temperature data. (inset) Schematic of the device layout Taken from Bunch (2000)

CHAPTER 3

GRAPHENE PHOTOCONDUCTIVE SWITCH FABRICATION USING ELECTROSTATIC DEPOSITION

3.1 Methodology

In this chapter, the electrostatic deposition of graphene will be explored in detail. This process will differ from the electrostatic deposition method as explained in the previous chapter. Improvements to the process have been introduced to better control the number of graphene layer deposited and to improve the control of the size and shape of the deposited graphene sheets.

This approach combines the HOPG island etching process found in micro-mechanical deposition of graphene with the electrostatic deposition method and includes improvements to the cleaving process to achieve more homogeneous results in terms of loosening the top graphene layer while also creating an upper boundary for the size of the depositions. By making the size of the etched HOPG islands smaller than the average deposition size normally reported for electrostatic deposition, the size of the deposited graphene sheets will be homogenized to this upper boundary. The HOPG islands also create smaller areas for the cleaving process, it is thought that a smaller cleaving surface will result in more homogenously loosened graphene layer since the chances of defects resulting in inhomogeneous cleaving within each surface is lower.

Deposition substrate etching has also been incorporated in this process. By etching features onto the deposition substrate, the strength of the electrical field during the deposition process can be changed locally. This can be used as another method of controlling the position of the graphene deposition. Etching features such as trenches or holes onto the deposition substrate can also be used to create suspended graphene devices.

3.1.1 Set-up and Materials

A set-up similar to the one explained in the previous chapter was used. HOPG grade SPI-1 and HOPG grade SPI-3 which exhibits mosaic angles of 0.4°±0.1° and 3.5°±1.5° with typical lateral grain size of 3nm and 30nm respectively were used as the bulk graphitic material, these HOPG samples were bought from SPI Supplies®. The HOPG sample was glued to the top electrode using silver epoxy. The top electrode is made of a 99% 0.5" copper rod, cut and polished to 3 cm in height. The top electrode was threaded to accommodate a 0.25" x 1" ThorLab cap screw which was connected to the positive terminal of the high voltage power supply. The top electrode with the cap screw was placed inside a custom made PVC holder and held by a x-y-z micro precision stage. The x-y-z micro precision stage was used to bring the HOPG into contact with the deposition substrate and to move the HOPG laterally to control the deposition location on the substrate. A piece of rigid foam of 2mm in height was attached to the bottom of the PVC holder to homogenize horizontal forces present on the HOPG during the contact with the deposition substrate. Figure 3.1 shows the set-up for the top electrode that was used for this project.

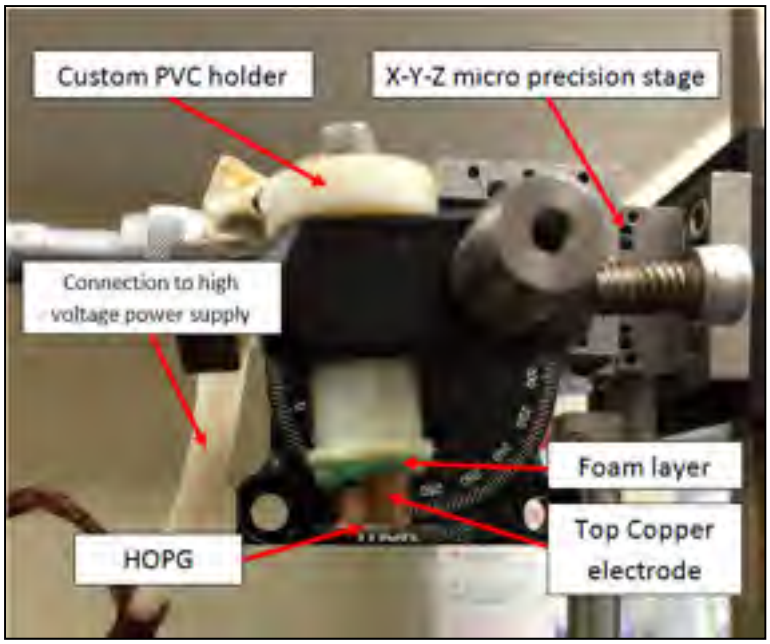

Figure 3.1 Image of the top electrode set-up for electrostatic deposition of graphene

The bottom electrode is made of a 4" diameter 99% copper puck of 3cm in height, it was also threaded to accommodate a 0.25" x 0.5" ThorLab cap screw which was connected to the ground terminal of the high voltage power supply. Three layers of 0.25mm mica sheets where glued to the top of the bottom electrode with Loctite® UV cured PVC bonding adhesive to create an insulating layer between the bottom electrode and the deposition substrate. The bottom electrode was attached to a levelling stage to ensure that the HOPG and the deposition substrate came into complete contact. Figure 3.2 shows the set-up used for the bottom electrode in this project. A Stanford Research Systems model PS375 +20kV 10W, was used as the high voltage power supply which was connected to the top and bottom electrodes with a high voltage cable. Figure 3.3 shows the complete set-up for electrostatic deposition of graphene that was used in this project, the high voltage power supply is shown in figure 3.4. The set-up was placed in a Labconco® Precise® Controlled Atmosphere glove box purged with nitrogen to stop arcing between the two electrodes. The glove box is shown in figure 3.5.

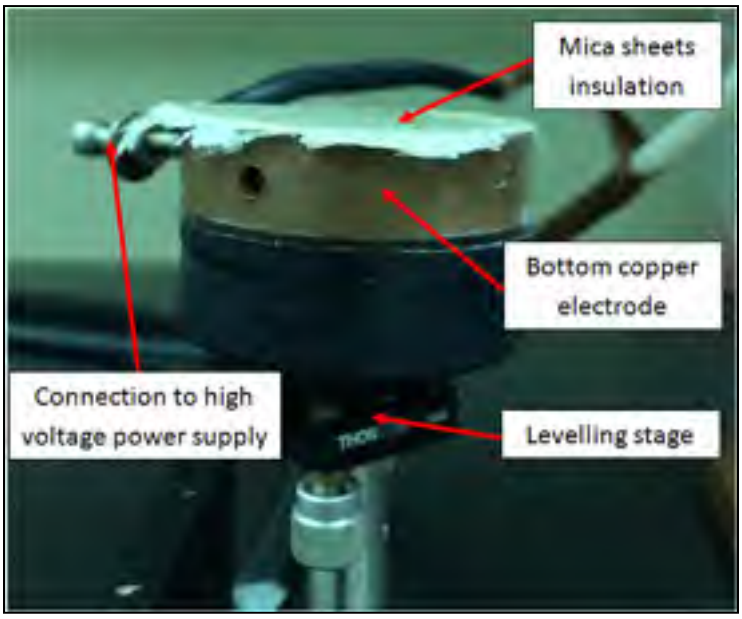

Figure 3.2 Image of bottom copper electrode set-up for electrostatic deposition of graphene

Figure 3.3 Electrostatic deposition set-up

Figure 3.4 Face view of the Stanford Research System Model PS375 +20kV 10W used as the high voltage power supply for the electrostatic deposition of graphene

Figure 3.5 Labconco® Precise® Controlled Atmosphere Glove Box

3.1.2 Electrostatic Deposition with HOPG

3.1.2.1 Etching HOPG

The pristine HOPG samples can be etched to create an array of islands that set an upper boundary on the feature size of the deposited graphene sheets. A Samurai UV laser marking system from DPSS laser inc. was used to etch the pattern on the HOPG. Operating at 355nm with a spot size of ~25 μm, this marking system was found to be ideal for the precise etching of HOPG. The etching pattern was first drawn using *WinLase® Professional.* It was found that the electrostatic deposition of graphene sheets occurred more readily for smaller graphene sheet area. Therefore, a pattern of the smallest island was created. The smallest feasible sub-squares using the Samurai UV laser marking system where found to be in the order of 20x20 μm. Below this threshold, the islands where more pyramidal in shape, became more fragile and broke easily during the cleaving process.

The etching depth is another important parameter. The etching depth should be of the same order or smaller than the side length of a islands. If the etching depth is large compared to the side-length of the islands (~20 times), the pattern becomes very fragile and the islands are prone to damage. If the etching depth is small in general (<10 μm), then the repeated cleaving process before each deposition can remove whole island features. The etching depth of the Samurai UV laser marking system on the HOPG can be controlled using the number of passes the laser makes in a certain area. Figure 3.6 shows experimental data of the etching depth of the Samurai UV laser marking system in single line mode. The etching depth was measured using an Olympus LEXT confocal optical microscope.

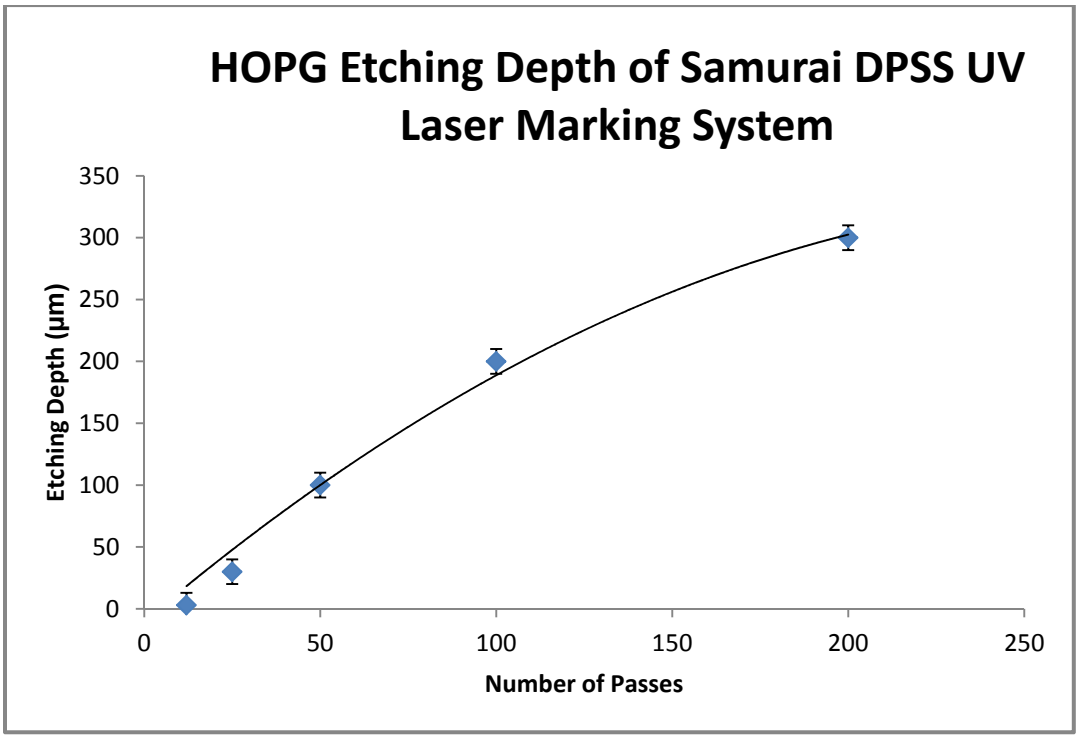

Figure 3.6 HOPG etching depth of Samurai DPSS UV Laser Marking System

Diminishing returns on the etching depth are seen as the number of passes is increased. This is due to two phenomena, first as the laser etches deeper it starts to un-focus as the distance increases slightly. Then, graphite powder and dusts falls in the trenches etched thus making the following passes less effective as the laser etches the HOPG. An etching depth of 50-100 µm depending on the island side-length was used for all following etchings. This depth was found to be shallow enough to leave the islands strong enough to manipulate and clean the HOPG and for electrostatic deposition. An etching depth of 50-100 µm was also found to be deep enough to enable repeated HOPG cleavage and thus multiple (>20) depositions between etching processes.

It was observed that the etching process leaves graphite dust inside the etched trenches. The HOPG must be cleaned of all residual dust before deposition otherwise the dust will be deposited alongside the graphene sheets. A gentle nitrogen flow over the etched HOPG sample is used to remove the excess dust without damaging the etched islands. Sonicating the HOPG in any solution to remove the excess graphite dust was found to result in damage

to the island features. For larger island features (>400x400 μm) it was found that sonicating the HOPG in distilled water can be used to remove the graphite dust with minimal damage to the island features.

3.1.2.2 SiO2 Substrate with Heat Sink Features

The deposition substrate can also be etched to create features such as trenches or holes for suspended graphene devices. These features will change the homogeneity of the strength of the electrical field around them, this can be used to control the position of the deposition of the graphene sheets (Sidorov, 2009). These features were etched using the same Samurai UV laser marking system from DPSS laser inc. The smallest etching features possible for the trenches and holes are of the order of the laser spot size (~25μm). Similarly to the HOPG etching process, the etching depth can be controlled with the number of passes. The etching depth was also found to vary extremely with the size of the etched features, with smaller features equating to shallower etched features for the same number of passes. This has been attributed to substrate dust accumulating within the smaller features. It was found that the etching depth saturated at around the size of the feature. Figure 3.7 shows experimental data for the etching depth versus the number of passes for holes of 50μm in diameter in a SiO2 substrate.

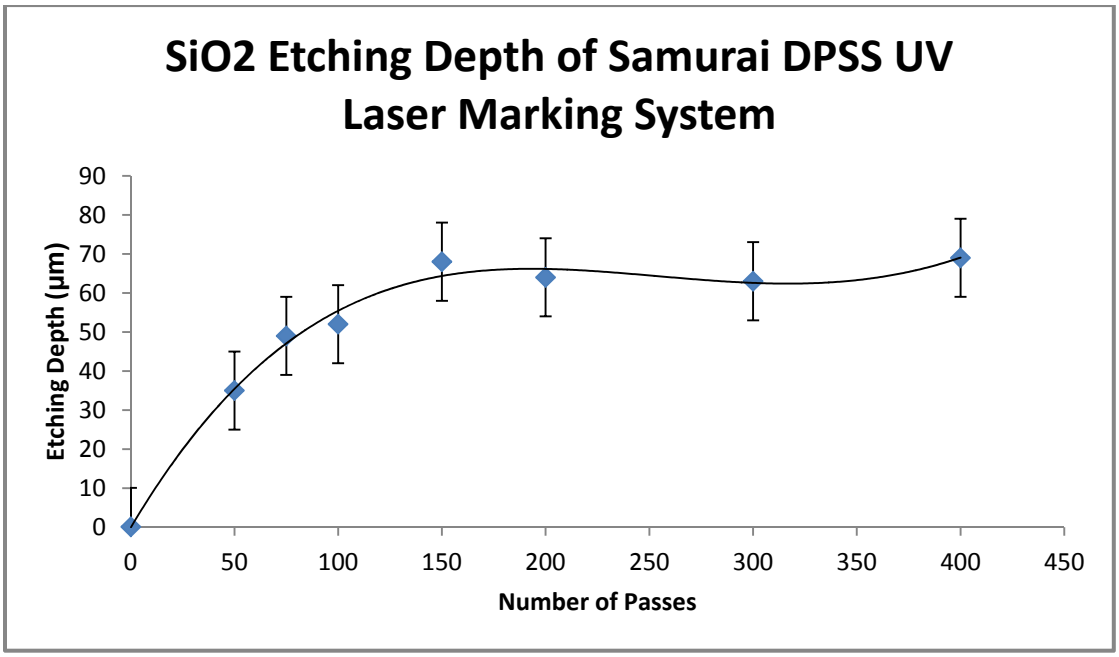

Figure 3.7 SiO2 Etching depth of Samurai DPSS UV Marking System for 50µm features

An example of 200µm trenches and 50µm holes etched (red arrow) on an SiO2 substrate are shown in figure 3.8 and 3.9 respectively.

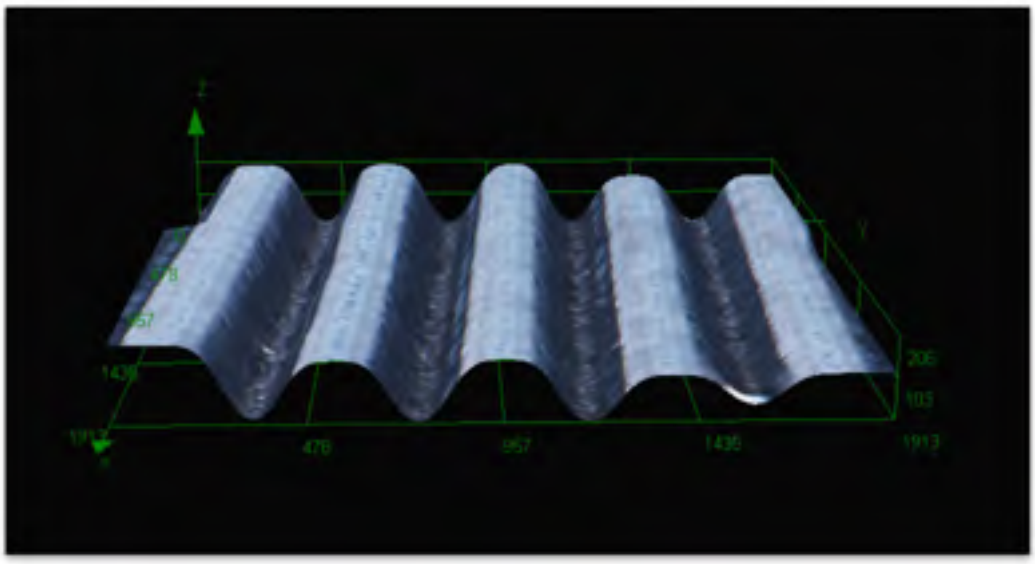

Figure 3.8 3D optical image of 200µm trenches in SiO2 substrate etched with a Samurai DPSS UV Marking System. All axis values are in µm

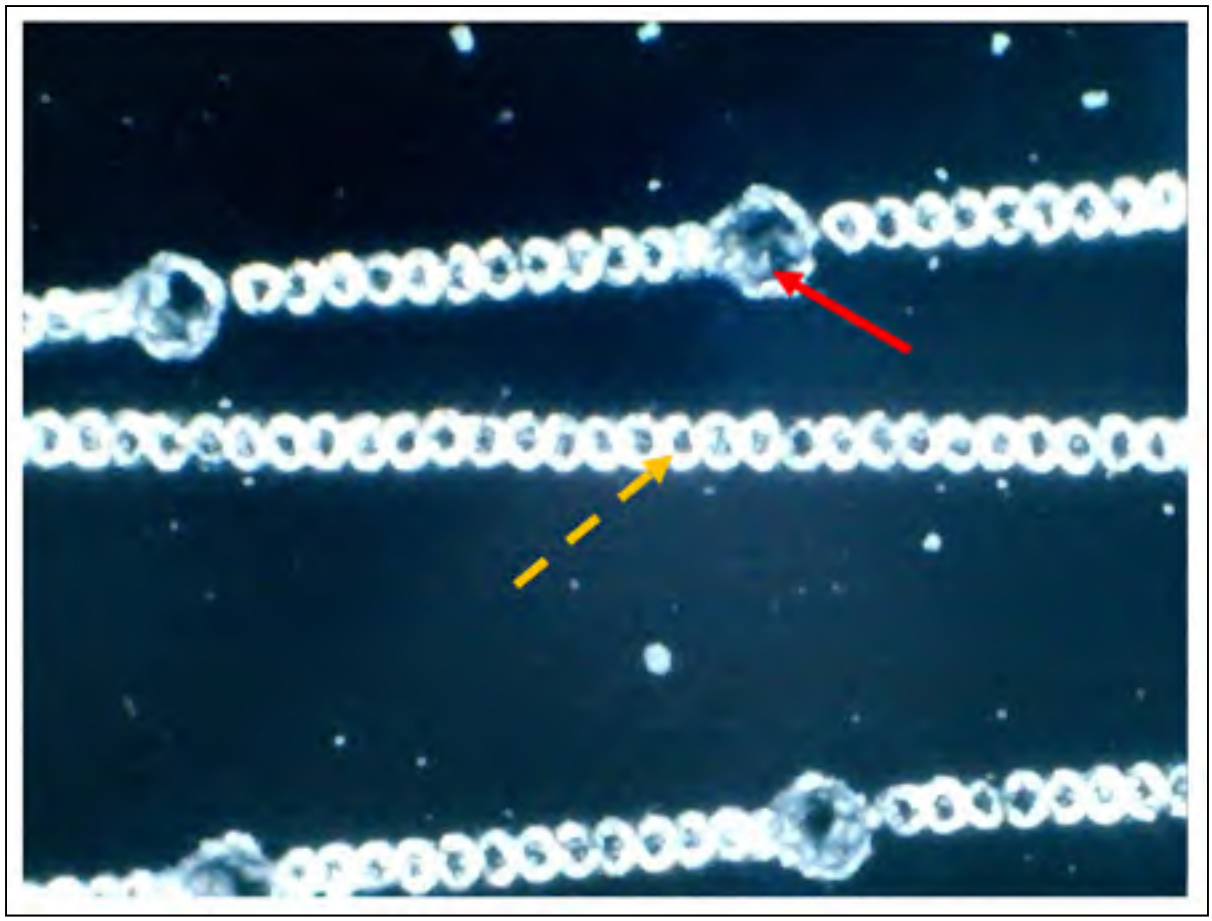

Figure 3.9 Top view of 50µm holes (red arrow) and artefacts (dashed orange arrow) etched in SiO2 substrate with Samurai DPSS UV Marking System

In figure 3.9 it can be observed that some unintended features were also etched onto the substrate (orange dashed arrow). The series of dots between each hole are due to the laser staying active while moving between each feature. These dots are the same size as the laser spot size (~25µm) and their depth is <1µm. The effect of these dots on the strength of the electrical field during deposition will be minimal compared to the intended etched features due to their shallow depth and therefore should have minimal effect to the deposition process.

3.1.2.3 Optimising Deposition Parameters

Due to the inhomogeneous process of scotch-tape cleaving of the graphene, repeatability and control over the quality of the deposited graphene is a main drawbacks of electrostatic deposition of graphene (Sidorov, 2009). The scotch-tape cleaving method will be analysed in greater detail in the next part of this chapter. Other parameters important for deposition must then be controlled and optimised to allow for the best possible control over the quality of the deposited graphene. The most important parameters to control for are: the deposition voltage, the size of the etched graphene islands and the ambient atmosphere (Sidorov, 2009).

The size of the etched graphene islands was found to affect the deposition voltage needed to controllably deposit a full graphene island with the desired number of layers, with a larger island needing a higher deposition voltage. At larger etched island sizes, it becomes impossible to deposit fully-shaped graphene layers as shown for electrostatic deposition without the HOPG etching procedure. Figure 3.10 shows an optical overview of the electrostatic deposition results for 700µm x 700µm etched graphene islands at a deposition voltage of 8kV and in a nitrogen atmosphere. It can clearly be seen that the electrostatic deposition using these parameters is completely inhomogeneous. Smaller deposited graphene sheets are also wanted as they are created to act as the active layer in photoconductive switches and/or microbolometers. The graphene islands were etched as small as possible with the Samurai UV laser marking system used (20µmx20µm). The upper size limit for the etched graphene island was found to be 90µm x90µm to allow for full deposition of graphene layers.

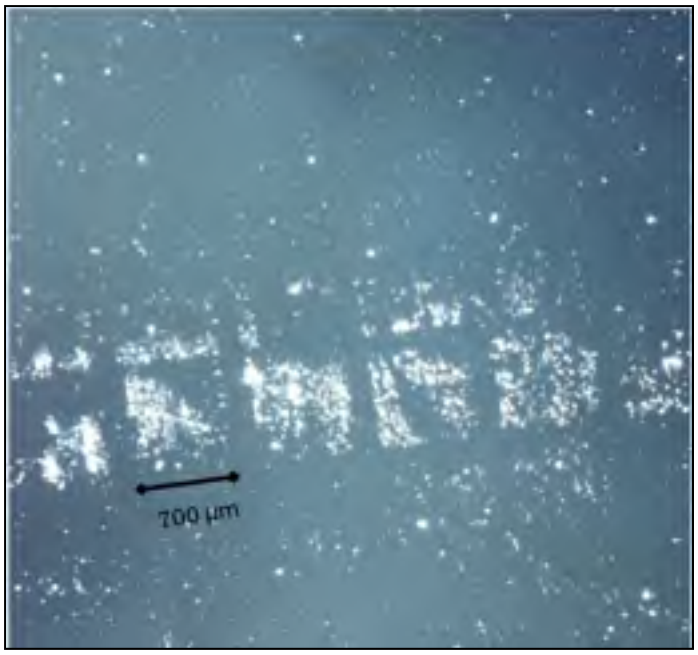

Figure 3.10 Optical image of electrostatic deposition of 700µm x700µm graphene islands on SiO2 substrate at 8kV in nitrogen atmosphere

A controlled atmosphere is needed for the electrostatic deposition of graphene (Sidorov, 2009). It is possible to deposit graphene electrostatically in ambient air, however, humidity levels in the air can fluctuate and can cause electrical shorting between the graphene and the deposition substrate to occur spontaneously at varying applied deposition voltages (Sidorov, 2009). Therefore, a dry nitrogen atmosphere is needed to prevent any electrical shorting between the graphene and the deposition substrate. As explained previously in this chapter, this was achieved by placing the electrostatic deposition set-up inside a Labconco® Precise® Controlled Atmosphere glove box, constantly purged with dry nitrogen. This allowed for a much better control over the deposition voltage.

With the controlled dry nitrogen atmosphere and the size of the etched graphene island set at 20µm x20µm, the deposition voltage can then be optimised. Other parameters will also affect the deposition voltage needed for a deposition of a wanted number of graphene layers, these parameters include everything that will have an effect on the electrical field created (Sidorov, 2009). The thickness of the oxide layer and of the insulating mica sheets will have an effect

on the global electrical field strength (Sidorov, 2009), whereas, any pattern etched on the deposition substrate will have an effect on the local electrical field strength (Sidorov, 2009). Calibrating the voltage necessary to deposit a wanted number of graphene layers will therefore be unique to every set-up. Although the applied voltages reported in this work give similar numbers of deposited graphene layers to the ones reported in other works (Sidorov, 2009), it is advisable to take these numbers with some reservation as they can be very sensitive to the setup and the environment. Table 2 shows the number of layers deposited for 20μm x 20μm etched graphene islands onto SiO2 substrate in a nitrogen atmosphere for different applied voltages. The most homogeneous deposition occurred at a deposition voltage of 2.5 to 3.5 kV, full 20μm x 20μm graphene sheets were deposited with mostly 4 full layers and a few sheets with 3 full layers and a partial fourth graphene layer. Below 2.5kV, the ability to deposit full 20μm x 20μm graphene sheets is lost. Most deposition below 2.5kV result in partial graphene sheets of 1 to 3 layers. Above 3.5 kV, full 20μm x 20μm graphene sheets are deposited readily with an increased number of full layers. For this work, the most homogenous graphene deposition with the least number of layers is wanted, therefore the full 20μm x 20μm graphene sheets of 4 layers that are deposited from 2.5 to 3.5 kV are utilised to continue this work.

Table 3.1. Deposition voltages with resulting number of deposited graphene layers for 20μm x 20μm etched islands onto SiO2 substrate in nitrogen atmosphere

Deposition Voltage	Number of Layers
0-1.5 kV	--
1.5 2.5 kV	1 to 3
2.5-3.5 kV	3 to 4
3.5 -4.5 kV	3 to 5
4.5 5.5 kV	4 to 5+
5 5 kV +	5–

3.1.2.4 HOPG Cleaving between deposition

Another step in the process of electrostatic deposition of graphene that is important in the homogeneity of the deposited graphene is the cleaving process of the HOPG before each new depositions. This inhomogeneity explains the range in the number of layers deposited for any given voltage seen previously (Sidorov, 2009). This step loosens the graphene sheets so that they can be removed from the bulk HOPG block and deposited onto the wanted substrate via electrostatic forces. In of itself, this process is inhomogeneous but steps can be taken to reduce this inhomogeneity. The cleaving method used in this work is known in layman's terms as the scotch-tape cleaving method. This method originates from the Nobel prize winning works of Andre Geim and Konstantin Novoselov where they were able to create single layered graphene by repeatedly cleaving graphite with household scotch tape. Many different adhesives were tested for this step but 3M brand single sided scotch-tape performed

the best in terms of a homogeneous cleave and least amount of material removed from the bulk HOPG.

To make this process as homogeneous as possible, care must be taken to apply a constant pressure over the surface of the HOPG when applying the tape and to remove the tape with a constant force. To do this, the tape was first applied lightly to the etched side of the HOPG. Then using the tip of the thick rubber glove attached to the Labconco® Precise® Controlled Atmosphere Glove Box, a small constant pressure is applied to flatten the tape and remove any bubbles between the tape and etched HOPG. Once the tape is flatten and devoid of bubbles, it is removed slowly at a constant speed starting at one corner and pealing diagonally to the opposite corner. Different works report different methods of applying and removing the tape; some report that a fast and sharp removal of the tape or that flattening the tape with the back of plastic tweezers for bubble removal works best. How effective each method is at creating homogeneous cleaves will highly depend on the dexterity and preference of the researcher.

Each cleave of the patterned HOPG surface removes some of the material until the patterned islands are removed completely and a flat HOPG surface is re-created. It was observed that upon a subsequent deposition, once the patterned island are removed from bulk HOPG via cleaving, that large scale single layer graphene sheets (> 120μm x120μm) can be deposited. It is thought that this is due to an anchoring effect of the patterned island on the bulk HOPG when they are removed via cleaving. This anchoring effect is thought to loosen the underlying graphene sheet periodically at each removed patterned island to create a very homogeneously loosened up graphene sheet which can then be deposited electrostatically. Figure 3.11 illustrate this considered phenomena.

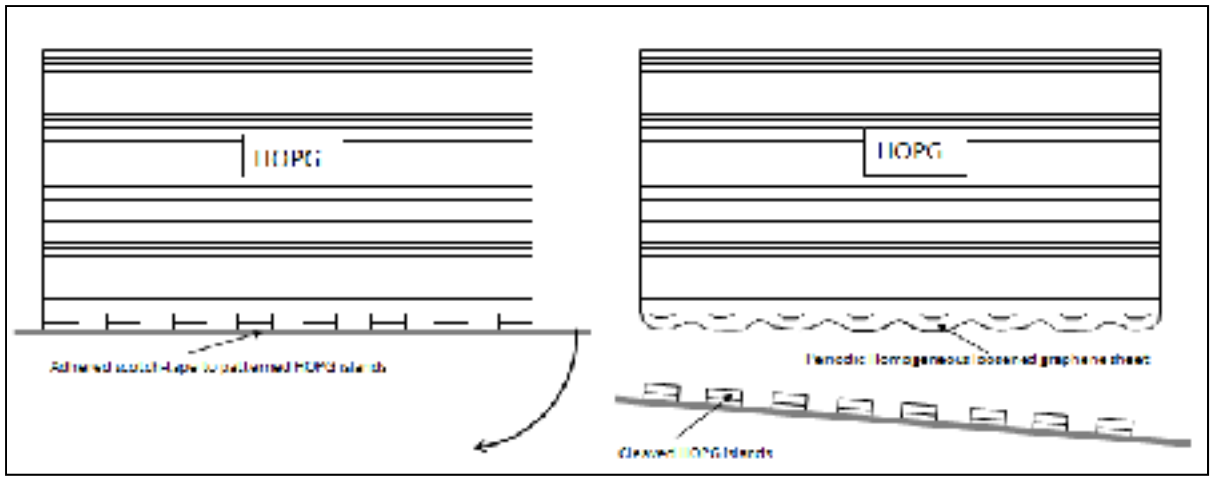

Figure 3.11 Homogeneous periodic loosening of underlying graphene sheet via anchoring effect of HOPG island cleaving

The large area single layer graphene deposition results of this particular effect will be analysed further in this chapter. It is important to note that this effect is not yet fully understood and that it did not constantly lead to large scale single layer graphene deposition.

3.2 Results of Electrostatic Deposition of Graphene

The deposition results for this work are divided into four different sections. The first section shows the preliminary results from the deposition with flat HOPG and deposition substrate. The second section shows the results from the deposition using flat HOPG and a patterned substrate, highlighting the effects of altering the local electrical field strength. The main results for this work are found in the third section, showing the results from deposition using a patterned HOPG onto a flat substrate. The last sections finally shows the results of deposition after the removal of the patterned HOPG island via scotch-tape cleaving.

3.2.1 Preliminary deposition

Preliminary electrostatic deposition using lower quality HOPG without island pre-patterning and also un-patterned SiO2 deposition substrate was performed to acquire a baseline for the deposition voltage needed for further depositions and to acquire the know-how to perform this type of graphene deposition. The preliminary deposition results in conjuncture with the subsequent results from the deposition onto a patterned SiO2 deposition substrate were used in developing a fast identification method to identify the number of layers of graphene present. This identification method will be looked at in detail in the next chapter, it uses the 2D graphene Raman peak center position to identify the number of graphene layers. The corresponding number of graphene layers have been added to all the Raman image scale bars for the ease of the reader.

The resulting graphene deposition is found to be inhomogeneous in terms of the number of graphene sheets deposited for any given deposition voltage and in terms of the shape of the graphene sheets. Similarly to the deposition voltages shown in the "Optimising Deposition Parameters" sub-chapter; below a 1.0kV deposition voltage, no deposition occurred; between 1.0kV and 4.0kV, 4 layers or less of graphene where deposited, and above 4.0kV, up to graphite material was deposited (5 or more layers). Figure 3.12 shows typical results of such electrostatic deposition at a deposition voltage of 3.0kV, the image on the right is a Raman image mapping the 2D peak center position. In this figure, a mostly 2 layered graphene sheet can be seen with sporadic single layer deposition surrounding it.

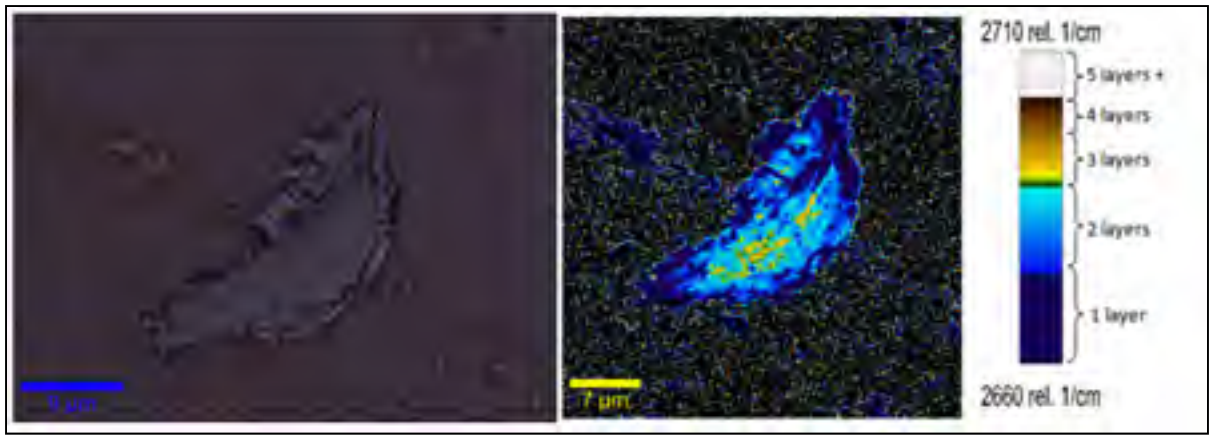

Figure 3.12 Optical and Raman image of typical electrostatic deposition at 3.0kV with un-patterned HOPG onto un-patterned SiO2 substrate

Figure 3.13 shows typical results for a preliminary deposition at 5.0kV, showing deposition up to 5 or more layers. This figure shows a larger range of number of layers deposited; from single layer deposition all the way up to graphite material deposition.

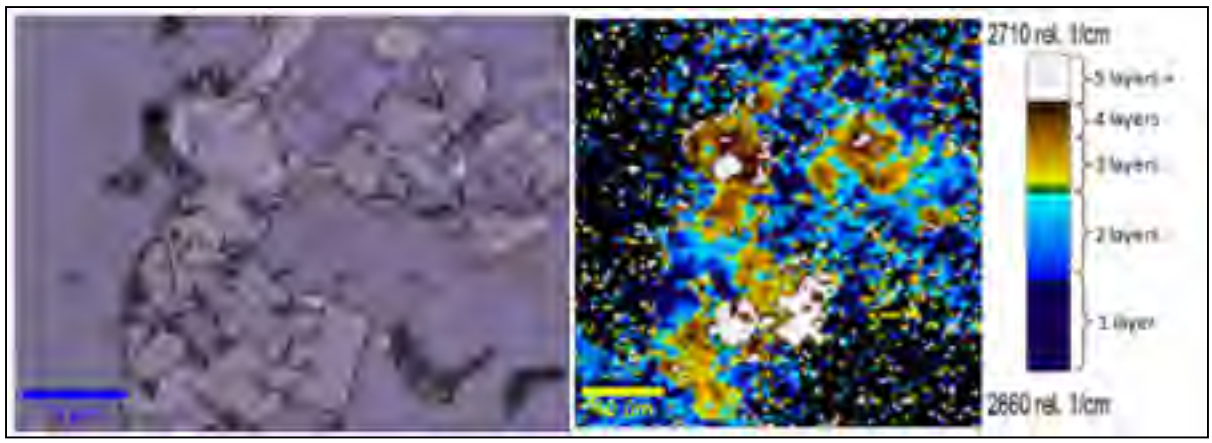

Figure 3.13 Optical and Raman image of typical electrostatic deposition at 5.0kV with un-patterned HOPG onto un-patterned SiO2 substrate

3.2.2 Deposition on pre-patterned substrate

Deposition of an un-patterned HOPG onto a pre-patterned SiO2 substrate was performed to examine the effects of changes in the local field strength. The patterning procedure for the SiO2 substrate is explained in an earlier chapter of this work. However the resulting change in electrical field is not explained in detail. Simply put, by patterning the SiO2 surface, the local permittivity of the SiO2 (ε_r =3.9) is replaced by the permittivity of air (ε_r = 1.0) which increases the resulting electrical field at those locations since the electrical field strength is inversely proportional to the relative permittivity of the material.

Figure 3.14 to 3.16 show the effect of the localised electrical field strength increase, it can be seen that deposition occurs more readily at the etched features in the SiO2 deposition substrate. Deposition onto the etched features happened more readily at deposition voltages as low as 0.5kV. However, for full coverage of these patterned features the minimum voltage required was found to be 1.0kV.

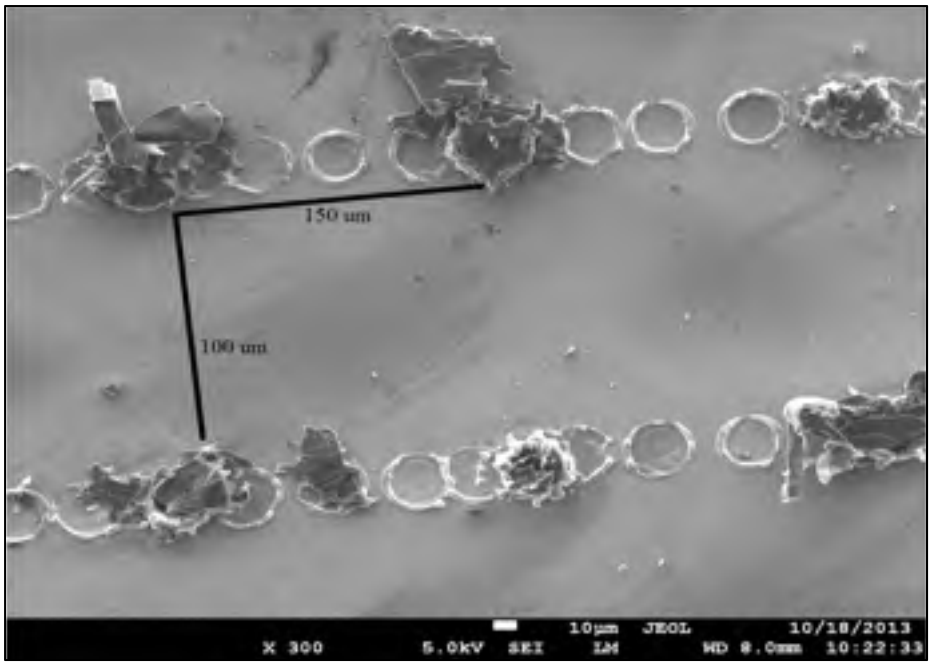

Figure 3.14 SEM image of electrostatic deposition at 5kV with un-patterned HOPG onto pre-patterned SiO2 substrate

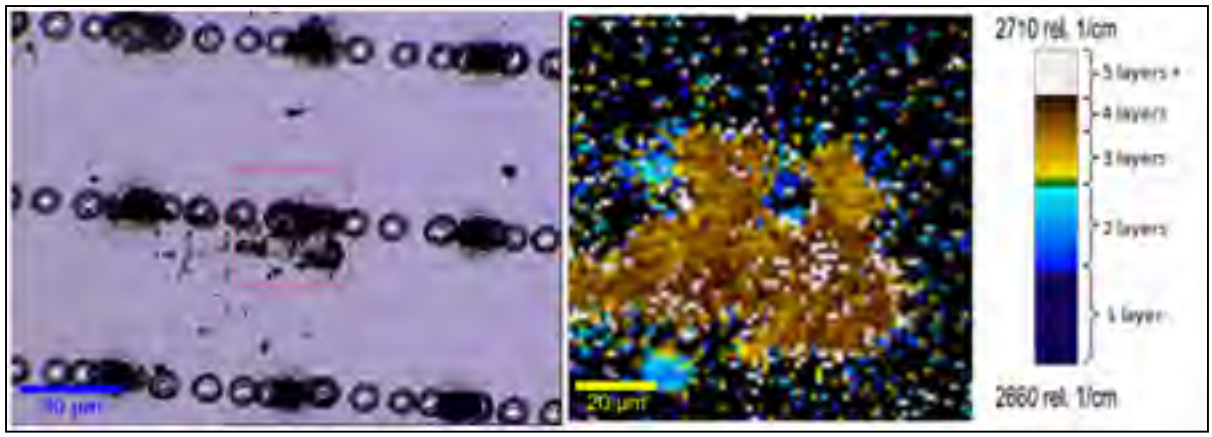

Figure 3.15 Optical and Raman image of typical electrostatic deposition at 1.0kV with un-patterned HOPG onto patterned SiO2 substrate

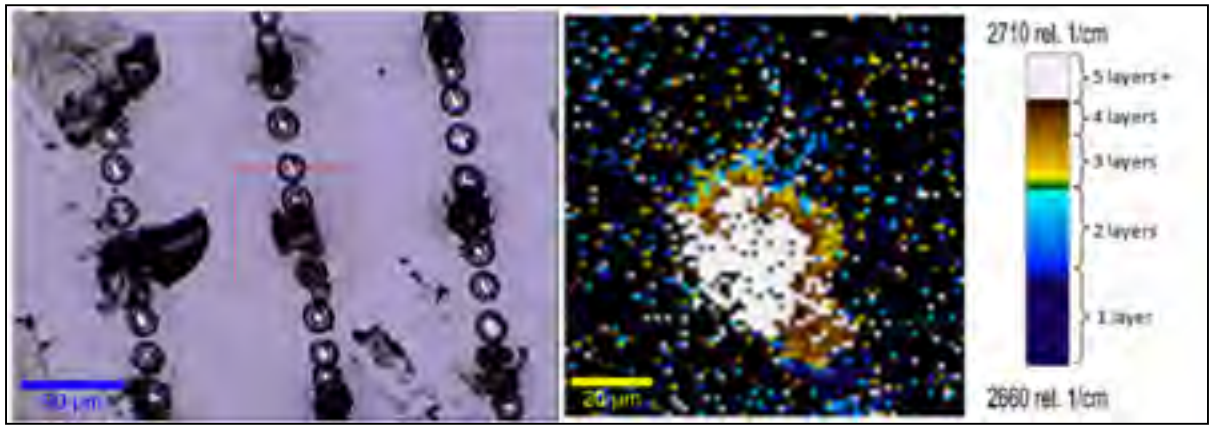

Figure 3.16 Optical and Raman image of typical electrostatic deposition at 3.0kV with un-patterned HOPG onto patterned SiO2 substrate

As can be seen from figures 3.15 and 3.16, increasing the deposition voltage also increases the density of etched features covered.

3.2.3 Micro Sheet Deposition

In this part of the chapter, the results for the electrostatic deposition of the patterned HOPG onto SiO2 substrate will be analysed. Figures 3.17 to 3.21 show typical results for different deposition voltages.

Below 2.5kV deposition voltage, most deposited graphene consisted of partial sub-square deposition of one (1) to three (3) layers of graphene. Figure 3.17 shows an optical image and the corresponding Raman image mapping the 2D peak center position for electrostatic deposition at 1.8kV. At deposition voltages lower than 1.8kV similar results are obtained however the density of deposition becomes lower with decreasing deposition voltages.

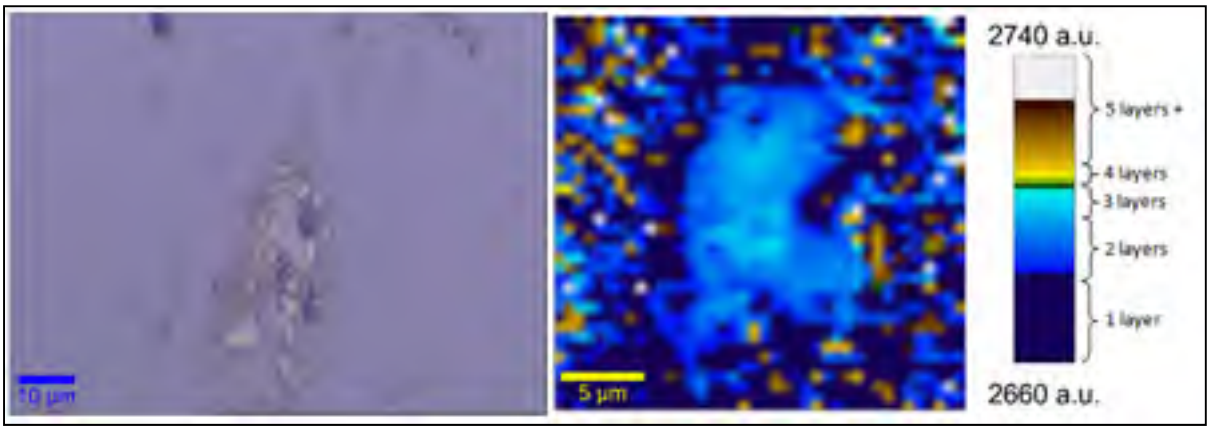

Figure 3.17 Optical and Raman image of typical electrostatic deposition at 1.8kV with patterned HOPG

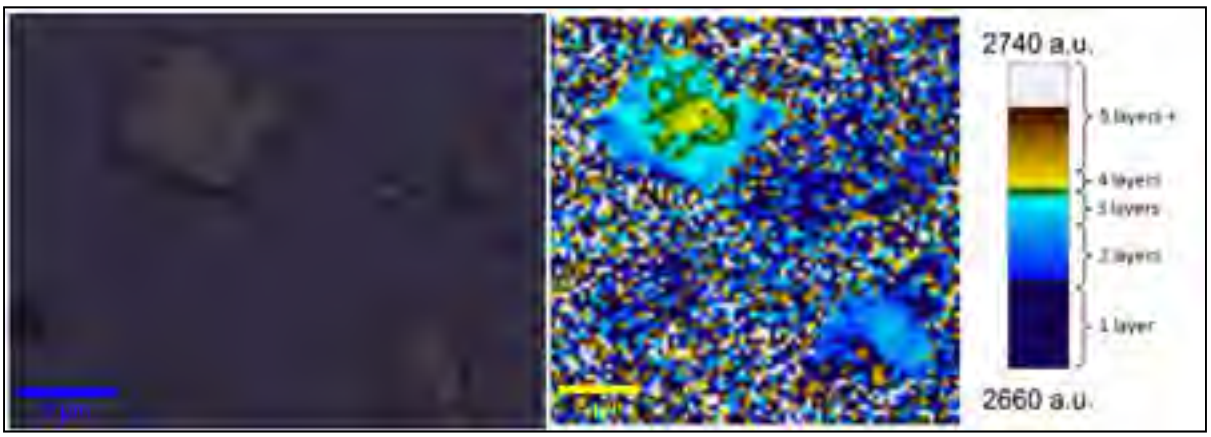

Figure 3.18 Optical and Raman image of typical electrostatic deposition at 2.5kV with patterned HOPG

Starting from 2.5kV, complete sub-square deposition takes place and the number of layers deposited becomes more constant. Three layer graphene deposition is more prevalent at the lower end of this range of deposition voltages and 4 layer graphene deposition happens more

readily at the upper end of this range. Figure 3.18 shows an optical and the corresponding Raman image mapping the 2D peak center position for a deposition voltage of 2.5kV. Around a deposition voltage of 3kV, the deposition density of complete sub-squares is high enough for it to be considered a deposition of a matrix of graphene sub-squares. This deposited matrix of sub-squares is shown in figure 3.19 1), in this figure it can also be noticed that there is some evidence of micro-mechanical deposition. The overlap of graphene sheet sub-squares seen in figure 3.19 2A) is similar to results of graphene deposition obtained from previous micro-mechanical deposition works (Xuekun, et. al., 1999). Even when there is an overlap of deposited graphene sheets due to micro-mechanical deposition effects, the individual graphene sheets are of constant number of layers.

For deposition voltages above 3.5kV, the resulting deposited graphene sheets are mostly four to five layers and above 4.5kV deposition most deposited graphene sheets consisted of five or more layers. Figures 3.20 and 3.21 show optical and Raman images mapping the 2D peak center position of electrostatic deposition performed at 4.0kV and 5.0kV, respectively.

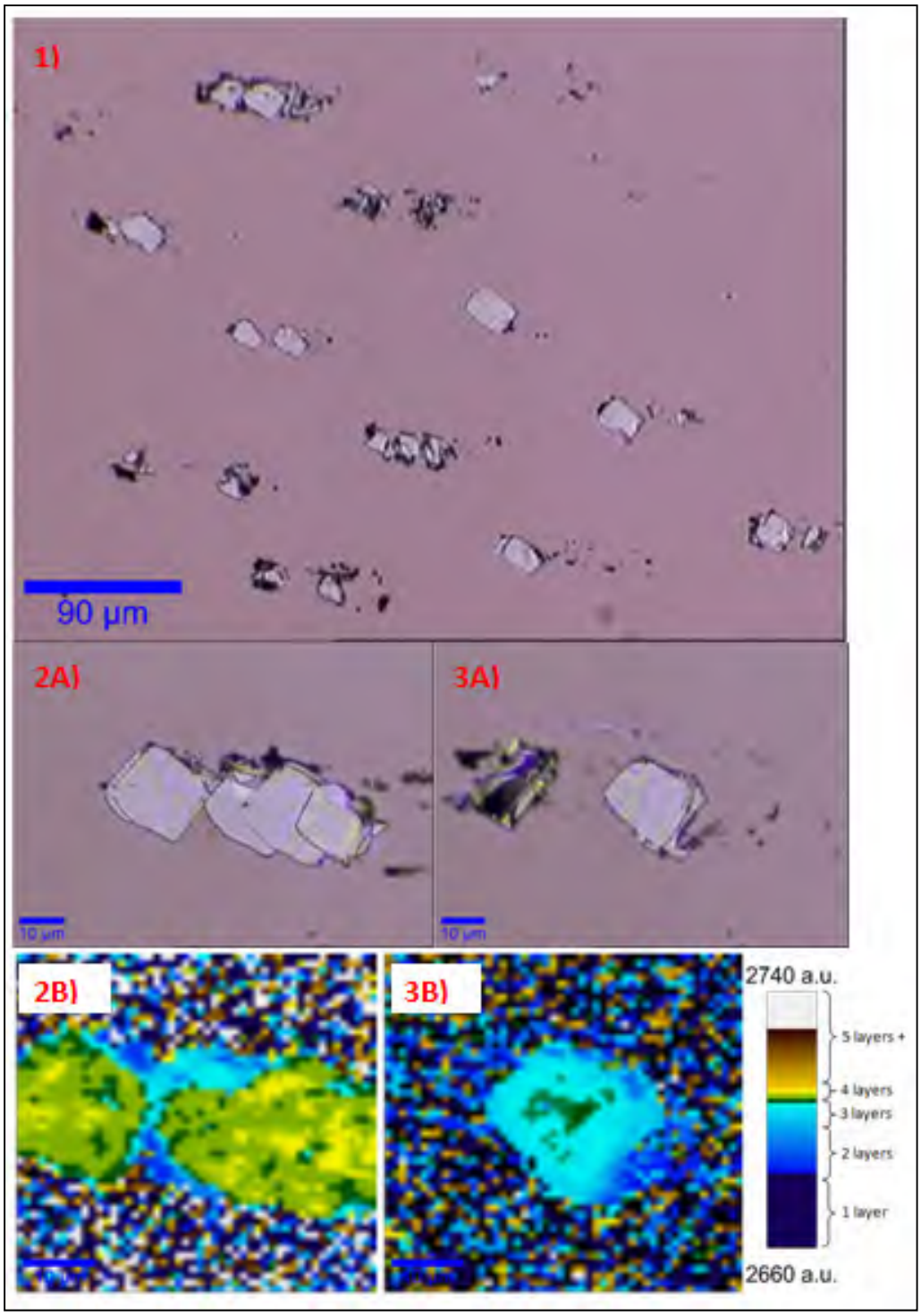

Figure 3.19 1): Optical image of deposited arrays of micro graphene sheets. 2A) & 3A): optical image of single micro graphene sheets. 2B) & 3B): Raman image mapping 2D peak center position. Electrostatic deposition at 3.0kV with patterned HOPG

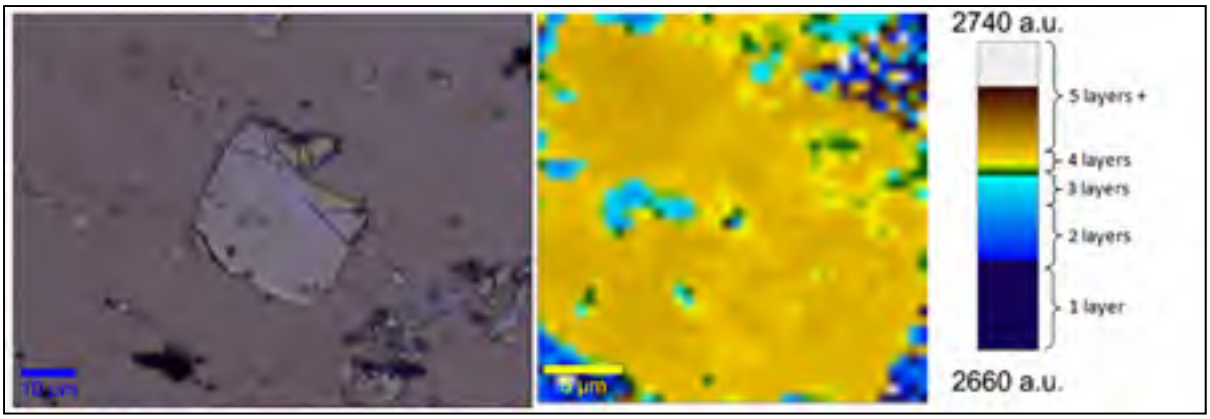

Figure 3.20 Optical and Raman image of typical electrostatic deposition at 4.0kV with patterned HOPG

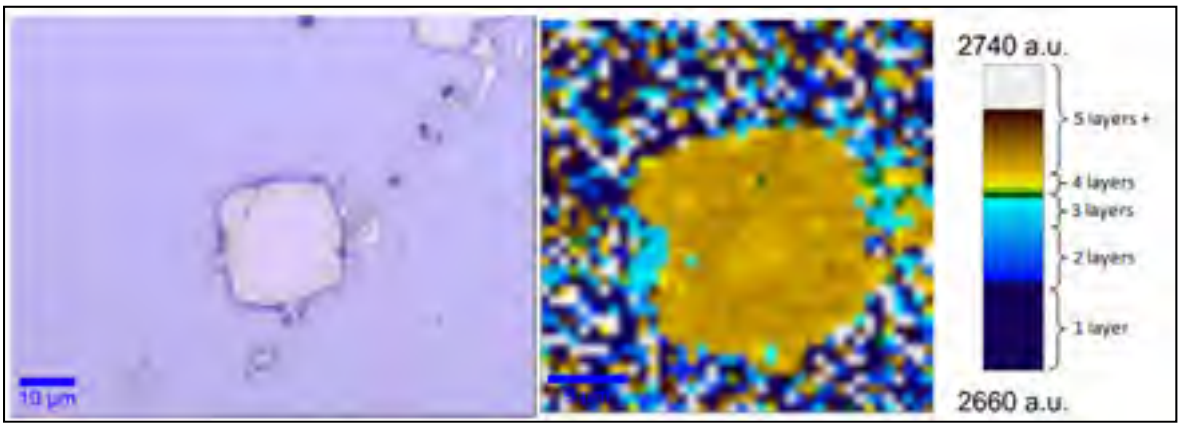

Figure 3.21 Optical and Raman image of typical electrostatic deposition at 5.0kV with patterned HOPG

3.2.4 Large Area Deposition

The large scale graphene depositions were performed at a deposition voltage of 3kV after the removal of the etched HOPG island pattern via scotch-tape cleaving. As can be seen from figure 3.22, the deposited graphene is mostly single and double layered with some sporadic multi-layer deposition. In the optical images, single layered graphene cannot be seen due to its low light absorption (~2-4%) (Bonaccorso et. al., 2010), double layered graphene can barely be seen optically in figure 3.22B as shaded areas and multi-layered graphene can easily be differentiated from the SiO2 deposition substrate. The Raman images show the

spatially resolved 2D peak center position and the single graphene layer becomes clearly visible.

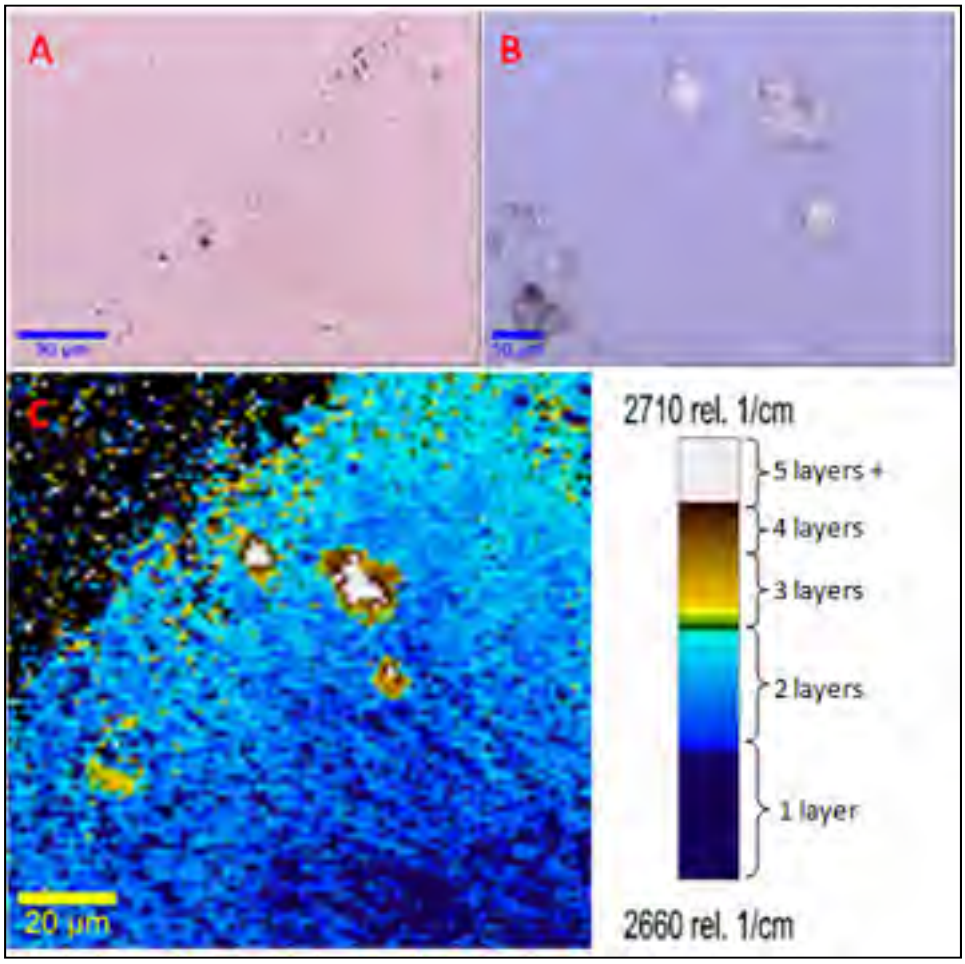

Figure 3.22 A) & B) Optical images of large scale single layer graphene deposition. C) Raman image of same deposition showing spatially resolved 2D peak center position

These are very interesting results in view of the fact that single layered electrostatically deposited graphene of this scale has never before been reported. However, the process to obtain these results still needs to be refined and understood more fully to make it more reproducible and consistent.

CHAPTER 4

GRAPHENE CHARACTERISATION

4.1 Methodology

In this chapter the method of characterisation of the number of layers and of the optoelectronic properties of the deposited graphene, that is used for this work, will be detailed. For the characterisation of the number of deposited graphene layers, SEM imaging is used with Raman spectroscopy. SEM imaging is used to support and calibrate the Raman 2D peak evolution characterisation method. In the case of the optoelectronic properties of the deposited graphene, calorimetric measurements and direct electrical response from an incident coherent light source is investigated.

4.1.1 Characterisation of the Number of Graphene Layers Deposited

As stated before, SEM imaging is an accurate method of characterisation for the number of graphene layers. This method can be time consuming and has some limitations such as the size of the sample which can be imaged and the makeup of the deposition substrate. To create a fast and accurate method of characterisation for the number of graphene layers, SEM images are taken in tandem with Raman scans. These can then be used together to improve the accuracy of the 2D Raman peak evolution technique and calibrate it for the equipment used in this work.

SEM imaging was done at l'Ecole Polytechnique de Montreal with a JEOL JSM7600F scanning electron microscope equipped with a field emission gun operated at an acceleration voltage of 5kV. Images 4.1 shows a resulting image from deposited graphene with an un-patterned HOPG onto a patterned SiO2 substrate, depositions with a wide range of deposited graphene layers were chosen for this calibration. The same deposition samples were then

scanned with a 300R Alpha Raman microscope system (shown in figure 4.3) from Witec with a 532nm excitation laser source.

Figure 4.1 SEM image from deposited graphene onto patterned SiO2

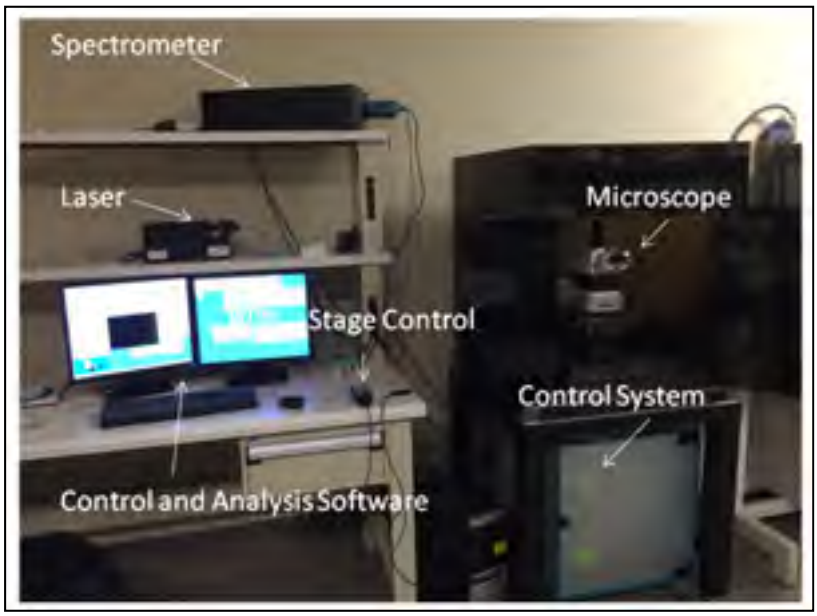

Figure 4.2 300R Alpha Raman microscope system from Witec with 532nm excitation laser source

Figure 4.3 shows the resulting Raman image mapping the 2D Raman peak center along with the optical image for one of the deposited samples.

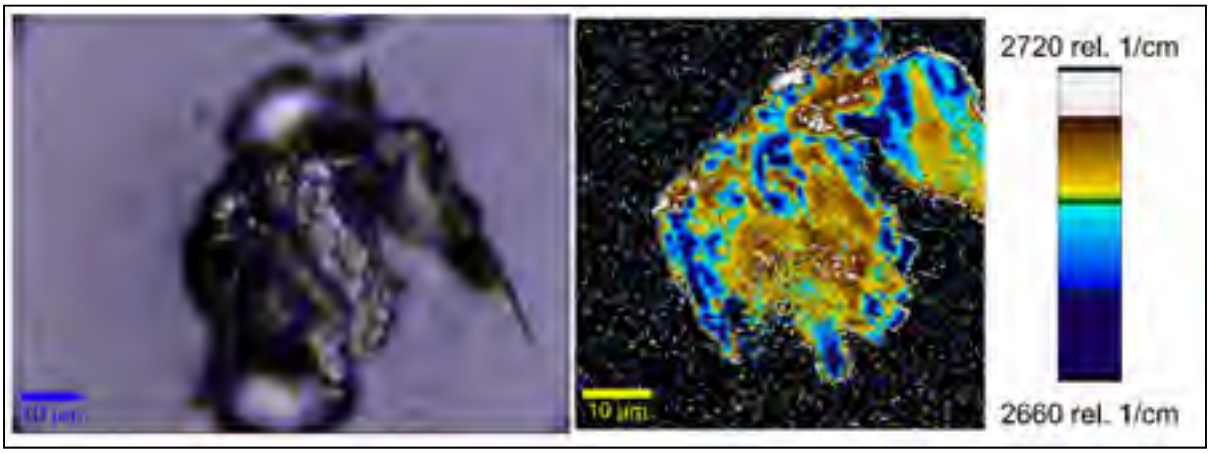

Figure 4.3 Optical and Raman image showing spatially resolved 2D Raman peak center position of deposited graphene from un-patterned HOPG onto patterned SiO2 substrate

With the help of both the Raman and the SEM images an average spectrum can be accumulated over areas for each of the number of graphene layers. Figure 4.4 shows these average spectra around the 2D Raman peak taken from one of the deposition samples, the intensities of the spectra have been shifted for easier viewing. A dashed line at 2700cm^{-1} has been added for easy identification of the shift towards higher wavenumbers with increased number of graphene layers.

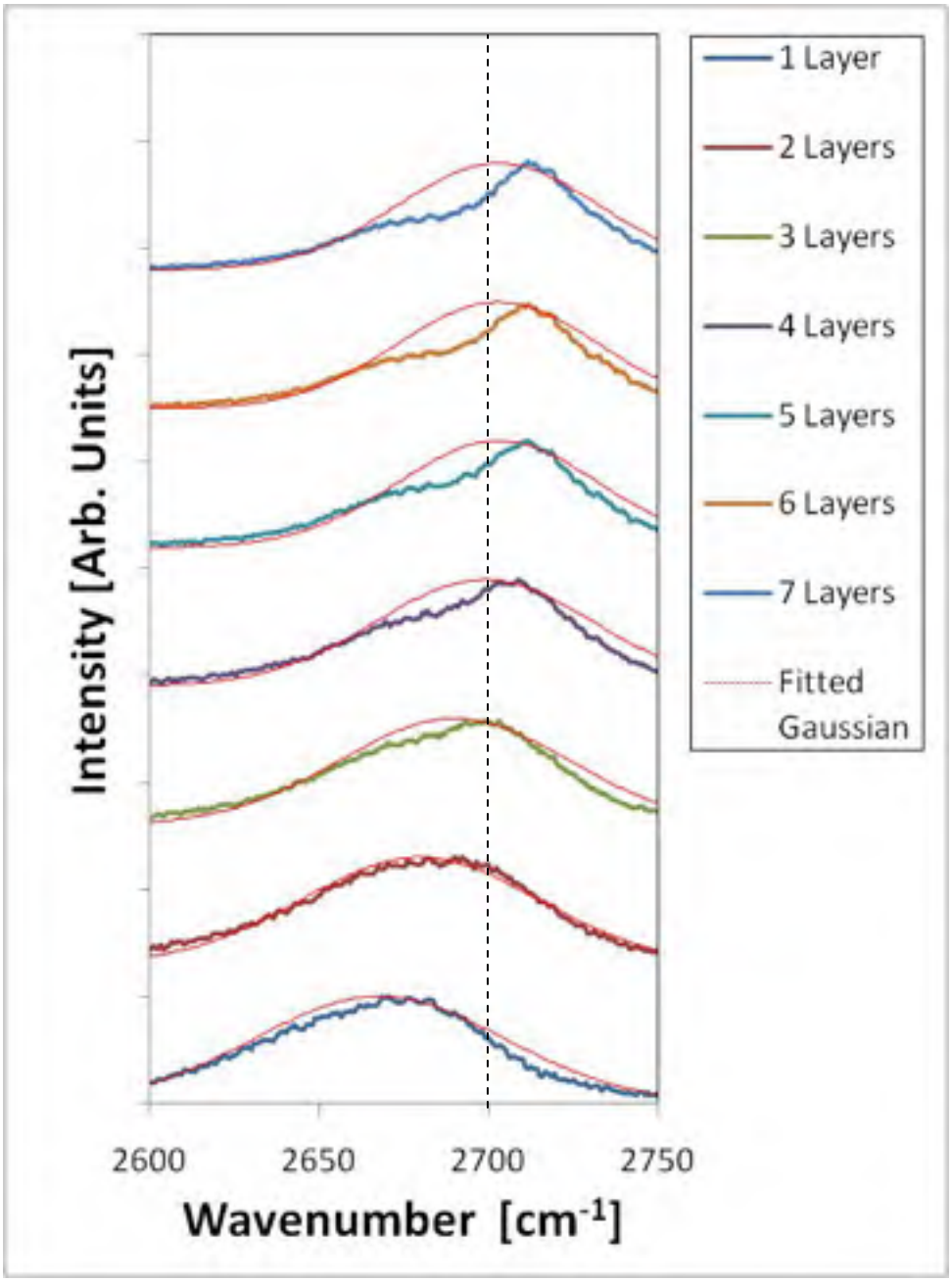

Figure 4.4 Evolution of 2D Raman peak with increasing number of graphene layers. Intensities in arbitrary units and shifted for easy viewing. Dashed line at 2700cm^{-1}

Above 5 layers of graphene, the 2D Raman peak stops evolving and stays constant, therefore this method of layer characterisation is only accurate up to 5 layers. Although the 2D peak splits and moves away from a Gaussian peak, gaussian curves can be fitted onto the 2D

Raman peak spectra. The center and full width at half maximum were extracted from the fitted curves and shown in Table 3. The ranges in table 3 are due to varying peak centers and widths from different samples, this can be attributed to a number of reasons such as relaxation of layer thicknesses with time. Since these ranges do not overlap it can be concluded that this method of characterisation is accurate, even without taking into account the error on the gaussian curve fitted due to the peak shape evolution. An effect of this error is the decreasing FWHM with the increasing number of layers, the actual width of the 2D peak seems to be increasing with the number of layers. However the split in the 2D peak changes the shape of the peak and the fitted Gaussian calculates the FWHM to be lower due to the right part of the peak (after the 2700cm^{-1} dashed line seen in figure 4.4) that is narrower and more intense than the left part of the 2D peak. This peak shape evolution also effects the fitted Gaussian center since the 2D peak is more weighted to the right for increased number of graphene layers.

Table 4.1. 2D Raman peak evolution for increasing number of graphene layers. Showing 2D peak center position and full width at half maximum

# Layers	2D Peak Center [cm^{-1}]	2D peak FWHM [cm^{-1}]
1	2660 - 2671	85.8 - 87.1
2	2673 - 2683	81.7 - 82.8
3	2686 - 2690	79.3 - 80.5
4	2698 - 2700	75.6 - 75.8
5	2702 - 2704	70.1 - 70.3

The values in table 3 can be used as an accurate characterisation of the number of graphene layer deposited by direct inspection of the 2D graphene Raman peak center position and FWHM.

4.1.2 Optoelectronic Measurements of Graphene

The optoelectronic properties of the deposited graphene samples where studied. First the calorimetric or the temperature-dependent resistivity measurements of the deposited graphene is studied. The samples where set in a continuous flow liquid nitrogen cryostat and connected via micropositioners to a Keithley 2400 source measure unit, the 2-point resistance was measured from the I-V curves collected with a custom LabView VI. Figure 4.5 shows the continuous flow liquid nitrogen set-up with a connected measured sample. Cryogenic temperatures down to -200 °C where reached with this set-up. In total 10 deposited graphene samples were tested, their 2-point resistances at room temperature (20°C) is plotted in figure 4.6. It can be seen from this figure that 80% (8/10) of the sample tested have 2-point room temperature resistances between 1 and 5 kΩ. Whereas the remaining 2 samples (sample 2 & 9) have much greater 2-point room temperature resistances (>15kΩ), possibly due to tears and defects present in these samples.

Figure 4.5 Liquid Nitrogen constant flow Cryostat set-up with contacts on graphene sample

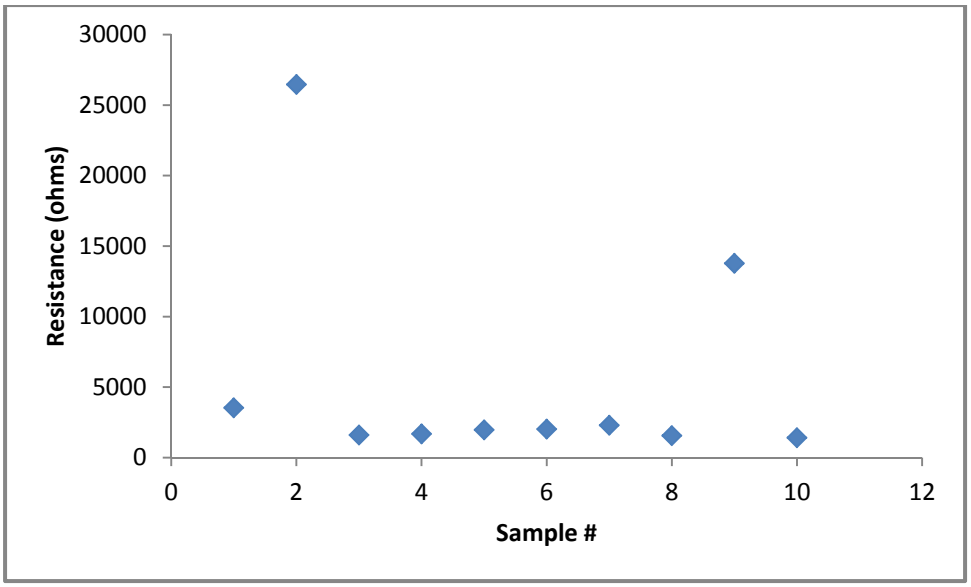

Figure 4.6 Room temperature resistance of electrostatically deposited graphene sheets

Similar 2-point resistances were measured at intervals of 20 °C from 20°C to -200°C to evaluate the temperature-dependence of these resistances. Figure 4.7 shows the measured temperature-dependent 2-point resistances of the 10 deposited graphene samples. As can be seen from this figure, a general negative relationship can be seen between the 2-point resistance and the temperature of the deposited graphene samples. These results generally agree with 2-point resistance of graphite samples (Bunch, 2000), however a specific temperature-dependent resistance relationship could not be developed due to the large variation in measurements. The ratio between the room temperature 2-point resistance and the -200°C 2-point resistance is also plotted in figure 4.8. With the help of figures 4.6 to 4.8 the deposited graphene samples can be separated into 4 different quality categories, these categories are summarized in table 4.

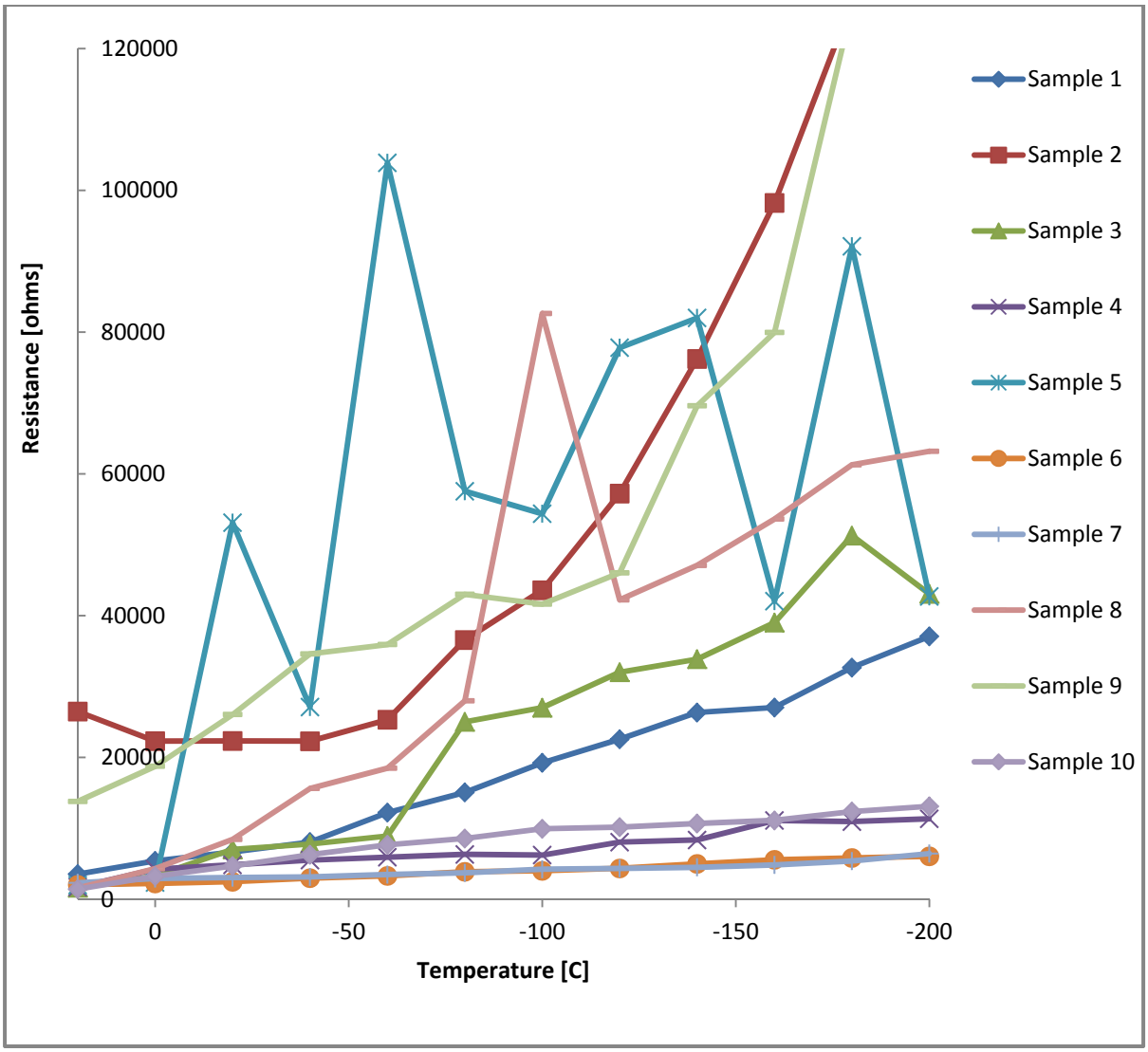

Figure 4.7 2-point temperature-dependent resistances of electrostatically deposited graphene sheets

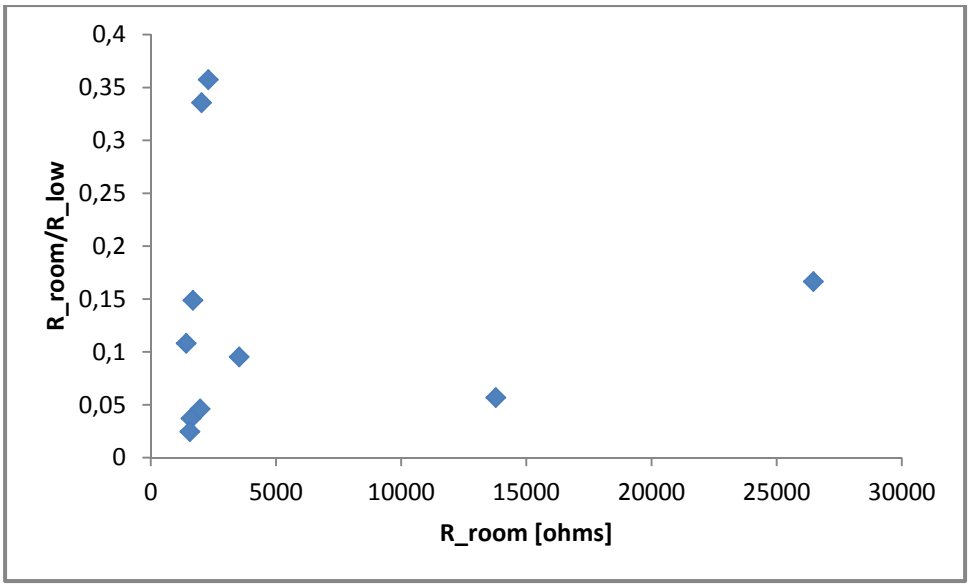

Figure 4.8 A scatter plot of the ratio of the low (T ~ -200°C) to room temperature 2-point resistance versus the room temperature 2-point resistance for all the devices for which there is low temperature data

Table 4.2. Electrostatically deposited graphene sheets separated into quality categories

Quality Category	Properties	Sample #
Very Low Quality	• High room temperature resistance	2 & 9
Low Quality	• Low room temperature resistance • Low R_room/R_low ratio (0 - 0.05)	3, 5 & 8
Medium Quality	• Low room temperature resistance • Medium R_room/R_low ratio (0.1 - 0.2)	1, 4 &10
High Quality	• Low room temperature resistance • High R_room/R_low ratio (>0.3)	6 & 7

The samples were also studied for the direct electrical response from incident light. These measurements were taken inside the cryostat which was set to a constant temperature of 0°C to help with the response time of the devices. The light sources used consisted of a Melles Griot 594nm 10mW laser and a Santec tunable semiconductor TSL-200 laser set at 1540nm

and 0.7mW power. These light sources were set-up outside the cryostat with their aligned beams passing through the protective anti-reflective top glass cover of the cryostat and hitting the deposited graphene devices at normal incidence. The I-V curves of the graphene devices were once again taken with a Keithley 2400 source measure unit and a custom Labview VI. For each source, the first measurement was taken in the dark, then the light source was switched on for 1 minute and again measurements were taken, the light source was switched off for 10 minutes to let the device cool, these measurements were repeated a second time. Figures 4.9 & 4.10 shows the I-V curves resulting from the direct response measurements for the 594nm and 1540nm light sources respectively.

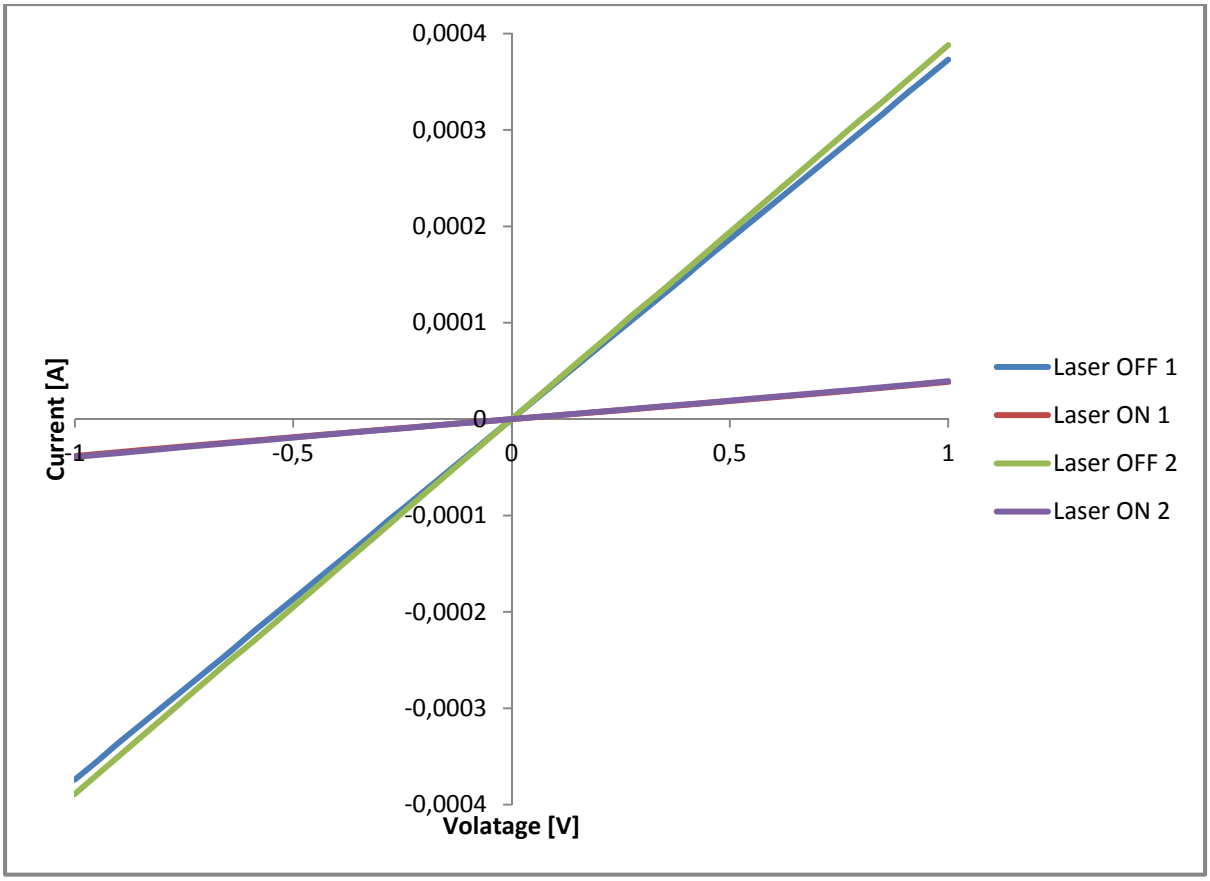

Figure 4.9 I-V curves of electrostatically deposited graphene sheets as photo-conductive switch excited with a Melles Griot 594nm 10mW laser. 10 minutes between readings

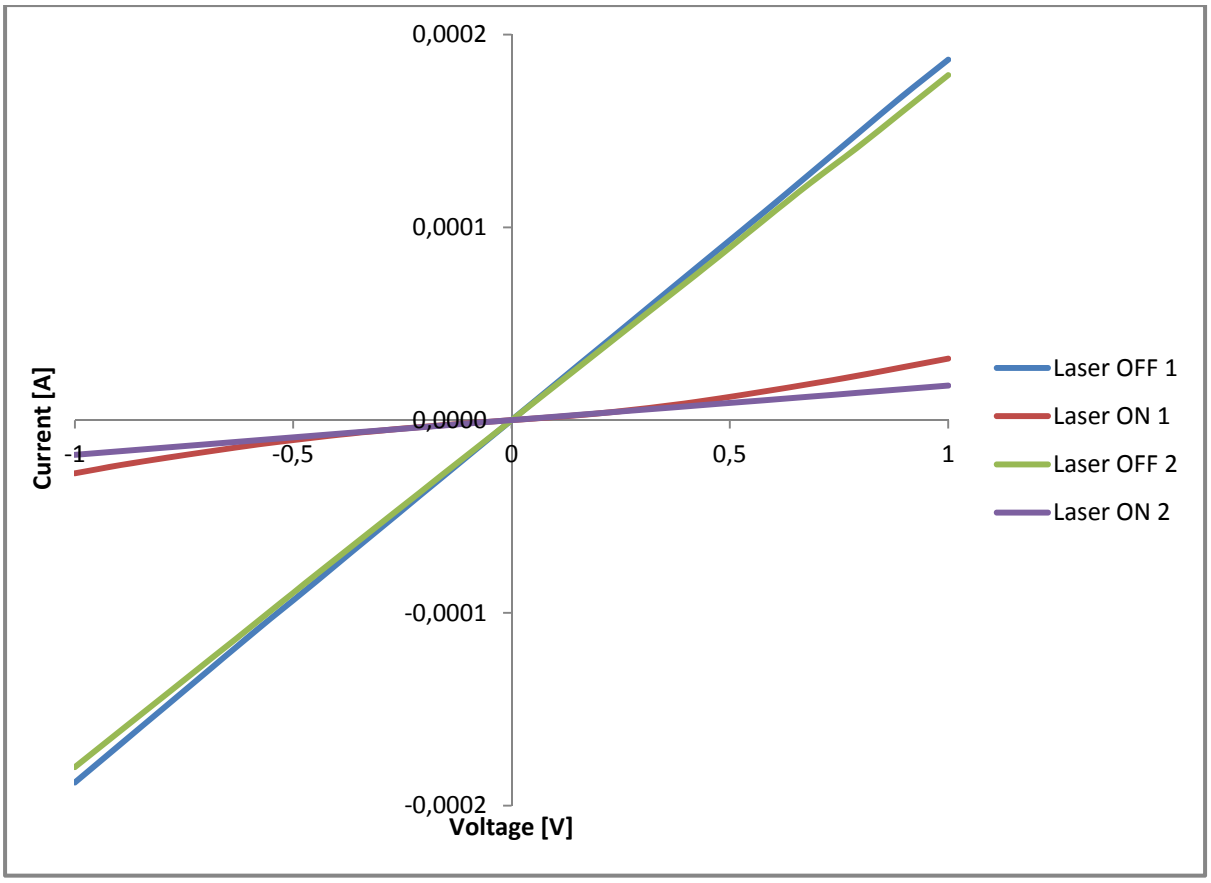

Figure 4.10 I-V curves of electrostatically deposited graphene sheets as photo-conductive switch excited with a Santec tunable semiconductor TSL-200 laser set at 1540nm 0.7mW. 10 minutes between readings

The results shown in figures 4.9 & 4.10 are very interesting, they show an inverse relationship to the temperature-dependence shown in the calorimetric measurements taken and to results from other works (Gilgueng et. al., 2009) (Zhang et. al., 2013). These results prompt questions concerning interactions between the SiO2 substrate of deposition with the deposited graphene. Do these interactions affect the absorption and heating effects of the device, do they introduce a new temperature dependence in the two point resistance of the devices? Further investigation in the subject must be done to answer these questions. These results still show a direct change in resistance with incident light power and thus, the devices in their current state, can be used as rudimentary photoconductive switch devices and potentially bolometers.

CONCLUSION

In conclusion, this work showed that graphene is indeed a unique material with peculiar properties that can be integrated into a multitude of devices. The "wonder material" reputation that is evoked when talking about graphene is well deserved. It was shown that graphene can be directly deposited onto insulating substrates via electrostatic forces and that these depositions can be controlled in terms of number of layers and in the deposition size and position. Some promising results showing large scale deposition of single layered graphene have been presented and offers new advantages to the electrostatic method of graphene deposition. It was also shown that these graphene sheets can be directly deposited onto a patterned substrate to form the active layer in photo-conductive switch devices. These devices have been shown to be sensitive to light sources in the visible and in the infrared spectrum. A small array of these photo-conductive switches were able to be deposited at once, however inhomogeneities in the cleaving process between depositions make this an inconsistent occurrence. A fast identification method using the evolution of the 2D graphene Raman peak was developed to count the number of graphene layers deposited. This identification method was calibrated and tested against SEM imaging and optical imaging techniques of layer counting.

LIST OF REFERENCES

Allen, M. T., J. Martin et A. Yacoby. 2012. « Gate-defined quantum confinement in suspended bilayer graphene ». Nat Commun, vol. 3, p. 934.

Arend M. van der Zande, Robert A. Barton, Jonathan S. Alden, Carlos S. Ruiz-Vargas, William S. Whitney, Phi H. Q. Pham, Jiwoong Park, Jeevak M. Parpia, Harold G. Craighead, Paul L. McEuen. 2010. « Large-Scale Arrays of Single-Layer Graphene Resonators ». Nano Letters. no 10, p. 4869-4873.

Beidaghi, Majid et. al. 2012. « Electrostatic spray deposition of graphene nanoplatelets for high-power thin-film supercapacitor electrodes ». Journal of Solid State Electrochemistry (New York -- United States). October 2012, p. 3341-3348.

Berry, C. W., N. Wang, M. R. Hashemi, M. Unlu et M. Jarrahi. 2013. « Significant performance enhancement in photoconductive terahertz optoelectronics by incorporating plasmonic contact electrodes ». Nat Commun, vol. 4, p. 1622.

Bonaccorso, F., Z. Sun, T. Hasan et A. C. Ferrari. 2010. « Graphene photonics and optoelectronics ». Nat Photon, vol. 4, no 9, p. 611-622.

Bunch, Joseph Scott. 2008. « Mechanical and electrical properties of graphene sheets ». Dissertation in Partial fulfillment of the requirements for the degree of doctor of philosophy. Cornell University, 140 p.

Chernozatonskii, L. A., P. B. Sorokin et A. A. Artukh. 2014. « Novel graphene-based nanostructures: physicochemical properties and applications ». Russian Chemical Reviews, vol. 83, no 3, p. 251.

Chun-Hu, Chen, M. Reddy Kongara et P. Padture Nitin. 2012. « Site-specific stamping of graphene micro-patterns over large areas using flexible stamps ». Nanotechnology, vol. 23, no 23, p. 235603.

Coron, N. 1976. « Infrared Helium cooled bolometers in the presence of background radiation: Optimal parameters and ultimate performances ». Infrared Physics, vol. 16, no 4, p. 411-419.

Dai, Xiaoyu, Leyong Jiang et Yuanjiang Xiang. 2015. « Tunable optical bistability of dielectric/nonlinear graphene/dielectric heterostructures ». Optics Express, vol. 23, no 5, p. 6497-6508.

Dharmendar, Reddy, F. Register Leonard, D. Carpenter Gary et K. Banerjee Sanjay. 2011. « Graphene field-effect transistors ». Journal of Physics D: Applied Physics, vol. 44, no 31, p. 313001.

Dirk M. Guldi, G.M.A. Rahman, Francesco Zerbetto, Maurizio Prato. 2005. « Carbon Nanotubes in Electron Donor-Acceptor Nanocomposites ». Accounts of Chemical Research, no 38, p. 871-878.

Draine, B. T., et A. J. Sievers. 1976. « A high responsivity, low-noise germanium bolometer for the far infrared ». Optics Communications, vol. 16, no 3, p. 425-428.

Eberlein, T., U. Bangert, R. R. Nair, R. Jones, M. Gass, A. L. Bleloch, K. S. Novoselov, A. Geim et P. R. Briddon. 2008. « Plasmon spectroscopy of free-standing graphene films ». Physical Review B, vol. 77, no 23, p. 233406.

Fal'ko, Vladimir I. 2008. « Electronic properties and the quantum Hall effect in bilayer graphene » (2008-01-28 00:00:00), 366. Journal Article. 1863. 205-219 p.

Ferrari, A. C., J. C. Meyer, V. Scardaci, C. Casiraghi, M. Lazzeri, F. Mauri, S. Piscanec, D. Jiang, K. S. Novoselov, S. Roth et A. K. Geim. 2006. « Raman Spectrum of Graphene and Graphene Layers ». Physical Review Letters, vol. 97, no 18, p. 187401.

Geim, A. K. 2012. « Graphene prehistory ». Physica Scripta, vol. 2012, no T146, p. 014003.

Geim, A. K., et K. S. Novoselov. 2007. « The rise of graphene ». Nat Mater, vol. 6, no 3, p. 183-191.

Gildemeister, Jan Mathias. 2000. « Voltage-biased superconducting bolometers for infrared and mm-waves ». University of California, Berkeley.

Gilgueng, Hwang, Juan Camilo Acosta, E. Vela, S. Haliyo et S. Regnier. 2009. « Graphene as thin film infrared optoelectronic sensor ». In Optomechatronic Technologies, 2009. ISOT 2009. International Symposium on. (21-23 Sept. 2009), p. 169-174.

Gorecki, Krzysztof, Witold J. Stepowicz et Andrzej Lozinski. 2004. « Thermal performance of LSCO and LSFO films for IR detectors ». In. Vol. 5505, p. 84-88. < http://dx.doi.org/10.1117/12.577905 >.

Graf, D., F. Molitor, K. Ensslin, C. Stampfer, A. Jungen, C. Hierold et L. Wirtz. 2007. « Spatially Resolved Raman Spectroscopy of Single- and Few-Layer Graphene ». Nano Letters, vol. 7, no 2, p. 238-242.

Gunasekaran, V., et S. J. Kim. 2009. « Observation of diode-like characteristics in planar-type structures of graphite flakes ». Journal of Physics: Conference Series, vol. 150, no 2, p. 022039.

Hancock, Y. 2011. « The 2010 Nobel Prize in physics—ground-breaking experiments on graphene ». Journal of Physics D: Applied Physics, vol. 44, no 47, p. 473001.

Y. Hatsugai: JPSJ Online-News and Comments [September 10, 2010]

Hidefumi, Hiura, Miyazaki Hisao et Tsukagoshi Kazuhito. 2010. « Determination of the Number of Graphene Layers: Discrete Distribution of the Secondary Electron Intensity Stemming from Individual Graphene Layers ». Applied Physics Express, vol. 3, no 9, p. 095101.

Jayasena, B., C. D. Reddy et S. Subbiah. 2013. « Separation, folding and shearing of graphene layers during wedge-based mechanical exfoliation ». Nanotechnology, vol. 24, no 20, p. 205301.

Jianjun, Wang, Wang Sigen, P. Miraldo, Hou Kun, R. Outlaw, Zhu Mingyao, Zhao Xin et B. C. Holloway. 2006. « Carbon Nanosheet Cathodes for Use in Milliamp Class Field Emission Devices ». In Vacuum Nanoelectronics Conference, 2006 and the 2006 50th International Field Emission Symposium., IVNC/IFES 2006. Technical Digest. 19th International. (July 2006), p. 403-403.

Kazi, H., Y. Cao, I. Tanabe, M. S. Driver, P. A. Dowben et J. A. Kelber. 2014. « Multi-layer graphene on Co(0001) by ethanol chemical vapor deposition ». Materials Research Express, vol. 1, no 3, p. 035601.

Kliros, G. S. 2010. « Quantum capacitance of bilayer graphene ». In Semiconductor Conference (CAS), 2010 International. (11-13 Oct. 2010) Vol. 01, p. 69-72.

Kotaki, Y., M. Matsuda, M. Yano, H. Ishikawa et H. Imai. 1987. « 1.55μm wavelength tunable FBH-DBR laser ». Electronics Letters. Vol. 23, no 7, p. 325-327. < http://digital-library.theiet.org/content/journals/10.1049/el_19870241 >.

Krökel, D., D. Grischkowsky et M. B. Ketchen. 1989. « Subpicosecond electrical pulse generation using photoconductive switches with long carrier lifetimes ». Applied Physics Letters, vol. 54, no 11, p. 1046-1047.

Kymakis, Emmanuel, et Gehan AJ Amaratunga. 2005. « Carbon nanotubes as electron acceptors in polymeric photovoltaics ». Reviews on Advanced Materials Science, vol. 10, no 4, p. 300-305.

Kymakis, E., et G. A. J. Amaratunga. 2002. « Single-wall carbon nanotube/conjugated polymer photovoltaic devices ». Applied Physics Letters, vol. 80, no 1, p. 112-114.

Liu, Zhi-Bo, Yan-Fei Xu, Xiao-Yan Zhang, Xiao-Liang Zhang, Yong-Sheng Chen et Jian-Guo Tian. 2009. « Porphyrin and Fullerene Covalently Functionalized Graphene Hybrid Materials with Large Nonlinear Optical Properties ». The Journal of Physical Chemistry B, vol. 113, no 29, p. 9681-9686.

Low, Frank J. 1961. « Low-Temperature Germanium Bolometer ». Journal of the Optical Society of America, vol. 51, no 11, p. 1300-1304.

Malard, L. M., M. A. Pimenta, G. Dresselhaus et M. S. Dresselhaus. 2009. « Raman spectroscopy in graphene ». Physics Reports, vol. 473, no 5–6, p. 51-87.

McMullan, D. 1995. « Scanning electron microscopy 1928–1965 ». Scanning, vol. 17, no 3, p. 175-185.

Mi, Zhou, L. Pasquale Frank, A. Dowben Peter, Boosalis Alex, Schubert Mathias, Darakchieva Vanya, Yakimova Rositza, Kong Lingmei et A. Kelber Jeffry. 2012. « Direct graphene growth on Co 3 O 4 (111) by molecular beam epitaxy ». Journal of Physics: Condensed Matter, vol. 24, no 7, p. 072201.

Miller, D. A. B. 2001. « Photonic analog to digital converter using ultrafast photoconductors». In Lasers and Electro-Optics Society, 2001. LEOS 2001. The 14th Annual Meeting of the IEEE. (2001) Vol. 1, p. 251-252 vol.1.

Ni, Zhenhua, Lei Liu, Yingying Wang, Zhe Zheng, Lain-Jong Li, Ting Yu et Zexiang Shen. 2009. « G-band Raman double resonance in twisted bilayer graphene: Evidence of band splitting and folding ». Physical Review B, vol. 80, no 12, p. 125404.

Novoselov, K. S., A. K. Geim, S. V. Morozov, D. Jiang, M. I. Katsnelson, I. V. Grigorieva, S. V. Dubonos et A. A. Firsov. 2005. « Two-dimensional gas of massless Dirac fermions in graphene ». Nature, vol. 438, no 7065, p. 197-200.

Novoselov, K. S., A. K. Geim, S. V. Morozov, D. Jiang, Y. Zhang, S. V. Dubonos, I. V. Grigorieva et A. A. Firsov. 2004. « Electric Field Effect in Atomically Thin Carbon Films ». Science, vol. 306, no 5696, p. 666-669.

Obraztsov, Alexander N. 2009. « Chemical vapour deposition: Making graphene on a large scale ». Nat Nano, vol. 4, no 4, p. 212-213.

Palser, Adam H. R. . 1999. « Interlayer interactions in graphite and carbon nanotubes ». Physical Chemistry Chemical Physics, vol. 1, no 18, p. 4459-4464.

Pollard, Benjamin. 2011. « Growing Graphene via Chemical Vapor Deposition ». Master Thesis. 47 p.

R.E. Camacho, A.R. Morgan, M.C. Flores, T.A. McLeod, V.S. Kumsomboone, B.J. Mordecai, R. Bhattacharjea, W. Tong, B.K. Wagner, J.D. Flicker, S.P. Turano, W.J. Ready. 2007. « Carbon Nanotube Arrays for Photovoltaic Applications ». Nanomaterials for Electronic Applications Research Summary.

Richards, P. L. 1994. « Bolometers for infrared and millimeter waves ». Journal of Applied Physics, vol. 76, no 1, p. 1-24.

Sidorov, Anton N. 2009. « Novel techniques to produce and deposit n-layer graphene: Their physical properties ». Doctoral Thesis in Electrical and Computer Engineering. Ann Arbor -- United States, University of Louisville, 190 p. ProQuest Dissertations & Theses Full Text.<http://search.proquest.com/docview/304916336?accountid=2723>.

Sidorov, Anton N. et. al. 2007. « Electrostatic deposition of graphene ». Nanotechnology (Bristol -- United Kingdom). April 4,, p. 4pp.

Smith, F. W., H. Q. Le, V. Diadiuk, M. A. Hollis, A. R. Calawa, S. Gupta, M. Frankel, D. R. Dykaar, G. A. Mourou et T. Y. Hsiang. 1989. « Picosecond GaAs-based photoconductive optoelectronic detectors ». Applied Physics Letters, vol. 54, no 10, p. 890-892.

Venugopal, Archana, Jack Chan, Xuesong Li, Carl W. Magnuson, W. P. Kirk, Luigi Colombo, Rodney S. Ruoff et Eric M. Vogel. 2011. « Effective mobility of single-layer graphene transistors as a function of channel dimensions ». Journal of Applied Physics, vol. 109, no 10, p. 104511-104511-5.

Vito Sgobba, Dirk M. Guldi. 2007. « Carbon nanotubes as integrative materials for organic photovoltaic devices ». Journal of Materials Chemistry. p. 141-248.

Wood, R. Andrew. 1993. « Uncooled thermal imaging with monolithic silicon focal planes ». In. Vol. 2020, p. 322-329. < http://dx.doi.org/10.1117/12.160553 >.

Xuekun, Lu, Yu Minfeng, Huang Hui et S. Ruoff Rodney. 1999. « Tailoring graphite with the goal of achieving single sheets ». Nanotechnology.

Yoneoka, S., M. Liger, G. Yama, R. Schuster, F. Purkl, J. Provine, F. B. Prinz, R. T. Howe et T. W. Kenny. 2011. « ALD-metal uncooled bolometer ». In Micro Electro Mechanical Systems (MEMS), 2011 IEEE 24th International Conference on. (23-27 Jan. 2011), p. 676-679.

Yu, Qingkai, Luis A. Jauregui, Wei Wu, Robert Colby, Jifa Tian, Zhihua Su, Helin Cao, Zhihong Liu, Deepak Pandey, Dongguang Wei, Ting Fung Chung, Peng Peng, Nathan P. Guisinger, Eric A. Stach, Jiming Bao, Shin-Shem Pei et Yong P. Chen. 2011. « Control and characterization of individual grains and grain boundaries in graphene grown by chemical vapour deposition ». Nat Mater, vol. 10, no 6, p. 443-449.

Zhang, By Yongzhe, Tao Liu, Bo Meng, Xiaohui Li, Guozhen Liang, Xiaonan Hu et Qi Jie Wang. 2013. « Broadband high photoresponse from pure monolayer graphene photodetector ». Nat Commun, vol. 4, p. 1811.

Zhang, Y., Z. Jiang, J. P. Small, M. S. Purewal, Y. W. Tan, M. Fazlollahi, J. D. Chudow, J. A. Jaszczak, H. L. Stormer et P. Kim. 2006. « Landau-Level Splitting in Graphene in High Magnetic Fields ». Physical Review Letters, vol. 96, no 13, p. 136806.

« Highly Ordered Pyrolytic Graphite ». 2013. In http://www.2spi.com/catalog/new/hopgsub.php. Visited 5th June 2013.

« High-Purity Metal Foils ». 2015. In http://www.sigmaaldrich.com//materials-science/material-science-products.html?TablePage=108832768. Visited 5th August 2015.